Commercial Production of Non-Proprietary Ultra High Performance Concrete

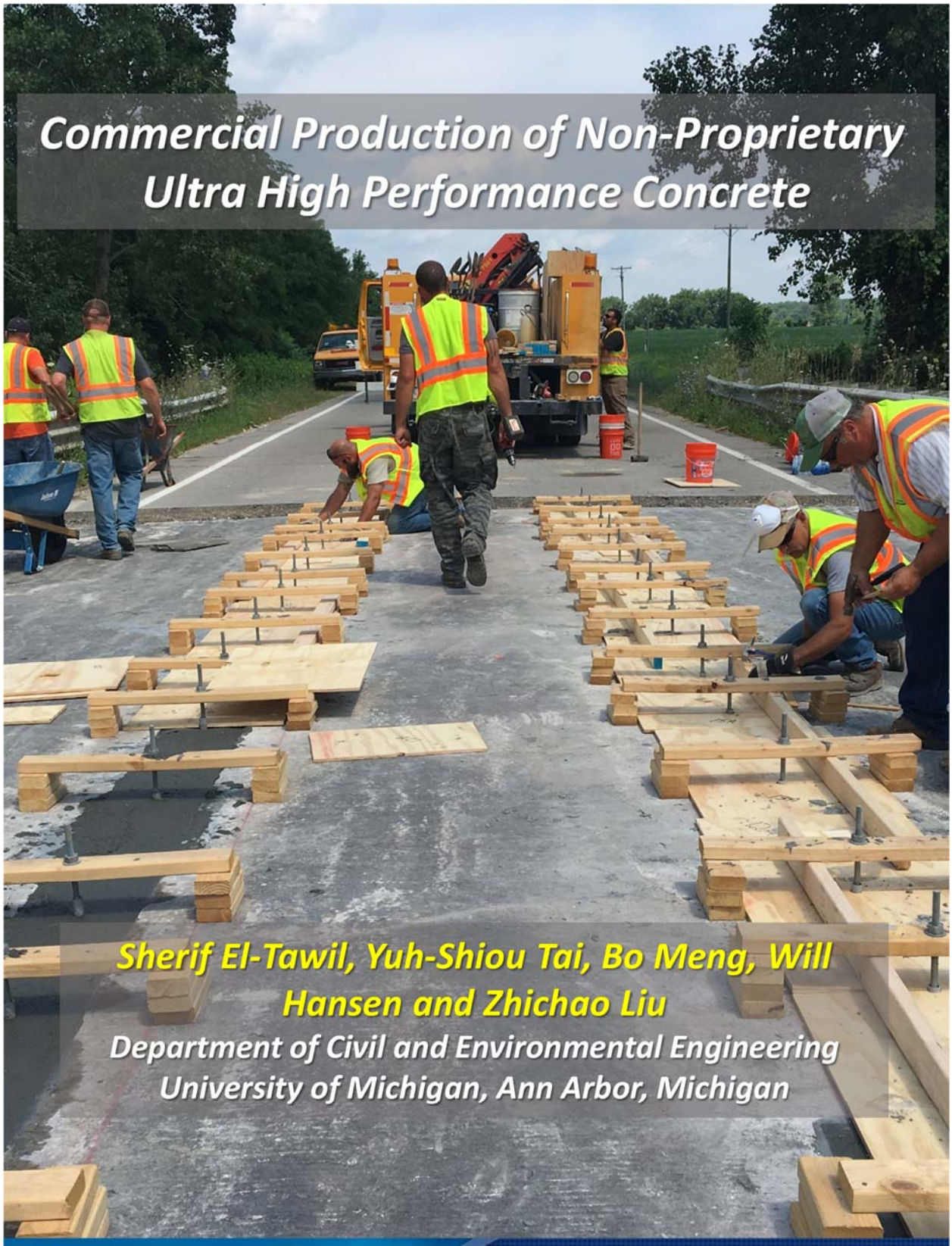

Sherif El-Tawil, Yuh-Shiou Tai, Bo Meng, Will Hansen and Zhichao Liu

Department of Civil and Environmental Engineering
University of Michigan, Ann Arbor, Michigan

MichiganEngineering
University of Michigan College of Engineering

1. Report No. SPR-1670	**2. Government Accession No.** N/A	**3. MDOT Project Manager** Steve Kahl
4. Title and Subtitle Commercial Production of Non-Proprietary Ultra High Performance Concrete		**5. Report Date** 12/31/2018
		6. Performing Organization Code N/A
7. Author(s) Sherif El-Tawil, Yuh-Shiou Tai, Bo Meng, Will Hansen and Zhichao Liu		**8. Performing Org. Report No.** N/A
9. Performing Organization Name and Address The Regents of the University of Michigan Office of Research and Sponsored Projects Wolverine Tower First Floor, Room 1058 3003 S. State St. Ann Arbor, MI 48109-1274		**10. Work Unit No. (TRAIS)** N/A
		11. Contract No. Contract 2016-0068
		11(a). Authorization No. Z6
12. Sponsoring Agency Name and Address Michigan Department of Transportation Research Administration 8885 Ricks Rd. P.O. Box 30049 Lansing MI 48909		**13. Type of Report & Period Covered** Final Report 4/1/2017 – 12/31/2018
		14. Sponsoring Agency Code N/A
15. Supplementary Notes N/A		

16. Abstract

The vast majority of field usage of UHPC in the US, to date, has employed pre-packaged, proprietary materials. A previous project funded by MDOT developed a generic, cost-optimized UHPC mix (named MI-UHPC) that performed exceptionally well in the lab but was not well-suited for field implementation. This project explored the reasons why the generic UHPC mix did not scale up. Successful field mixing was achieved by optimizing the mix proportions and changing the mixing procedure. In addition and in order to achieve truly generic UHPC technology, this project also proposed a family of mixes with components sourced from a variety of local suppliers. One of these mixes was used in the Kilgore Road Bridge Restoration Project on the Pine River in Kenockee, Michigan and is one of the earliest field applications of a non-proprietary blend of UHPC in the US. Extensive material testing was conducted to explore the influence of a number of variables on the short and long term properties of the proposed UHPC mix. The effect of component source and quantity was investigated with a specific focus on cement, silica fume and fibers. Recommended special provisions for commercial production of UHPC were proposed.

17. Key Words Ultra-high performance concrete, non-proprietary, durability, strength, mixing, field pour, bridge, freeze-thaw.	**18. Distribution Statement** No restrictions. This document is available to the public through the Michigan Department of Transportation.

19. Security Classification - report Unclassified	**20. Security Classification - page** Unclassified	**21. No. of Pages**	**22. Price** N/A

DISCLAIMER

This publication is disseminated in the interest of information exchange. The Michigan Department of Transportation (hereinafter referred to as MDOT) expressly disclaims any liability, of any kind, or for any reason, that might otherwise arise out of any use of this publication or the information or data provided in the publication. MDOT further disclaims any responsibility for typographical errors or accuracy of the information provided or contained within this information. MDOT makes no warranties or representations whatsoever regarding the quality, content, completeness, suitability, adequacy, sequence, accuracy or timeliness of the information and data provided, or that the contents represent standards, specifications, or regulations.

ACKNOWLEDGEMENT

This project was funded by the Michigan Department of Transportation. The authors would like to acknowledge the support and efforts of Mr. Steve Kahl and Mr. David Juntunen for initiating and directing this research and Mr. John Belcher for his ideas, support and many discussions during the course of the research. The authors also wish to acknowledge the continuing assistance of the Research Advisory Panel (RAP) members in contributing to the advancement of this study.

TABLE OF CONTENTS

ACKNOWLEDGEMENT iv
TABLE OF CONTENTS 1
LIST OF FIGURES 5
LIST OF TABLES 9
EXECUTIVE SUMMARY 1
1. INTRODUCTION 5
1.1. What is Ultra-High Performance Concrete (UHPC)? 5
1.2. Research Objectives 6
1.3. Organization of the Report 7
2. BACKGROUND AND LITERATURE REVIEW 8
2.1. Development of UHPC 8
2.2. Material Constituents 10
2.3. Mixing procedure 15
3. DEVELOPMENT OF NONPROPRIETARY UHPC MIXTURES 17
3.1. Component selection 17
3.1.1. Cement 18
3.1.2. GGBS 19
3.1.3. Silica fume 21
3.1.4. Silica Sands 22
3.1.5. High Range Water Reducers (HRWRs) 23
3.1.6. Fibers 24
3.2. Particle Size Distribution and Packing Density Models 25
3.3. Effect of Mixing Speed 28

3.4. Effect of Mixing Protocol 31

4. TEST PROCEDURES AND METHODS 36

4.1. Mixing and casting processes 36

4.2. Fresh characteristic and quality control 36

4.2.1. Flowability 36

4.2.2. Setting time 37

4.2.3. Hydration heat 38

4.2.4. Ultrasonic pulse velocity 38

4.2.5. Shrinkage 38

4.3. Hardened UHPC mechanical Properties 40

4.3.1. Compression testing 40

4.3.2. Direct tension testing 41

4.4. Durability characteristics 42

4.4.1. Air void analysis 42

4.4.2. Rapid chloride penetration test (RCPT) 44

4.4.3. Freeze-thaw resistance 45

5. EXPERIMENTAL RESULTS 48

5.1. Effect of Superplasticizer Source on Spread 49

5.2. Effect of GGBS Dosage 53

5.2.1. Flowability and air content characteristics 53

5.2.2. Hydration heat and degree of hydration 60

5.2.3. Autogenous shrinkage 64

5.2.4. Capillary absorption and F-T test 67

5.2.5. Compressive strength development 70

5.3. Compressive strength characteristics of UHPC 75

5.4. Tensile behavior of UHPC 80

5.5. Effect of fiber characteristics 88

5.6. Durability 90

5.6.1. Analysis of air void distribution 91
5.6.2. Chloride penetration resistance test results 95
5.6.3. Freeze-thaw (F-T) resistance of UHPC 96
6. SCALING UP TO FIELD IMPLEMENTATION 100
6.1. Introduction 100

6.2. Laboratory trial batches 100

6.3. Field demonstration of UHPC application 103

6.3.1. Mixing equipment 104
6.3.2. Mixing process 105
6.3.3. Casting process 107
6.3.4. Post-curing inspection 108
6.3.5. Comparison between lab and field properties 109
6.4. A note about cost 110

6.5. Summary and conclusions 110

7. SUMMARY, MAJOR CONCLUSIONS AND FUTURE RESEARCH 112
7.1. Summary 112

7.2. Why field-mixing failed in the previous project 113

7.3. Major Conclusions 113

7.4. Commercial Potential of UHPC 117

8. REFERENCES 119
9. APPENDIX A – STRESS-STRAIN PLOTS FOR ALL UHPC MIXES 131
9.1. LA CEMENT MIXES 132

9.2. ST CEMENT MIXES 135

9.3. LE CEMENT MIXES 138

10. APPENDIX B – RESULTS OF FREEZE-THAW TESTING – RILEM 142

11. APPENDIX C – RECOMMENDED SPECIAL PROVISION 145

LIST OF FIGURES

Figure 3-1 GGBS activity test results 21

Figure 3-2 Color of silica fume 22

Figure 3-3 The silica sands used for the preparation of UHPC 23

Figure 3-4 Types of fibers used for this project 25

Figure 3-5 Particle size distributions of solid materials used in this project 27

Figure 3-6 Analysis of actual particle size distributions of particles in the different mixes with the modified A&A model. 27

Figure 3-7 Mixer effect on the turnover of UHPC 31

Figure 3-8 The new mixing sequence 34

Figure 3-9 Flow test and determination of flow 34

Figure 3-10 Comparison of turnover time and flow of the mixtures with different amounts of premixed silica sands 35

Figure 3-11 The weight variation of mixtures with different amounts of premixed silica sands 35

Figure 4-1 Paste penetration resistance test 37

Figure 4-2 Autogenous shrinkage measurement 39

Figure 4-3 Testing set-up for compression tests of cube specimens 41

Figure 4-4 Tensile test set up and specimen dimension 42

Figure 4-5 Photograph of the linear traverse method point count instrument 43

Figure 4-6 Treated and untreated UHPC cross section for air void analysis 44

Figure 4-7 Rapid Chloride Permeability test setup 45

Figure 4-8 Diagrammatic presentation of the F–T test 47

Figure 5-1 The spread of UHPC with H1 and different cement and silica fume combinations 51

Figure 5-2 The spread of UHPC with H2 and different cement and silica fume combinations 52

Figure 5-3 The spread of UHPC with H3 and different cement and silica fume combinations 52

Figure 5-4 Effect of cement replacement by GGBS on the spread of UHPC 54

Figure 5-5 Effect of steel fiber addition on the fresh air content of UHPC mixes 57

Figure 5-6 Air Content as a Function of Power's Spacing Factor 58

Figure 5-7 Air void size distribution based on the chord length from linear traverse method (air content of the regular air-entrained concrete is normalized to the paste content of UHPC mixes) 59

Figure 5-8 Air void profiles for the UHPC mixes with different GGBS contents 60

Figure 5-9 Temperature evolution in UHPC mixtures with different GGBS contents 61

Figure 5-10 Evolution of the degree of hydration reaction with time in UHPC mixtures with different GGBS contents 63

Figure 5-11 Shrinkage strain development of UHPC mixes with different GGBS contents 64

Figure 5-12 (a) Penetration resistance of UHPC paste mixes and (b) correlation between dormant time and setting time 65

Figure 5-13 Simultaneous representation of temperature and strain evolution 66

Figure 5-14 Shrinkage development in the steady state 67

Figure 5-15 Moisture uptake curves of UHPC mixes 69

Figure 5-16 Normalized moisture uptake between different concrete mixes 69

Figure 5-17 The capillary suction and associated sorptivity 70

Figure 5-18 The segregation caused by high dose of HRWR 71

Figure 5-19 Effect of different grade of GGBS on the compressive strength of cube 73

Figure 5-20 Effects of different combinations on compressive strength 79

Figure 5-21 Relationship between compressive strength and spread 79

Figure 5-22 Typical Tensile Strain Response in UHPC [115] 80

Figure 5-23 Effects of the different variables on post-cracking strength 83

Figure 5-24 Effects of different variables on strain capacity 84

Figure 5-25 Effects of different variables on energy absorption capacity 86

Figure 5-26 Effects of different variables on average fiber stress 87

Figure 5-27 Effect of fiber type, length and dosage on mechanical properties of UHPC 90

Figure 5-28 Comparison between modified point count method and linear traverse test method 93

Figure 5-29 Air void profiles for the UHPC mixes with different HRWR contents 94

Figure 5-30 Air void size distribution based on the chord length from linear traverse method 94

Figure 5-31 Total charge passed for UHPC and regular concrete 96

Figure 5-32 Moisture uptake curves of UHPC 98

Figure 5-33 Evolution of the surface scaling for UHPC 98

Figure 5-34 Effects of freeze-thaw cycling on the relative dynamic modulus of UHPC 99

Figure 6-1 Bridge repair plan and site 104

Figure 6-2 (a) Closure pour and (b) transportation of UPHC to pour location 104

Figure 6-3 Field mixing process 107

Figure 6-4 Casting of UHPC into the longitudinal connection 108

Figure 6-5 Field cast result 109

LIST OF TABLES

Table 3-1 Physical and chemical properties of cement 19

Table 3-2 Properties of GGBS mortar mixes..... 20

Table 3-3 Properties of silica fume..... 22

Table 3-4 High range water reducer 24

Table 3-5 Properties of fibers 25

Table 3-6 Rotational speeds of the three Hobart mixers..... 29

Table 3-7 Mix design of UHPC mortar for three Hobart mixers..... 30

Table 3-8 Spread and turnover time for three different mixers at two different speeds..... 30

Table 5-1 Mixture proportions by weight..... 49

Table 5-2 Air content and void parameters for UHPC mixes..... 58

Table 5-2 Performance of UHPC with different grades of GGBS 74

Table 5-4 Compressive and tensile properties of UHPC..... 77

Table 5-5 Effect of fiber effect on mechanical properties of UHPC 89

Table 5-6 Air void analysis results for different mixes 93

Table 6-1 Field mix proportions (by weight)..... 100

Table 6-2 Mechanical properties of laboratory and field batches..... 102

Table 6-3 Cost per component of Mix 3 in 2017 dollars..... 103

Table 6-4 UHPC fresh test results 106

EXECUTIVE SUMMARY

Introduction:

Ultra-high performance concrete (UHPC) has drawn the attention of researchers and practitioners because of its unique properties that make it particularly well-suited for infrastructure applications. The US Federal Highway Administration (FHWA) and multiple state Departments of Transportation (DOTs) have exhibited strong interest in UHPC and its application to bridges. For example, the third round of the FHWA Every Day Counts (EDC-3) program focused on demonstrating the advantages that UHPC offers for connecting prefabricated bridge elements (FHWA 2017). The fourth round of the program, EDC-4, will focus on that general theme as well.

The vast majority of field usage of UHPC in the US, to date, has employed pre-packaged, proprietary materials. A previous project funded by MDOT developed a generic, cost-optimized UHPC mix (named MI-UHPC) that performed exceptionally well in the lab but was not well-suited for field implementation. This project explored the reasons why the generic UHPC mix did not scale up. In addition and in order to achieve truly generic UHPC technology, this project also proposed a family of mixes with components sourced from a variety of local suppliers. One of these mixes was used in the Kilgore Road Bridge Restoration Project on the Pine River in Kenockee, Michigan and is one of the earliest field applications of a non-proprietary blend of UHPC in the US. It is hoped that this research will spur commercial production and utilization of non-proprietary UHPC and broaden its appeal and range of application.

Objectives:

The objective of this project was to systematically investigate the characteristics of non-proprietary UHPC, while considering cost optimization, feasibility of field construction, and providing relevant information for the development of a special provision for field use of UHPC. Specific research objectives were: 1) Investigate why the earlier UHPC mix did not scale up for field application; 2) Conduct further optimization studies of fibers and cementitious components, to determine the range of material properties that will lead to a successful larger scale mix regardless of potential sources of key ingredients; 3) Provide material properties for engineering design and specifications; and 4) Demonstrate constructability of the mix on large scale closure pours in a field environment.

Summary of Research:

This research examined the fresh, short-term, and long-term properties of generic UHPC made from components sourced from a variety of suppliers. The research also investigated the effect of the activity level of slag cement, which is a key component of UHPC, and the impact of slag cement content on UHPC properties. The material tests conducted included workability, hydration heat, autogenous shrinkage, rapid chloride penetration, freeze-thaw, air void distribution as well as compression and direct tension testing. Steel fibers with two different aspect ratios were also investigated and the possibility of replacing steel fibers with polyethylene fibers was explored. A field application that implemented one of the mixes in the Kilgore Road Bridge Restoration Project on the Pine River in Kenockee, Michigan led to valuable lessons for field production and

casting of generic UHPC. Recommended special provisions for commercial production of UHPC were proposed.

Summary of Results:

Field efforts to mix generic UHPC in an earlier project failed for four key reasons: 1) the silica fume used in the field had a high carbon content, which drove up water demand, 2) the dosage of the high range water reducer (HRWR) was too low to compensate for the higher water demand, making mixing more difficult, 3) the silica fume was a densified product that posed an additional challenge for the mixer as it tried to deagglomerate the material and sufficiently disperse it during dry mixing, and 4) the field mixer did not have sufficient capacity to induce turnover in the wet mix, compromising the mixing process.

Results from this research project showed that generic UHPC can be successfully mixed using components sourced from a variety of suppliers as long as a proper HRWR dose is selected. Too low of a dose will prevent the mix from turning over as in the earlier project. Increasing the HRWR dose can lead to mildly lower mechanical properties but does not compromise the long term properties of UHPC. Too high of a dose can lead to fiber segregation, which is undesirable and should be avoided. An appropriate HRWR dosage can be identified through field trial batches in order to achieve a mix that meets the required performance criteria and can be mixed in the field.

With few exceptions, the 28-day compressive strength and peak tensile strength of all mixtures (sourced from the various suppliers considered in this work) were higher than 21.7 ksi (150 MPa) and 1.2 ksi (8.3 MPa), respectively, fulfilling the minimum requirement for field-cast

UHPC. The material testing program showed that partial replacement of cement by slag cement can improve the workability of UHPC paste, lead to favorable self-consolidating characteristics and reduce air voids and porosity, which is beneficial for the durability of UHPC. A new mixing protocol reduces the burden on field mixers and allows for larger mix loads in the field. This project demonstrated conclusively that field application of truly generic UHPC technology is feasible.

The Promise of UHPC - An Opportunity for the State of Michigan:

The extremely high freeze-thaw resistance, negligible chloride penetration, and ability to mobilize the material's strain hardening response in tension to limit crack width, suggests that UHPC structures can be extremely long-living and low maintenance at the same time. The material's characteristics open up new applications, such as ultra-long span structures, and offer an opportunity to build the next generation of infrastructure that is significantly more robust, resilient and sustainable. Although this project investigated field cast applications of UHPC and successfully executed them, it is obvious that UHPC is better suited for precast construction, where mixing can be conducted under controlled conditions in a plant.

Even though it is still a nascent material and expensive with respect to regular concrete, UHPC usage in the US is growing exponentially. The Michigan Department of Transportation is one of the earliest DOTs to investigate production and implementation of generic UHPC. Encouraging growth in UHPC usage will encourage growth in the demand for steel fibers, which are a key component of UHPC. AS UHPC usage grows, the State of Michigan, with its strong manufacturing base, could become a leader in steel fiber production, opening up manufacturing opportunities and leading to the creation of new jobs in this burgeoning technology.

1. INTRODUCTION

1.1. What is Ultra-High Performance Concrete (UHPC)?

Ultra-high performance concrete (UHPC) is a cementitious material that achieves a compressive strength of at least 21.7 ksi (150 MPa) and has self-consolidating properties (Wille et al. [1], Graybeal [2]; Wille et al. [3-4]). It is comprised of component materials with particle sizes and distributions carefully selected to maximize packing density [5,6]. The high packing density, which means that constituent particles are arranged as compactly as possible, is the reason for the extremely high mechanical and durability properties of the material. Another key feature of UHPC is that it is reinforced with a small percentage by volume (typically 1% to 2%) of short steel fibers. Changes in the type and quantity of steel fibers directly affect the ductility, durability, strength and energy dissipation capacity of the material (Wille et al. [1,3,4]; Kim [7-15]; Pyo [16-20]).

The US Federal Highway Administration (FHWA) and multiple state Departments of Transportation (DOTs) have exhibited strong interest in UHPC and its application to bridges. For example, the third round of the Every Day Counts (EDC-3) program focused on demonstrating the advantages that UHPC offers for connecting prefabricated bridge elements (FHWA 2017). The fourth round of the program, EDC-4, will focus on that general theme as well.

The use of UHPC as a field-cast material is not new, but most of the experience has been with proprietary materials. Proprietary UHPC has been used in Europe [21] and across the US, particularly for field-cast connections as outlined in [22]. A common thread in UHPC applications is that the required volume of material is not large, primarily because proprietary UHPC is expensive. UHPC must be purchased from specific suppliers and the contractors that work with it must be specially trained and certified, further increasing the cost per cubic yard. In a 2016

Michigan Department of Transportation project that required 8 cubic yards of proprietary UHPC, the total cost for the project was estimated at $5,500 per cubic yard. This included about $2,500 per cubic yard for purchase of the material itself. The other $3,000 per cubic yard was for the specialized construction and technical services required by the supplier.

In a previous effort funded by MDOT [5], the PIs had developed a non-proprietary UHPC mixture that doesn't require specialized crews or curing procedures. The resulting material had performance characteristics similar to the commercially available material as discussed in numerous publications (Wille et al. [3,4,23,24], Pyo et al. [16,17,25] and Alkaysi et al [6, 26]). However, although the material could be mixed successfully in the lab, the mixing process could not be scaled up to permit field application. This project examines the challenges associated with field mixing and investigates the reasons behind the failed batches.

1.2. Research Objectives

The objectives of this research project are as follows:

- Investigate the failed mix attempts in the previous MDOT project and through further optimization studies of fibers and cementitious components, determine range of material properties that will lead to a successful larger scale mix regardless of potential sources of key ingredients.
- Provide material properties for engineering design (minimum strength, for example) and specifications.
- Demonstrate constructability of the mix on large scale closure pours in a field environment.

1.3. Organization of the Report

The main body of the report is preceded by detailed contents including lists of figures and tables. This is followed by an introduction giving briefly the scope and objectives of the study and importance of the topic.

- Chapter 2 provides background information about UHPC and discusses the literature.
- Chapter 3 outlines development of non-proprietary UHPC mixes geared for field applications. The chapter discusses the sources, selection and characteristics of UHPC ingredients. It also discusses various mixing protocols and the effect of different mixing parameters on the fresh properties of UHPC.
- Chapter 4 addresses the test procedures and methods used to characterize the properties of the various UHPC mixes used in this research.
- Chapter 5 presents and discusses the extensive test results obtained during the course of this project.
- Chapter 6 reports on a successful field mixing effort to cast UHPC bridge joints. The chapter presents information on the bridge site and how the field mix differed from the lab one. It also reports on the lessons gained from the field experience.
- Chapter 7 provides a summary of the research, the most important conclusions and future work.

2. BACKGROUND AND LITERATURE REVIEW

This chapter provides background information about UHPC and discusses the literature. It starts with a review of the historical development of UHPC and follows up with a discussion of the material's key ingredients and their properties. A review of mixing procedures used by others is also provided.

2.1. Development of UHPC

Researchers around the world have been trying for decades to develop cement-based materials with exceptionally high performance. Macro defect free (MDF) cement, which is a blend of hydraulic cement and water-soluble polymer, was one of the first trials. The material was formulated such that large voids or defects in the hardened cement product were minimized, resulting in a compressive strength that exceeded 43.5 ksi (300 MPa) [27]. Another noteworthy product is densified small particles (DSP) concrete, where micro silica was introduced to fill the voids between cement particles in order to maximize the density of the concrete mixture. Superplasticizer was used to ensure workability and it was shown that the material could achieve compressive strengths of up to 36.3 ksi (250 MPa) [28]. It was observed that the cementitious matrix of DSP became more brittle as its strength increased. To address this undesirable response and make the material more ductile, Bache introduced high-strength aggregates and steel fibers into the concrete matrix. The composite reached a compressive strength of 65.3 ksi (450MPa) and was named compact reinforced composites (CRC) concrete [29].

Slurry infiltrated fiber concrete (SIFCON) is a type of fiber-reinforced concrete, but its production method is very different from that of regular fiber-reinforced concrete. Regular fiber-reinforced concrete is usually produced by adding short discontinuous fibers to fresh concrete prior

to casting. SIFCON, however, is produced by placing long, continuous fibers into the empty mold first. Compared to regular fiber reinforced concrete where the fiber content is usually 2% - 6% by volume, the fiber content in SIFCON could be as high as 20% by volume. The placed fibers were then infiltrated with a cement slurry [30,31]. Although MDF, DSP and SIFCON all have excellent performance, their complicated production processes and high cost prevented their widespread use in industry.

Richard et al. [32,33] used finer and more reactive components to formulate reactive powder concrete (RPC). RPC is based on the principle of improving homogeneity by eliminating coarse aggregates, optimizing particle packing density, and applying heat and pressure before and during setting. Steel fibers with 0.5 inch (13 mm) length and 0.006 inch (0.15 mm) diameter were used to enhance the ductility of the composite. The performance of RPC was shown to depend on the type of aggregates used and curing methods applied. The highest performing RPC exhibited a compressive strength of up to 116 ksi (800 MPa) and had tensile flexural strength of up to 8.7 ksi (60 MPa). At about the same time RPC was proposed, de Larrard [34] employed optimized particle-packing and used a special selection of fine and ultrafine particles to develop a low porosity, high durability, and self-compacting concrete. The optimized particle-packing was theorized to be the reason behind the material's high compressive strength and durability.

Combining concepts from DSP and RPC, early versions of ultrahigh performance concrete (UHPC) were based on the ideas of eliminating coarse aggregates and optimizing particle packing density. They also required special mixing techniques and the application of heat, steam or pressure treatment before and during setting. These onerous requirements, which substantially increased cost, hindered the broad adoption of UHPC by industry, especially for field applications. Subsequent research since then has focused on eliminating these requirements, with many

successes reported [4,35]. These successes have enabled a multitude of UHPC applications in Europe [36], North America [37-41], and Malaysia [42-44]. The following sections review previous research on selection of raw materials, evolution of mixing methods and their influence on the microstructural characteristics, mechanical properties, and durability of UHPC.

2.2. Material Constituents

UHPC formulations are usually composed of ordinary Portland cement, fine aggregates, supplemental materials, high-range water-reducing admixture (HRWR), and steel fibers. [38]. The combination of these ingredients creates a dense packing matrix that increases the rheology and mechanical properties of the UHPC.

2.2.1 Portland Cement

Previous studies [26,45] have shown that cement for UHPC should have a low alkali content and low to medium fineness. To facilitate strength development, cement with a higher total content of tricalcium citrate (C_3S) and dicalcium citrate (C_2S) were usually selected. Tricalcium citrate (C_3S) rapidly hardens and is primarily responsible for initial set and early strength. In general, the early strength of Portland cement concrete grows with an increase in the C_3S content. Dicalcium citrate (C_2S) hardens more slowly, but contributes significantly to strength at ages beyond 7 days. Tricalcium aluminate (C_3A) provides a rapid hydration reaction and increases with the surface area of the particles. This leads to higher water demand and greater viscosity, which makes it challenging to reduce the w/c ratio. Sakai et al. [46] suggested that the use of cement with

<8% of tricalcium aluminate (C_3A) is preferred due to its low heat of hydration and delayed setting time.

Various types of Portland cement have been used in the manufacturing of UHPC. However, ASTM Types I/II and IV (ASTM C150/C150M-17) [47] cement are the most widely used and recommended by researchers [45,48,49]. White Portland cement is also recommended due to its moderate C_3A content and very high value of C_2S+C_3S [26,45]. The disadvantage of using white cement in UHPC mix designs is that it is expensive, costing about 2.5 times the price of ordinary Portland cement [26].

2.2.2 Aggregates

The coarse and fine aggregates used in traditional concrete form an internal skeleton that helps support external loads. To: 1) avoid the limitations of the strength of coarse aggregate, 2) overcome the inherent weakness between coarse aggregate and matrix, and 3) increase homogeneity and eliminate stress concentration at the contact points between aggregates, UHPC typically includes only fine aggregates or refined aggregates. Early trials to develop UHPC used silica sand with a diameter of 0.016 in (400 μm) [33] in an attempt to significantly decrease the size of micro-cracks in UHPC. Wille et al. [4] investigated the bulk density of various mixtures of two type of sands to optimize their proportion. The two sands had mean diameters of 0.0039 in (110 μm) and 0.02 in (500 μm) respectively. An optimum content of finer sand ranging between 30% and 50% was noted. While partially replacing coarse sand with finer sand resulted in a higher bulk density, it also increased the demand for water due to the larger surface area of the smaller particles of the fine sand.

Recent studies have shown that UHPCs containing an appropriate type and content of coarse aggregates have certain advantages [45,48]. For example, Wille [35] noted that UHPC that included coarse aggregate with a maximum grain size ranging from 0.27 to 0.63 inch (7 to 16 mm) showed a slightly higher compressive strength of 25.8 ksi (178 MPa), on average, compared to its counterpart with only fine aggregate, which reached a strength of 23.5 ksi (162 MPa). Rozalija et al. [51] reported that concrete containing basalt aggregate had higher mechanical properties than concrete containing limestone, which is mainly caused by the inherent strength of basalt. Ma et al. [52] reported that adding coarse aggregates was observed to increase the elastic modulus and change the workability of UHPC, as well as reducing its costs. Some researcher reported that UHPC that utilized coarse aggregates exhibited reduced autogenous shrinkage compared to mixes with only fine aggregates [53,54].

2.2.3 Supplemental Materials

Adding supplementary cementitious materials to a UHPC formulation has two advantages. First, they provide secondary pozzolanic reaction and convert calcium hydroxide (CH) into a calcium-silicate-hydrate (C-S-H) gel, which increases the compactness of the microstructure. Second, due to their fineness, supplementary materials fill the voids of concrete mixtures, reducing porosity and enhancing the mechanical and durability properties of the hardened concrete. Commonly used supplementary materials are silica fume, glass powder, fly ash, ground granulated blast-furnace slag (GGBS), and lime powder.

Most UHPCs contain silica fume, which is a byproduct of producing silicon metal or ferrosilicon alloys. Silica fume has a typical median particle size of 0.2 to 1 microns and is widely considered to be a key component of UHPC. Richard et al. [32,33] showed that the optimal content

of silica fume in UHPC should be about 25% of Portland cement. Chan [55] demonstrated that the best silica fume content is between 20% and 30% in terms of bonding properties between steel fibers and the surrounding matrix. However, the cost of silica fume is relatively high and its variable carbon content can adversely affect the fluidity of fresh UHPC. It has been shown in different studies that ground granulated blast furnace slag (GGBS), fly ash, metakaolin, and limestone powder, etc., can also be used to replace silica fume in UHPC [26,39, 45].

Granulated blast furnace slag (GGBS) has been used as a supplemental cementitious material in concrete technology for many years. GGBS is a by-product material obtained from the production of blast furnace pig iron and is composed of a mixture of iron ore soil components and limestone flux. GGBS has pozzolanic properties and is therefore a beneficial addition from that perspective. It also reduces porosity, the pores become finer, and the mineralogical change of the cement hydrate leads to a decrease in the mobility of chloride ions [56]. Yazici [57] prepared RPC with Portland cement replaced with 20%, 40%, and 60% GGBS. The compressive strength of RPC with high volume GGBS exceeded 36.3 ksi (250 MPa) after autoclaving treatment. When external pressure was applied during setting, the compressive strength could reach 58 ksi (400 MPa). It was further noted that the amount of silica fume could be decreased by increasing the amount of GGBS. Oner et al. [58] reached the same conclusion and further pointed out that after an optimum point, at around 55% of the total binder content, the addition of GGBS does not improve compressive strength. They also observed that the pozzolanic reaction is relatively slow and depends on the calcium hydroxide availability. Therefore strength gain is typically slower for UHPC with GGBS compared to regular UHPC.

2.2.4 Superplasticizer

The use of polycarboxylate-based high range water reducer (HRWR), also known as superplasticizer, in UHPC mixture design can significantly improve the rheological properties of cementitious suspensions. They can have a great influence on the kinetics and solidification characteristics of the cement hydration system. The rheological properties of fresh cementitious paste are controlled by many factors, for example by the dispersion characteristics between particles due to the mixing technique, amount of HRWR added, type of hydration products, particle packing determined by particle size distribution etc. In addition, laboratory experiments have shown that the rheological properties of certain types of cement are more sensitive to the type and amount of HRWR used [46,59,60].

Li et al. [59] showed that the dispersion ability of HRWR is determined by its chemical structure. They showed that the fluidity of the cementitious paste is exponentially related to the HRWR dosages. They also noted that the fluid retaining capacity of UHPC is sensitive to the ratio of water-to-powder and that further addition of HRWR does not increase flowability after a saturation dosage is reached. Hirschi et al. [60] studied the effect of eight polycarboxylate based HRWRs on the fresh and hardening properties of UHPC. They showed that using different HRWRs resulted in a noticeable change in setting time and that that was an excellent indicator of early strength development. The addition of HRWR also affected the processability of fresh UHPCs. Gradual additions significantly increased the dispersion of HRWR and increased the mobility of UHPC compared to a direct addition. This observation is supported by research in Wille [4,45] and Graybeal [61].

In the predecessor MDOT study [5], HRWR was used in the amount of 1.35% by weight of cement. However, because of it is sensitivity to the composition of silica fume and the activity

of cement [62], this particular dosage is not necessarily optimal when the component materials are sourced from different suppliers or their relative proportions change.

2.3. Mixing procedure

The mixing procedure is more complicated for UHPC mixtures than for conventional concrete. When preparing UHPC, careful consideration should be given to the mixing time, mixing speed, temperature, and mixing sequence to achieve the anticipated performance [63]. Different researchers have adopted various mixing protocols to achieve a homogeneous mixture. Wille et al. [35] and Alkaysi [6] mixed all dry ingredients first before adding water and HRWR. Graybeal [61] studied the influence of HRWR addition time on the properties of fresh UHPC. The HRWR was added to the UHPC in two different ways: direct addition and stepwise addition. An enhancement in dispersion and flowability was observed with the latter process. Hiremath et al. [64] indicated that improved mixing techniques are beneficial in enhancing the fresh and hardened properties of UHPC. However, as the mixing speed and duration increase, the percentage of pores in the RPC also increases, resulting in reduced fresh and hardened properties.

Pan mixers with high energy/high shear capacity have proved useful for mixing UHPC. Such mixers generally have a rotating blade that scrapes the material attached to the wall and bottom of the pan during mixing and therefore produce consistent results. However, pan mixers have a number of limitations. Among them is that they are not well suited for field construction because they require greater input energy than regular mixers. Their volume is also typically small, limiting the supply of UHPC. They also tend to cause the UHPC load to overheat, although that can be alleviated by modifying the mixing sequence.

Low shear mixers, such as rotating drum mixers, are not preferred for UHPC as they typically produce inconsistent mix quality. Rotating drum mixers have blades fixed to the interior, and the drum is rotated, often at an incline. Inconsistencies in mix quality can result in clumps of unmixed dry materials in the mixture. These inconsistencies can be mitigated by using more specialized mixing procedures, such as the half batch method used by Hale et al. [65]. In this procedure, half the mix is batched and mixed completely before the other half of the mix is added and mixed. Fibers are added once the entire mix becomes workable. A common ready-mix truck is not preferred for UHPC, either, because it can also result in clumps of unmixed dry materials [65].

The entrained air volume plays an important role in the quality control of the mix and its performance level. Due to these unfavorable effects, researchers have shown interest in methods to reduce the number of air bubbles. One possibility is mixing the UHPC under a reduced air pressure as demonstrated in [66].

3. DEVELOPMENT OF NONPROPRIETARY UHPC MIXTURES

In a project funded by MDOT, El-Tawil et al. [5] investigated the performance of several non-proprietary UHPC mix designs with a focus on minimizing cost. The study investigated the compressive and tensile characteristics of the hardened mixes as well as their resistance to freeze-thaw and chloride ion penetration. The experimental variables included four different quantities of silica fume, three different quantities of silica powder, three different cement types (white cement Type I, Portland cement Type V, GGBS/Portland cement Type I blend) and three different fiber volume contents (0.5%, 1.0%, and 1.5%) of straight, smooth, high strength steel fibers. The experimental results revealed that material behavior is mostly insensitive to silica powder quantity, suggesting that silica powder could be removed from the formula due to its high cost. It was also shown that UHPCs containing white cement Type I exhibited the best performance in almost all aspects of behavior including load carrying capacity, energy absorption capacity and multiple cracking behavior. However, white cement is expensive and raised the overall cost. It was therefore replaced with a mixture of ordinary Portland Type I cement and ground granulated blast slag (GGBS), which was substantially cheaper and yet still gave good performance. Building upon these results, this chapter discusses the feasibility of using locally-sourced generic ingredients with an eye towards large-scale field blending. The chapter also discusses the effect of mixing processes and variables on the fresh and hardened characteristics of UHPC.

3.1. Component selection

The ingredients investigated in this project include three types of ordinary Portland Type I cement, GGBS with two different slag activity levels, silica sands, three types of silica fumes, and

three types of superplasticizers. Steel fibers with two different aspect ratios were also investigated as well as replacing steel fibers with polyethylene fibers.

3.1.1. Cement

White Portland Type I cement was used in the initial development of UHPC [4] due to its low tricalcium aluminate (C_3A) and the high combination of di- and tricalcium silicate (C2S+C3S) resulting in exceptional performance in the fresh and hardened states. However, white cement is expensive (at $275 per ton). Research in [5,6] has shown that ordinary Portland cement Type I, which is much cheaper (at $150 per ton), can be successfully used. Cement with high C_3A tends to produce higher heat of hydration, resulting in lower performance of the HRWR. In general, the selected cement must have a tricalcium aluminate (C_3A) content lower than 8% and a relatively low Blaine fineness to reduce water demand during the hydration. Many suppliers in the US can meet this requirement.

Portland Type I cement is available from several major US supplier. The various blends balance the requirements of low alkali content, low to medium fineness, and low tricalcium aluminate (C_3A) content. Three types of Type I or II ordinary Portland cements were selected as shown in Table 3-1, where ST is sourced from St. Marys Cement, LA from LaFargeHolcim, and LE from Lehigh Cement Company, a division of Lehigh Hanson Inc.

The properties of the selected cements are presented in Table 3-1. The LE cement has a substantially higher C_3A than the others two, and as such, was selected to investigate the effect of C_3A on UHPC performance. In order to evaluate the average 28-day strength, mortar cubes were made from the various cements in accordance with ASTM C109 [67]. The proportion of cement,

standard sand, and water used in the test was 1:2.75:0.46. The result is shown in Table 3-1. The strengths lie within a 16% range.

Table 3-1 Physical and chemical properties of cement

Name	Type	C_2S %	C_3S %	$C_2S + C_3S$ %	C_3A %	C_4AF %	Blaine m^2/kg	Loss on ignition (%)	>45 μm, %	Avg. 28-day $f'_{c,N}$ MPa (ksi)
ST	St. Mary OPC I/II	19	51	70	7	9	382	2.0	2.8	43.3 (6.3)
LA	LaFarge OPC_I	13	58	71	7	9	374	2.1	1.7	39.9 (5.8)
LE	Lehigh OPC_I	8.5	62	70.5	9.4	6.5	421	2.9	4.8	46.2 (6.7)

3.1.2. GGBS

Unlike regular concrete, UHPC uses a lot of cement, which increases costs and has environmental and ecological burden. It also has a negative impact on the hydration heat, which can lead to shrinkage problems. Therefore, ground granulated blast slag (GGBS) cement is added to make the mixes more environmentally friendly since GGBS is a byproduct of the steel making industry. GGBS is a beneficial mineral mixture for concrete because of its pozzolanic property [57] and is known to positively affect the durability of concrete materials [57].

According to ASTM [68], GGBS is classified by its performance in the slag activity test. There are three grades, namely Grades 80, 100, and 120. Currently, Grades 100 and 120 are commonly available on the U.S. market. These two grades of GGBS were used in mortar mixes

with a ratio of cement:GGBS:standard-sand:water ratio of 0.5:0.5:2.75:0.46, whose fresh and hardened performance parameters were evaluated. Table 3-2 summarizes the properties of mortar mixes with the two grades of GGBS. The cement mortar uses LA cement. Its mortar strength is 5.8 ksi (39.9 MPa) and serves as the reference strength. Using that number, the activity indices of G1 and G2 are 103% and 125%, respectively (Figure 3-1).

The workability of a UHPC mixture can be substantially increased by partial replacement of Portland cement with GGBS. Mix flowability increases with the grade of GGBS because the material becomes finer as its grade increases. For example, Grade 120 GGBS particles are smaller than their Grade 100 counterpart (Blaine fineness of 5720 cm^2/g versus 5510 cm^2/g, respectively). The uniformly spherical particles of GGBS also facilitate the flow of the paste and result in a larger spread value. As shown in Table 3-2, the strength difference between both types of GGBS mortars is modest (6.0 ksi for G1 versus 7.3 ksi for G2).

Table 3-2 Properties of GGBS mortar mixes

Name	Type	Blaine m^2/kg	>45 μm, %	Avg. strength MPa (ksi)	
G1	GR100	551	0.6	41.1 (6.0)	St. Mary Cement
G2	GR120	572	0.4	50.0 (7.3)	LafargeHolcim

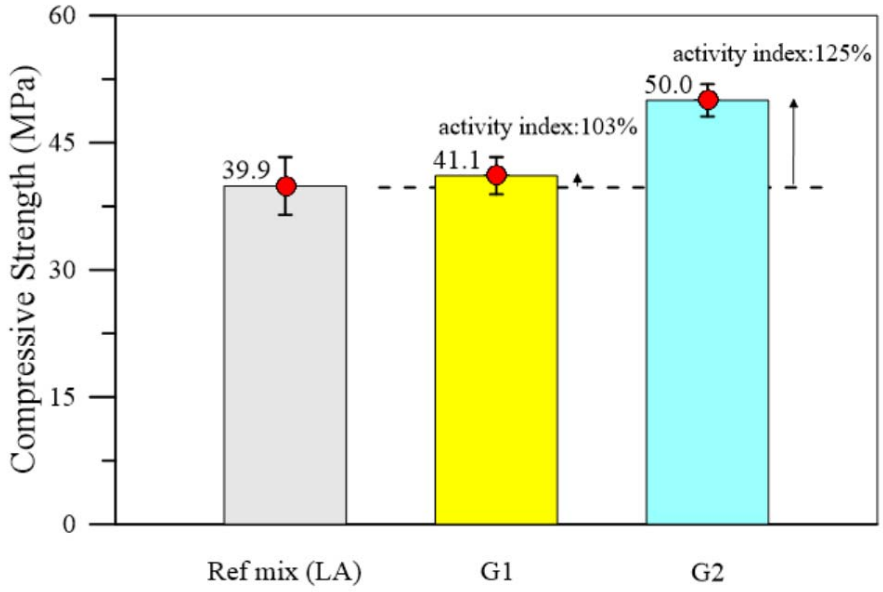

Figure 3-1 GGBS activity test results

3.1.3. Silica fume

The superfine spherical particles and pozzolanic reactivity of silica fume densify the microstructure and significantly improve the compressive strength of UHPC. The median particle size is in the range of 0.1 to 10 microns. In general, a lower carbon content is preferred because that decreases the water demand while promoting high flowability.

Three types of undensified silica fume were selected for investigation (Figure 3-2). The first (EL) was selected because it had a low carbon content. The second (NC) had a relatively high carbon content. Choosing a material with higher carbon content was deliberate to see if UHPC could be successfully mixed with such a component. The third material (WM) had a high zirconium dioxide content. According to [69], zirconium dioxide improves the flowability of the UHPC mixture compared to ordinary silica fume because it has a coarser particle size, although it

is still smaller than the cement particles. The chemical and physical properties of the silica fumes used in this project are given in Table 3-3.

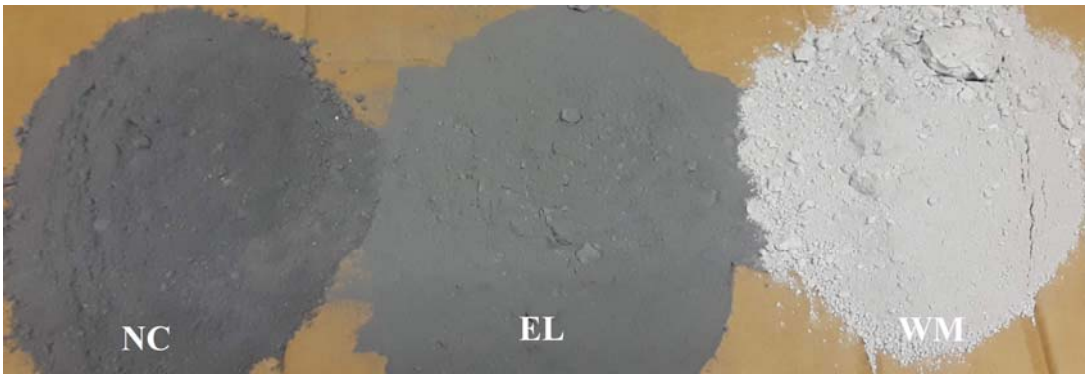

Figure 3-2 Color of silica fume

Table 3-3 Properties of silica fume

Name	Source	Appearance	SiO_2 %	C %	ZrO_2 %	SO_3 %	Na_2O %	K_2O %	Bulk Density (kg/m^3)	Median particle size (μm)
EL	Elkem	Gray	96.9	0.5	/	0.2	0.2	0.3	322	0.5
NC	Norchem	Dark gray	93.47	<6	/	/	<2	<2	225	1.73%
WM	Washington Mills (Zirconium silica fume)	Grayish white	>86	1.9	10	/	/	/	208	6

3.1.4. Silica Sands

Eliminating the coarse aggregate promotes high compressive strength. Therefore, instead of coarse aggregate, two types of quartz silica sand, with grain sizes of 80–200 μm and 400–800

μm were used (see Figure 3-3), named Sand A and Sand B, respectively. The two sands are blended in such a way to maximize the packing density. Wille et al [4] suggested that the optimal content of Sand A is 30-50%. Although the partial replacement of Sand B with Sand A results in a higher bulk density, due to the larger surface area of the smaller particles of sand A, the demand for water also increases. Therefore, in order to maintain proper spread and not compromise compressive strength, the ratio of Sand A to Sand B is selected to be 0.25 in this research.

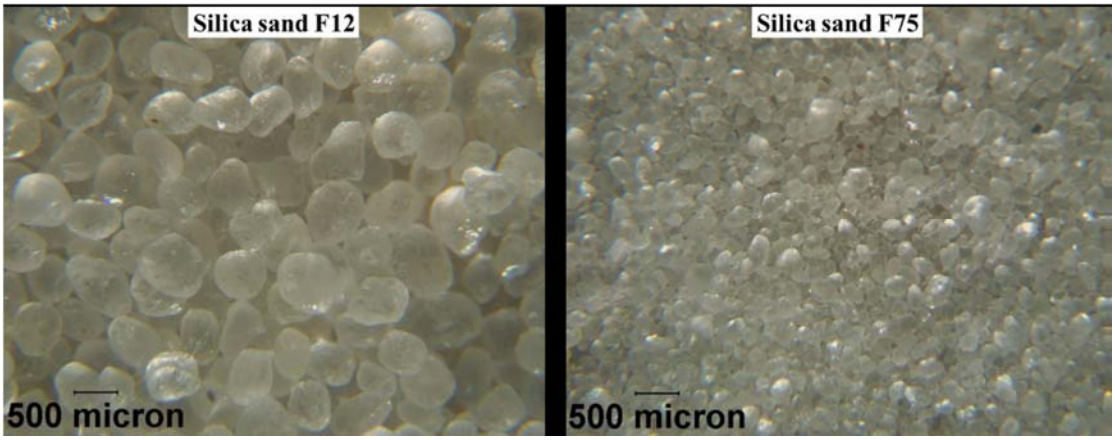

Figure 3-3 The silica sands used for the preparation of UHPC

3.1.5. High Range Water Reducers (HRWRs)

HRWRs have great influence on the fresh properties of concrete. The use of an appropriate amount of HRWR can reduce macro porosity because it makes the paste more flowable and easier to compact. An insufficient HRWR dosage would make UHPC compaction difficult and lead to a high level of porosity. On the other hand, excess HRWR dosage can cause chemical incompatibility issues and fibers segregation, resulting in non-uniform mixing or higher porosity. Moreover, the water-reducing effect is sensitive to the particle size and chemical composition of

the powder material. For this research, the most effective HRWR was determined to be a polycarboxylate-based superplasticizer. Three different HRWRs sourced from a variety of suppliers were used in the preliminary test mix design (Table 3-4).

Table 3-4 High range water reducer

Name	Type	Supplier
H1	ViscoCrete 2100	Sika
H2	Plastol 6400	Euclid
H3	ADVA Cast 575	GCP Applied Technologies

3.1.6. Fibers

The use of fibers enhances the mechanical performance of UHPC in terms of tensile strength, ductility, energy dissipation capacity, crack spacing and crack width. Their effect is dependent on the fiber material and strength, the bond between matrix and fiber, the fiber aspect ratio and the fiber volume fraction. In order to investigate the influence of these factors, two types of high strength straight steel fibers (Figure 3-4 (a) and (b)) were selected along with a high modulus polypropylene fiber (Figure 3-4 (c)). The fiber geometries and properties are summarized in Table 3-5.

Table 3-5 Properties of fibers

Fiber type	Density pound/in^3 (g/cc)	Diameter (d_f) inch (mm)	Length (l_f) inch (mm)	Modulus ksi (GPa)	Strength ksi (MPa)	Aspect ratio l_f / d_f	Supplier
Short steel fiber (F13)	0.28 (7.8)	0.008 (0.2)	0.5 (13)	30457 (210)	415 (2860)	65	Nycon
Long steel fiber (F19)	0.28 (7.8)	0.008 (0.2)	0.75 (19)	30457 (210)	285 (1965)	95	S. Korean
Polyethylene fiber (PF)	0.035 (0.97)	---	---	11457 (79)	379 (2610)	---	Honeywell

(a) Short Steel fiber (F13) (b) Long Steel fiber (F19) (c) Polyethylene fiber (PF)

Figure 3-4 Types of fibers used for this project

3.2. Particle Size Distribution and Packing Density Models

Packing theory is the basic method used for developing dense concrete using different sized particles. Proper application of packing theory can control the fresh and hardened properties of concrete because the improved particulate packing leads to more usable water as a lubricant. The

Andreasen and Andersen (A&A) model is commonly used [70] to design UHPC with various solid constituents and high fluidity. According to A&A theory, optimal packaging can be achieved when the cumulative particle size distribution (PSD) obeys the following equation:

$$\boldsymbol{P(D)(\%) = \left(\frac{D}{D_{max}}\right)^{q} \times 100\%} \qquad \textbf{Equation 3.1}$$

where, $P(D)$ is the fraction that can pass a sieve with opening D; D_{max} is the maximum particle size of the mix. The distribution modulus q has a value between 0 and 1. The Andreasen and Andersen model doesn't contain the minimum particle size. To account for that, a modified version of A&A model was suggested by Funk and Dinger [71] as follows:

$$\boldsymbol{P(D)(\%) = \left(\frac{D^{q} - D_{min}^{q}}{D_{max}^{q} - D_{min}^{q}}\right) \times 100\%} \qquad \textbf{Equation 3.2}$$

where, D_{min} accounts for the minimum particle size in the mix. Andreasen and Andersen found that optimum packing is obtained when q = 0.37. However, for mixtures with a high amount of powders (<250 μm), a smaller q value is recommended [72,73]. Hunger [74] suggested q values in the range of 0.22~0.25 for self-consolidating concrete.

The particle size distributions (PSD) of the various UHPC components listed above are graphically depicted in Figure 3-5 and Figure 3-6 based on the gradation tables given for each ingredient. The gradation curves based on A&A and the modified A&A are also shown in both figures. The figures show that the PSDs for the different slags and silica fumes combinations fit well between the modified A&A curves for q = 0.37 and 0.22. Figure 3-6 shows that the gradation curve of the modified A&A better accounts for powders than the gradation curve of Andreasen and Andersen.

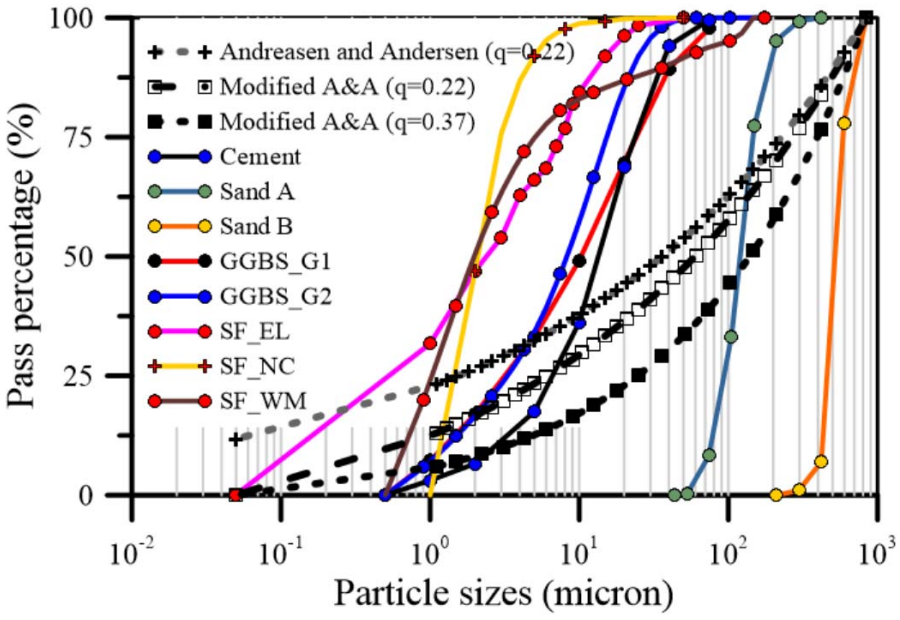

Figure 3-5 Particle size distributions of solid materials used in this project

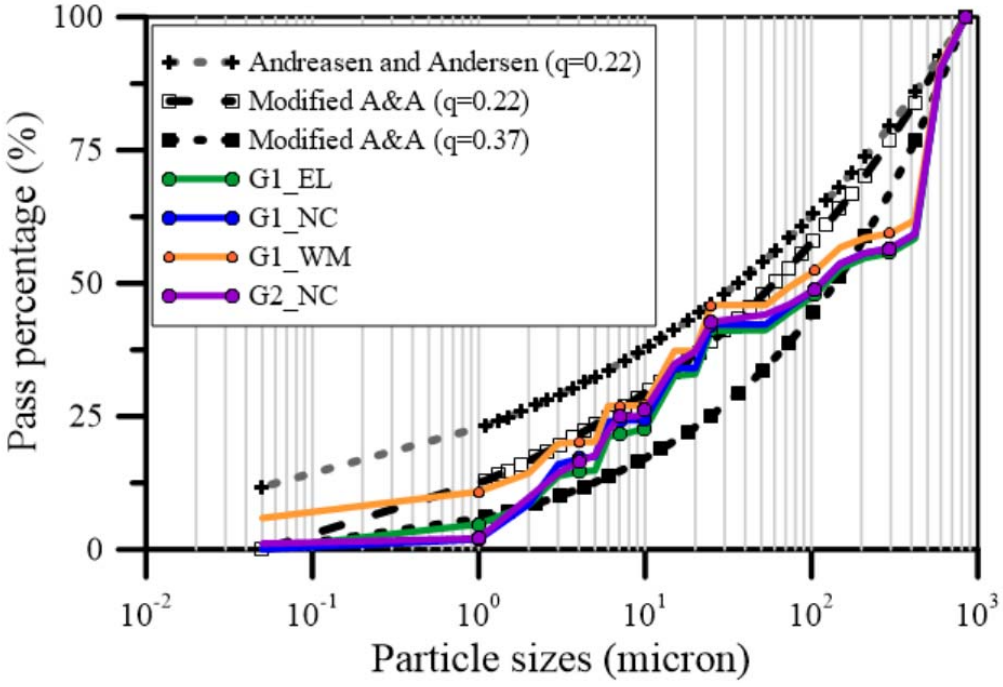

Figure 3-6 Analysis of actual particle size distributions of particles in the different mixes with the modified A&A model.

3.3. Effect of Mixing Speed

Conventional concrete is generally easy to mix using commonly available mixers and can be conveniently adapted to most construction conditions. However, mixing UHPC requires equipment that provides more energy and shear than regular concrete due to the low water content and high powder content (<75 um). In general, the expected performance (including fresh and hard-solid properties) of the selected mixture cannot be achieved when low-mix energy mixers are used to mix UHPC. Moreover, use of a low-energy mixer will also increase the turnover time of the mixture, causing the temperature of the mix to rise, which is detrimental to the UHPC mixing process (high temperature delays mix turnover).

A pan mixer is generally used to mix UHPC in the laboratory. Different paddle speeds and mixing volumes can be used for producing UHPC. To develop an appropriate UHPC mixing scheme that produces a homogeneous mixture, Hobart mixers with three different volumes (5, 12 and 30 quarts, see Table 3-6) were used to investigate the effect of mixing size on UHPC properties. The mix design in Table 3-7 is used and two different mixing procedures were evaluated.

The first mixing procedure is the standard one used in [5]. That mix procedure involved mixing at 2nd speed for 3-minutes after turnover. In the second mixing procedure, slower 1st-speed mixing was used throughout the mixing process. A slower speed was investigated because field mixers do not run as fast as the smaller lab ones. The measured fresh mortar parameters include spread and turnover time. The main purpose of the study was to investigate whether the turnover time is related to the energy input of the mixer delivered through the paddle.

The test results are shown in Table 3-8. It is clear that using 2nd-speed mixing leads to a shorter turnover time and increased spread. For example, in the case of the 30-qurt mixer, faster mixing resulted in 11.1 inch (283 mm) spread versus 9.9 inch (251 mm) at slower speed. The turnover time was also substantially less (0.5 minutes versus 2.33 minutes, respectively). Based on the assumption that the energy input to the mix is related to the turnover time and the agitator speed, an efficiency factor (multiplication of the turnover time by the agitator speed) is proposed and plotted in Figure 3-7. Although no clear trend emerged regarding the efficiency factor, it is obvious that the turnover time drops with increasing mix size.

Insufficient mix energy can result in improper water distribution throughout the mixture. In particular, it is difficult to break down the lumps formed during the mixing process. These unbroken lumps hoard water and HRWR, depriving other particles of their share of moisture and HRWR. Based on the observation from this study, it appears that the mixer used in this research can achieve uniform mixing of the UHPC mixture for a mix speed of 60 RPM. Although a faster mixing speed (100 RPM for the case of 30-quarts) is more beneficial to spread, a mixing speed of 60 RMP is adopted for mixing in this project.

Table 3-6 Rotational speeds of the three Hobart mixers

	Agitator (RPM)			Paddle (RPM)		
	5-quart	12-quart	30-quart	5-quart	12-quart	30-quart
1st -speed	136	104	94	60	60	54
2nd -speed	281	194	174	124	111	100
3rd -speed	580	353	317	255	203	183

Table 3-7 Mix design of UHPC mortar for three Hobart mixers

Ingredient		Cement	Silica fume	Sand A	Sand B	Water	HRWR
Weight ratio		1	0.25	0.3	1.19	0.24	0.03
Quantity, pound (g)	5-quart	0.8 (360)	0.2 (90)	0.24 (107.5)	0.95 (430)	0.19 (86.4)	0.02 (10.8)
	12-quart	2.2 (1000)	0.55 (250)	0.66 (300)	2.6 (1190)	0.53 (240)	0.07 (30)
	30-quart	5.7 (2600)	1.43 (650)	1.71 (777)	6.8 (3104)	1.38(624)	0.17 (78)

Table 3-8 Spread and turnover time for three different mixers at two different speeds

	5-quart		12-quart		30-quart	
	Spread, inch (mm)	Turnover time, minute	Spread, inch (mm)	Turnover time, minute	Spread, inch (mm)	Turnover time, minute
1st -speed	9.6 (244)	6	9.0 (229)	1.67	9.9 (251)	2.33
2nd -speed	9.8 (248)	1.25	9.6 (244)	1.42	11.1 (283)	0.5

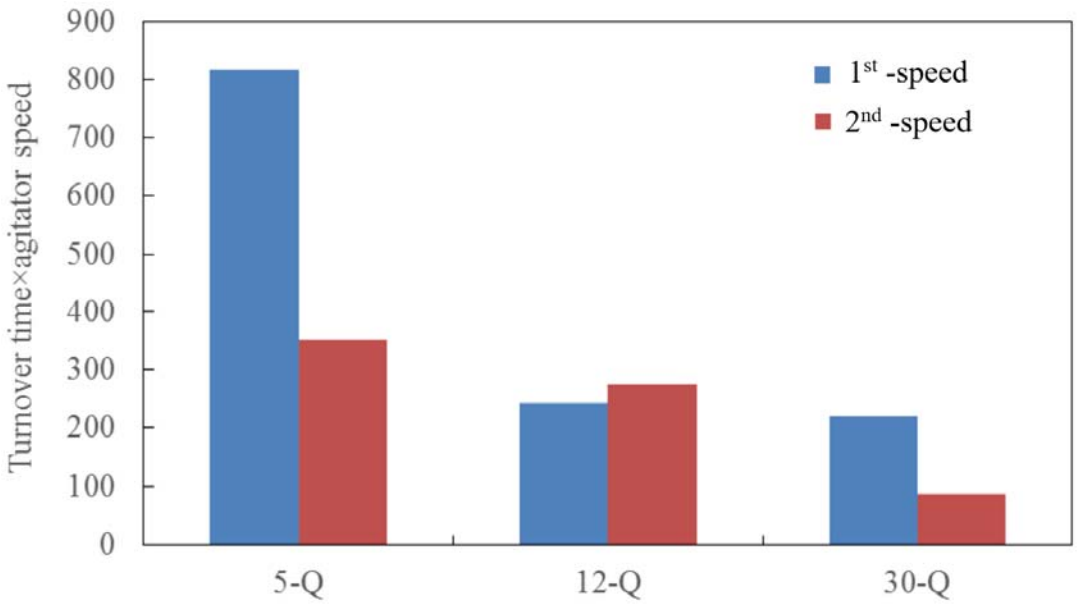

Figure 3-7 Mixer effect on the turnover of UHPC

3.4. Effect of Mixing Protocol

Different researchers have adopted various mixing protocols to achieve homogenization of the UHPC mixture in the shortest time [4, 75-77]. Although specific details of the overall mixing process differed, all researchers were unified in that UHPC components had to be dry mixed prior to adding water and HRWR. The intent of dry mixing is to ensure higher bulk density and lower moisture requirements.

Most of the mixing regimens advocated by other researcher were for lab mixing. However, for field mixing there are two key restrictions that do not apply to lab mixing: (1) Large-capacity mixers used for field construction generally have mixing speeds that are lower than those achievable in smaller lab mixers, (2) The powder materials and silica sands form lumps that can be quite large in field mixing applications, which hinder the mixing process. In order not to

decrease the amount of mixing per batch, and without compromising the fresh and hardened properties after the mixing, the mixing procedure proposed in de Larrard et al [34] is evaluated and compared to the process advocated by El-Tawil et al. [5]. The de Larrard [34] process is as follows:

1. Mix water, silica fume and 33% of superplasticizer till the slurry looks homogenous;
2. Add cement with 50 % of the superplasticizer;
3. Add sand, and mix for 1 min at high speed;
4. Add the residual 17% of superplasticizer and mix for 1 minute at high speed.

The de Larrard [34] procedure has the following two advantages. The addition of a high proportion of water in the initial stage of mixing facilitates the release of sufficient Ca^{2+} ions from the cement particles. These ions are subsequently adsorbed onto the superplasticizer chain, thereby achieving a lower viscosity of the mixture [78]. Mixing only the cement initially reduces the burden on the mixer during the initial phase of the mixture turnover, when viscosity is highest and demand on the mixer is therefore greatest. Due to the presence of the ultrafine particles (silica fume, cement, and GGBS), sufficient shear force is required to break apart the agglomerates during the UHPC mixing process. While the silica sands contribute to such a role, adding them later to reduce the initial burden on the mixer is beneficial from a practical point of view.

Keeping the above discussion in mind, the new mixing process explored in this project is shown schematically in Figure 3-8 and described as follows.

1. Dry mix cement, GGBS, silica fume, and a portion of the silica sands for 5 minutes;
2. Add water and superplasticizer till turnover and formation of thick slurry;
3. Incorporate remaining silica sands gradually and mix another 5 minutes;

4. Add fibers and continue to mix until fluidity is optimized (between 5 and 8 minutes).

The flow test was performed by using a conical mold as shown in Figure 3-9 (a) and discussed later on in the report (see Section 3.2.1). When the mortar ceases spreading (usually within 2 minutes), the base diameter of the mortar is measured from two perpendicular directions (Figure 3-9 (b)) and the average value is used as the flow value (i.e., the spread).

Figure 3-10 shows turnover time and flow of blends with different portions of silica sands. It can be observed that the fresh nature of UHPC is affected by the mixing method. When mixing UHPCs using the original mixing protocol in El-Tawil et al. [5], turnover occurs quickly, usually within two minutes. When the premixed material is free of silica sands, the turnover time exceeds six minutes, which demonstrates the importance of silica sands in facilitating mixing. Particles in the premixed part of the silica sand grind against the powder materials and aid in their dispersion.

Experiments were conducted to evaluate the effect of the portion size of the premixed sands. The premix portion variable ranged from zero to 60%. The test results can be seen in Figure 3-10. A premix amount of 40% resulted in a turnover time of 5 minutes. That reduced to 3 minutes when the premix amount reached 50%-60%. The spread was relatively independent of the premix potion as also shown in Figure 3-10.

Figure 3-11 shows the weight of initial part of the consitutents, which represents the burden on the mixer. For example, the original mixing sequence places 100% burden on the mixer, meaning that all the material is mixed initially. Reducing the premix portion decreases the burden, as explained earlier. As can be seen in Figure 3-11, premixing half of the silica sand reduces the burden on the mixer (weight of mixed components before turnover) by nearly 25%. These results imply that, even though turnover time may be delayed slightly by premixing just half of the silica

sands, the burden on the mixer can be decreased substantially allowing it to mix a larger load. It is therefore recommended that the revised mix protocol be used in the field with only half the silica sands premixed. The success of this mixing methodology in the field is discussed in Chapter 5.

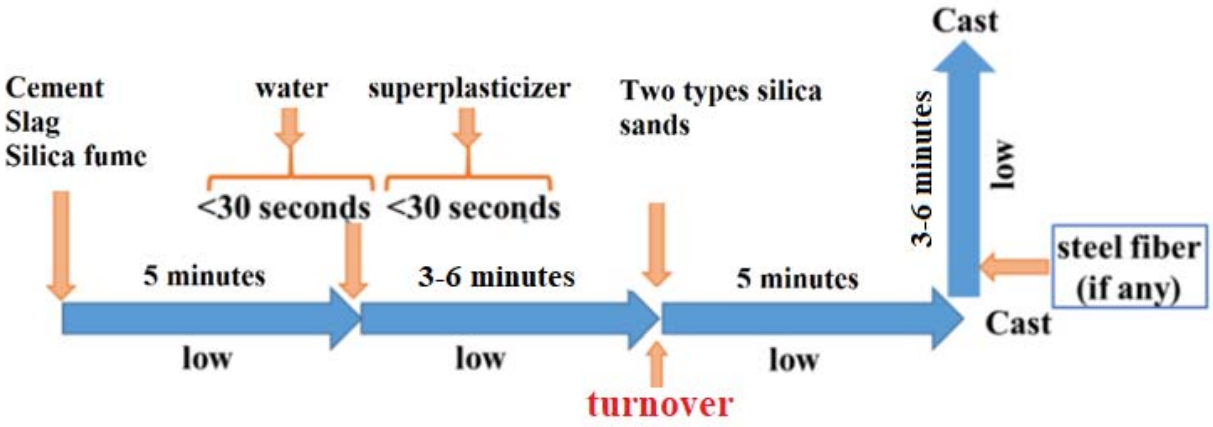

Figure 3-8 The new mixing sequence

(a) The conical mold for flow test [79] (b) Workability of UHPC paste mixed by new procedure

Figure 3-9 Flow test and determination of flow

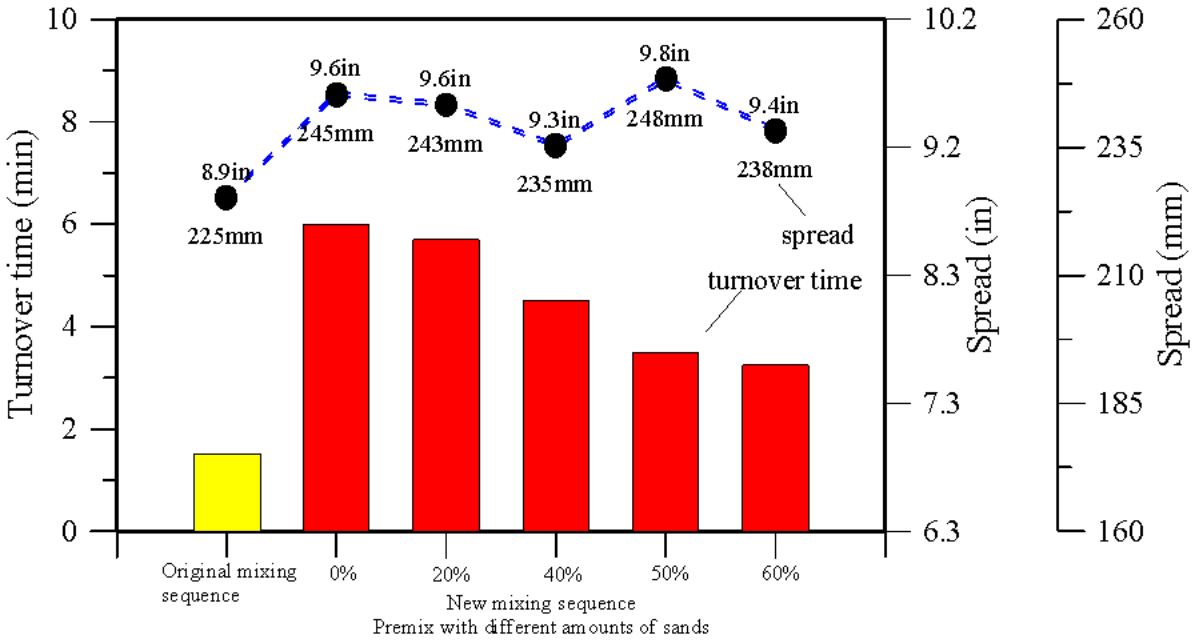

Figure 3-10 Comparison of turnover time and flow of the mixtures with different amounts of premixed silica sands

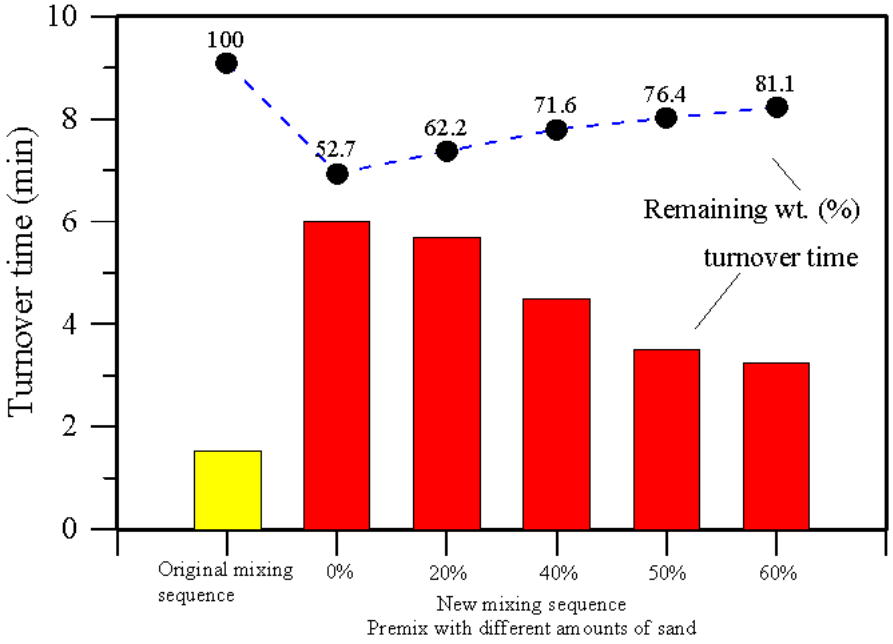

Figure 3-11 The weight variation of mixtures with different amounts of premixed silica sands

4. TEST PROCEDURES AND METHODS

There are no well-established tests to characterize the fresh, hardened and long-term behaviors of high-performance cementitious materials. According to the Federal Highway Administration (FHWA) [38] and ASTM [80], tests used for high-performance cementitious materials are generally similar to those used for conventional concrete or mortar, albeit with some adjustments to accommodate the unique properties of the new materials. This chapter describes the testing processes and practices used in this research.

4.1. Mixing and casting processes

Mixing was discussed in Sections 3.3 and 3.4. After successfully mixing and casting the specimens used in this work, the specimens were covered with plastic sheets for 24 hours, removed from the mold and placed in a temperature-controlled water bath. Compression and tensile tests were performed at different curing ages. For each mixture, at least 3 cube compressive specimens and 5 dog bone tensile specimens were prepared and tested.

4.2. Fresh characteristic and quality control

4.2.1. Flowability

The workability for freshly mixed UHPC was determined by testing the spread value in accordance with ASTM C1437 [81]. After mixing the paste, the fresh mix was placed into a spread cone (refer to Figure 3-9). Special care was taken to keep the spread cone and the base plate at the

same humidity level prior to testing. Due to the inherent high flowability of the paste, there was no need to compact the UHPC in the mold and no vibration was required or used. The spread cone was filled up to the rim and then lifted at a fixed speed. The leftover material sticking to the wall of the cone was scraped off and the material on the base plate was left to spread. After 2 min ± 5 sec had elapsed, the diameter of the spread UHPC paste was measured along two perpendicular directions and the average diameter was calculated and recorded as the spread value.

4.2.2. Setting time

The setting times for UHPC pastes were evaluated by using the Vicat apparatus as outlined in ASTM C191-13 [82] (Figure 4-1). The setting time was tested at room temperature (approximately 22 °C).

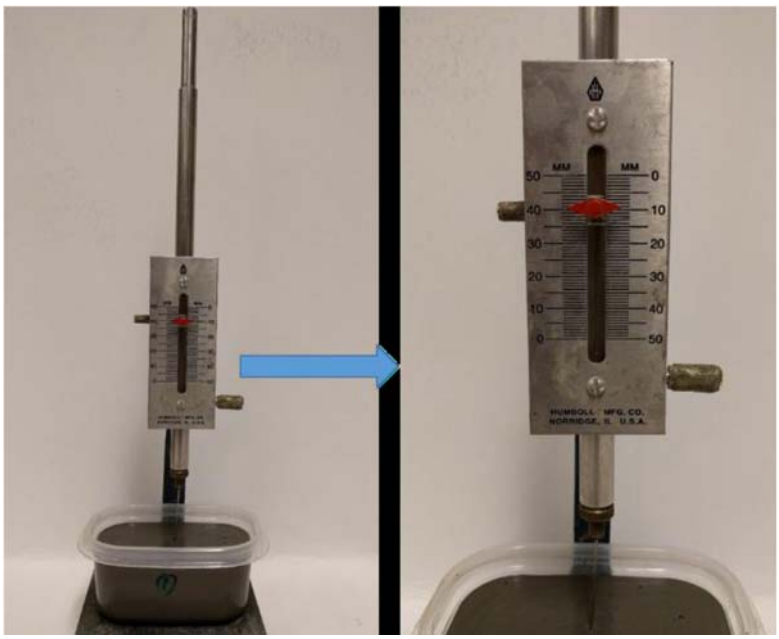

Figure 4-1 Paste penetration resistance test

4.2.3. Hydration heat

One major benefit of GGBS addition in concrete is the reduction of heat generation in the early age when young concrete is prone to cracking. The effect of different amounts of GGBS on the heat of hydration in the initial stage is characterized by the measurement of temperature evolution in a 6 inch x 12 inch (150 mm × 300 mm) cylinder stored in a semi-adiabatic chamber. Right after the freshly mixed mortar sample was cast into the cylindrical mold, it was sealed by a lid with a small hole punctured in the center. Two Type-T thermocouples were inserted halfway into the sample through the hole. The thermocouples were connected to a data acquisition system, from which temperature was monitored every 1 minute.

4.2.4. Ultrasonic pulse velocity

Ultrasonic transit time was measured on 0.2 inch x 6 inch (5mm×150mm) cylinders by a Pundit Plus ultrasonic digital tester with 54 kHz transducers. The ultrasonic pulse velocity (UPV) was then calculated and used as an indicator of strength development. Measurement commenced when specimens gained sufficient strength to be removed from the mold.

4.2.5. Shrinkage

The autogenous shrinkage that occurs in UHPC may cause early cracking due to its very fine pore structure and low water-binder ratio. This can ultimately lead to a serious reduction in the material's performance in terms of strength, appearance, and especially durability. Based on previous studies [83,84], when the amount of cement and/or SF is replaced by GGBS, not only is the heat of hydration reduced, but the autogenous shrinkage also decreases.

Autogenous shrinkage of UHPC was measured on a slender rectangular specimen (2.4 inch × 4 inch × 40 inch [60 × 100 × 1000 mm]) placed in a U-shaped stainless-steel ring, as shown in Figure 4-2. Fresh paste and mortar mixes were stored in a sealed bucket. Double polystyrene films were used to seal the specimen to prevent external drying. Two layers of 0.08 inch (2-mm) thick foam rubber were used to separate the sealed specimens and test rig to minimize friction. The specimens were positioned with one end fixed to the rig and the other end connected to a movable plate in contact with a LVDT with a 0.1 μm resolution. Specimen displacements were measured every 5 min and automatically converted to strain.

Figure 4-2 Autogenous shrinkage measurement

4.3. Hardened UHPC mechanical Properties

All specimens were de-molded 24 hours after casting and then cured in water at room temperature. On the day of testing, the specimens were removed from the water bath and dried in preparation for testing.

4.3.1. Compression testing

The uniaxial compressive strength tests at various ages up to 56 days were carried out on 2 in (50 mm) cubes using a 500 kips capacity servo-hydraulic testing machine as shown in Figure 4-3. The testing procedure was carried out according to ASTM C109/C109M [67]. Due to the ultra-high compressive strength of UHPC, testing under load rates of 50-100 psi/s (0.36-0.72 MPa) in accordance with ASTM C109/C109M means that the test will take much longer than usual. To reduce test time, an accelerated loading rate of 150 – 250 psi/s (1.0 – 1.7 MPa / s) has been shown to have no adverse effects and was used in this research [22]. Three specimens were tested for each age and the average result was reported. As discussed in Alkaysi et al. [26], it was not necessary to grind the loaded surfaces to a specified level of smoothness because the brass molds used ensured sufficient smoothness and parallel loading surfaces.

Figure 4-3 Testing set-up for compression tests of cube specimens

4.3.2. Direct tension testing

For this project, a direct tension test based on AASHTO T 132-87 [86] was chosen to test the specimens. In this test procedure, precast specimens were made and then tested under direct tension. As shown in Figure 4-4, the specimens were supported by plates that ensure anchored and rotation-capable boundary conditions. Each specimen had a gauge length of 3.14 in (80 mm) with a constant cross-sectional area of 1.0 in^2 (25.4 mm^2).

The test procedure started by carefully loading a tensile specimen into the MTS testing machine. A small preload (20% of the matrix cracking strength) was applied to the specimen. The specimen was then manually moved into the best-aligned position to insure uniaxial tension stress. The loading rate was set to 0.003 in/min, which resulted in an estimated strain rate of 1×10^{-4} s^{-1}.

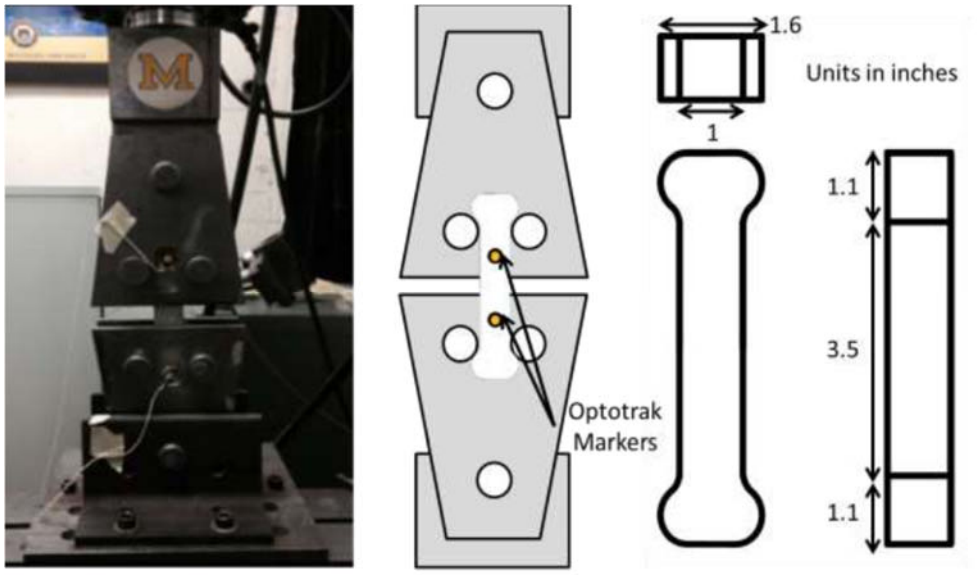

Figure 4-4 Tensile test set up and specimen dimension

4.4. Durability characteristics

The durability properties of the various UHPC mixtures were investigated by evaluating the presence and distribution of air voids, resistance to ingress of chlorides and resistance to freeze-thaw cycling.

4.4.1. Air void analysis

The air void analysis of the concrete was measured by the linear traverse method according to ASTM C457 [87]. The instrument employed is shown in Figure 4-5. Square specimens 4-inches (100 mm) by 4-inches (100 mm) were cut from the mid-depth portion of 6-inch (150 mm) diameter cores with the testing surface parallel to the finishing surface. Specimens were carefully polished with silicon carbide abrasives to obtain a smooth surface with undamaged paste and clearly defined

air voids. Then the point count method was used to determine the fractions of air void, paste and aggregate and the percentage of air voids with infillings. This step provided information on the quality of air void and input to the computation of the spacing factor in the next step. After the point count procedure, the polished surface was pretreated by filling all the air voids with a white powder (barium sulfate) and the rest of the surface was darkened by a permanent marker to produce a sharp contrast (Figure 4-6). Then, the linear traverse method was used to measure the chord length distribution and the total length of the traverse line over air void, based on which, the air void parameters can be calculated. A total of three specimens were tested for each of the material parameters.

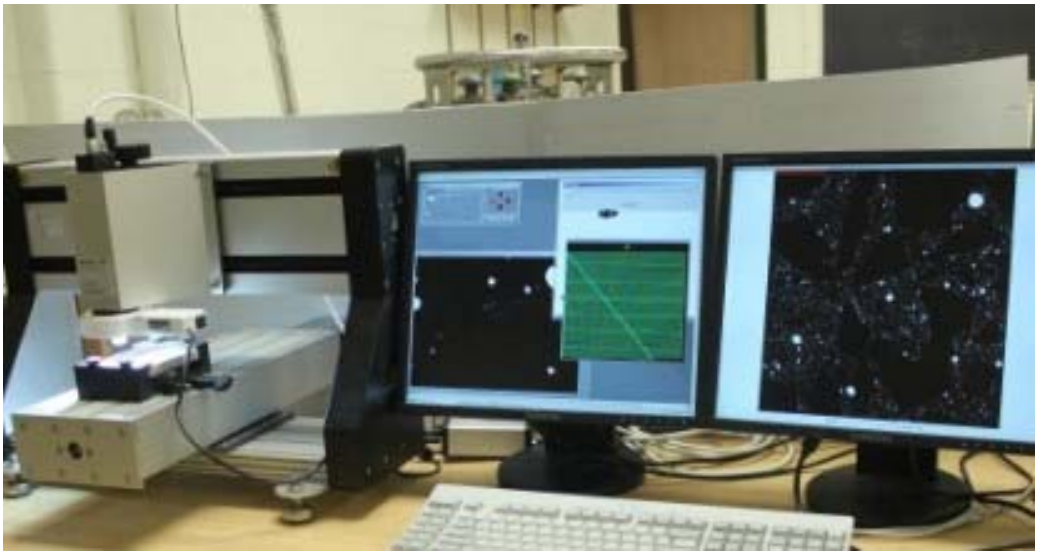

Figure 4-5 Photograph of the linear traverse method point count instrument

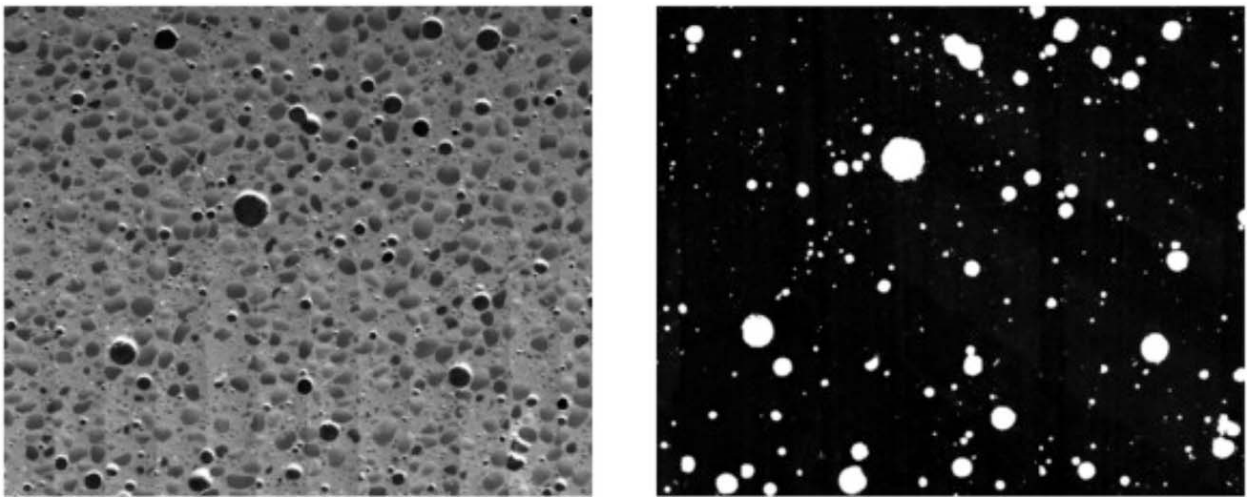

(a) Untreated surface (b) Coated surface

Figure 4-6 Treated and untreated UHPC cross section for air void analysis

4.4.2. Rapid chloride penetration test (RCPT)

A commercially available device, PROOVE'it, was used to evaluate the resistance of concrete to chloride ion ingress. In this approach, chloride ions are forced into a concrete specimen through the introduction of an external voltage on the specimen surface in accordance with the standard test method outlined in ASTM C1202 [88]. The schematic presentation of RCPT is illustrated in Figure 4-7.

Specimens 4-inches (100 mm) in diameter and 2-inches (50 mm) in width were positioned into the measuring cell. Each cell contained a fluid reservoir at each face of the specimen. One reservoir was filled with a sodium chloride solution (3.0% NaCl). The other reservoir was filled with a sodium hydroxide solution (0.3 M NaOH). The reservoir containing the NaCl was connected to a negatively charged terminal, the NaOH reservoir was connected to the positively

charged terminal of the device's microprocessor-controlled power unit. Once started, the test automatically measured the total electrical current passing through the concrete specimen for a standard period of 6 h, with a direct current voltage of 60 V. A total of two specimens were tested for each of investigated parameter.

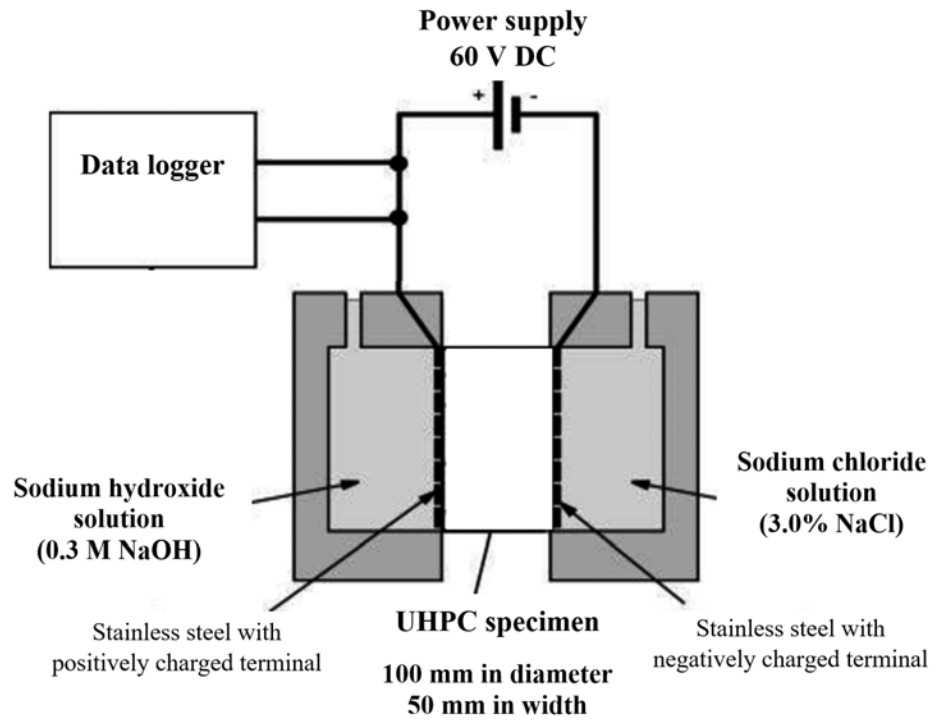

Figure 4-7 Rapid Chloride Permeability test setup

4.4.3. Freeze-thaw resistance

In this study, the RILEM CDF/CIF test equipment was used to perform freeze-thaw resistance procedures. Simultaneously, the UHPC samples were measured for room temperature adsorption and cumulative mass loss under exposure to water (w) and 3% NaCl solution (s). The test

configurations are shown in Figure 4-8. The freeze-thaw test was carried out on UHPC specimens having a thickness of 3 inches (70 mm) and a cross-section of around 4 inches × 4 inches (100 mm×100 mm). An F-T test machine was employed for the concurrent measurement of cumulative mass loss, bulk moisture uptake and internal cracking in the specimens (Figure 4-8). Prior to F-T test, specimens were dried in the oven at 50±2 °C, followed by pre-saturation in de-mineralized water to characterize the capillary absorption process. The preconditioned specimens were placed in the F-T chamber with the bottom surface immersed in a 3% sodium chloride (NaCl) solution while undergoing a specific temperature profile. One F-T cycle is 12 hours with the temperature decreasing from 20 °C to -20 °C and ultimately going back to 20 °C. After 6-8 cycles, measurements were taken when the temperature was brought back to 20 °C, including cumulative moisture uptake based on specimen weight gain, surface scaling based on cumulative mass loss and internal bulk cracking based on variation in the relative dynamic modulus of elasticity (RDM).

(a) Salt frost test machine

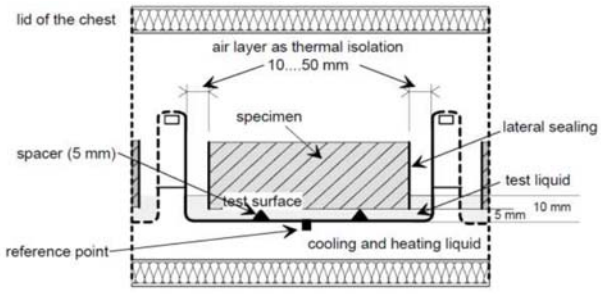

(b) Detailed F-T test close-up

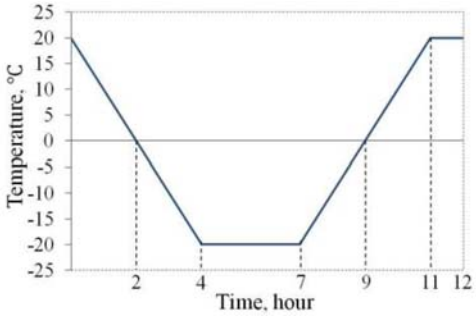

(c) F-T test temperature curve

Figure 4-8 Diagrammatic presentation of the F–T test

5. EXPERIMENTAL RESULTS

A series of test programs were carried out in order to characterize the fresh, short-term and long-term properties of UHPC. The tests were conducted in order to develop the knowledge needed to control the quality of the non-proprietary UHPCs developed in this project, facilitate field mixing, and provide pertinent information for developing a Special Provision for field implementation.

To ensure that the non-proprietary UHPC sought in this research is truly generic, its components were sourced from various suppliers. In particular, the ordinary Portland Type I cement, silica fume and superplasticizer used in the testing were each obtained from three different suppliers to study the effect of material source on the properties of UHPC. Another test variable was the slag activity levels of GGBS (two levels were considered). Of specific interest was the effect of GGBS content on the properties of UHPC. In particular, a key question was how much cement can be replaced by GGBS. Tests conducted to answer this question included workability, heat of hydration, ultrasonic pulse velocity (UPV), autogenous shrinkage and air void distribution. Steel fibers with two different aspect ratios were also investigated as well as replacing steel fibers with polyethylene fibers.

This chapter presents and discusses the extensive test results obtained during the course of this research project. Some test data is presented in Appendices A and B and the developed Special Provision presented in Appendix C.

5.1. Effect of Superplasticizer Source on Spread

The main variable in this section is the superplasticizer source. In previous work [5], the optimum ratio between cement and silica fume was determined to be 1:0.25, with a water to cement (w/c) ratio of 0.22. The previous research had also replaced 50% of the cement with GGBS. These values are used in the research reported in this Section. Studies in this project showed that the most appropriate amount of HRWR is in the 2% to 3% range by weight of the cement to ensure proper workability. With a view towards ensuring feasibility for field applications, the tests conducted in support of this Section use a fixed amount of 3% HRWR. Such a dosage of HRWR could lead to low workability for some combinations of components. For such cases, improvements can be made by adjusting the w/c ratio or increasing the amount of HRWR, although the information in Section 5.1 suggests that the ensuing side effects must be considered. Table 5-1 lists the mixing ratios of the mixtures considered in this Section.

Table 5-1 Mixture proportions by weight

Portland cement	GGBS	Silica fume	HRWR	Silica sand		Steel fiber
				Sand A	Sand B	
0.5	0.5	0.25	0.03	0.30	1.21	0.20 (2% by volume)

The following naming scheme was used to simplify the discussion of the batch test results. The second portion of the name represents the cement supplier used in the mix design, LA for LaFargeHolcim Inc., ST for St. Marys Cement Inc., and LE for Lehigh Hanson Inc. The second

portion of the name represents the silica fume supplier, for example, EL is for the Elkem Inc., WM for Washington Mills Inc., and NC for NorChem Inc. The third portion represents the superplasticizer type, i.e., H1 for ViscoCrete 2100 from Sika Inc., H2 for Plastol 6400 from Euclid Inc., and H3 for ADVA Cast 575 from GCP Inc. For example, LA-EL-H1 indicates a mix comprised of Lafarge cement, Elkem silica fume and HRWR from Sika.

The spread values of the various UHPC mixes were measured in accordance with ASTM C1437 as discussed in Section 4.2.1. The average spread values of the test are shown in Figure 5-1, Figure 5-2, and Figure 5-3. It should be emphasized that all the spread values were obtained by testing under static paste flow as outlined in Section 4.2.1.

Figure 5-1 shows that H1 was quite effective. In particular, all mixes exhibited static flow greater than 7 inches (178 mm). The effectiveness of H3 was not as good as H1, especially when using the NC silica fume, where there is almost no fluidity. This trend was attributed to the high carbon content in NC silica fume, which caused the demand for water to increase during mixing. H2 is almost as good as H1, although mixes with NC silica fume still presented a challenge.

It should be mentioned that UHPC flowability can be adjusted by changing the water usage, adjusting the mixed water temperature [61], or by changing the mixing speed. However, careful consideration should be given to these types of modifications to mix proportions or procedure as they can also affect other properties.

A type of zirconium silica fume (WM) was also adopted in this study because it is known to improve flowability of UHPC mixtures as compared to ordinary silica fume. This is because zirconium silica fume has much larger particle sizes than ordinary silica fumes, although they are

still smaller than Portland cement particles. Figure 5-1 through Figure 5-3 show that the best workability performance occurs for mixtures with WM.

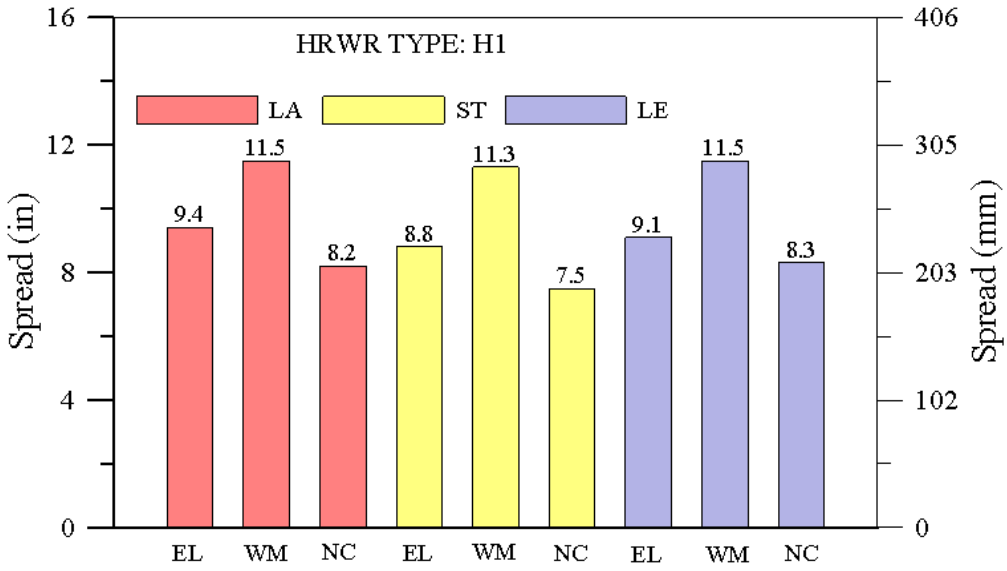

Figure 5-1 The spread of UHPC with H1 and different cement and silica fume combinations

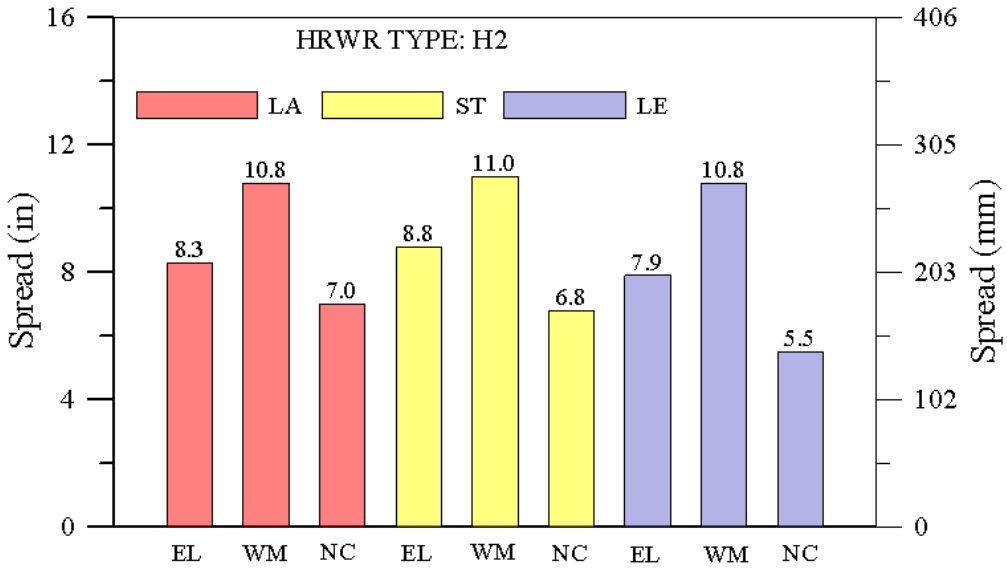

Figure 5-2 The spread of UHPC with H2 and different cement and silica fume combinations

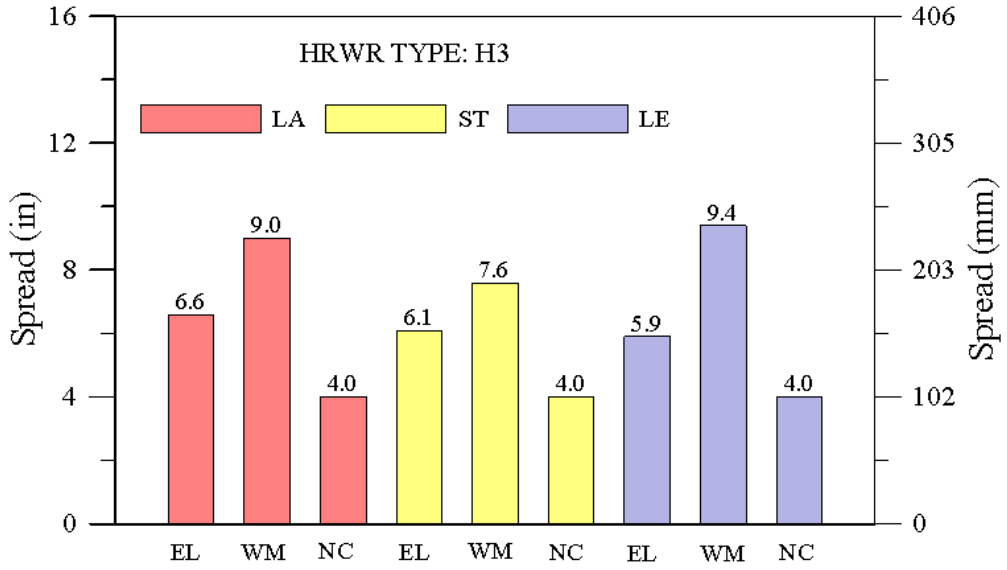

Figure 5-3 The spread of UHPC with H3 and different cement and silica fume combinations

5.2. Effect of GGBS Dosage

As noted earlier, GGBS serves the dual purpose of imparting high resistance to attacks by harmful substances in harsh environments and significantly reducing the heat of hydration. The amount of GGBS used in a cementitious mix influences multiple characteristics of the fresh and hardened product. There is a considerable amount of literature available on the effect of GGBS on the characteristics of regular concrete [89-92]. On the contrary, there is quite little on the effect of GGBS on UHPC properties [26,93]. To address this drawback, this project investigated the role of GGBS on the fresh and hardened properties of UHPC including flowability, setting time, autogenous shrinkage, air voids and strength development. The intent is to identify an optimal amount of Portland cement for replacement with GGBS. The test results reported in this Section are based on the LA-EL-H1 combination. In addition, the GGBS is of G1 grade (see Section 3.1.2). The replacement values considered are 0%, 25%, 50%, and 65%, respectively.

5.2.1. Flowability and air content characteristics

The test techniques used were described in Chapter 4. Flowability testing (see Section 4.2.1) showed that partial replacement of Portland cement with GGBS considerably increased the flowability of UHPC mixes. Figure 5-4 plots the effect of HRWR dosage and GGBS replacement quantity on flowability. Cases are designated XS, where X is the GGBS percent replacement. Hence case 65S indicates that 65% of the Portland cement was replaced with GGBS. The cases considered differentiate between mixes with and without fibers as shown in Figure 5-4.

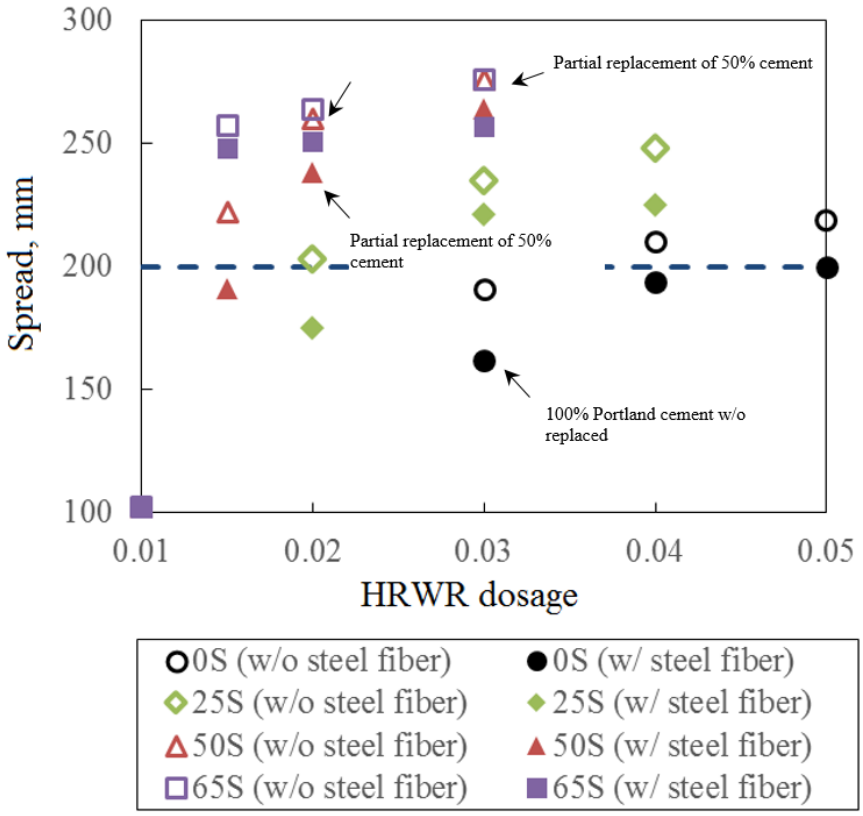

Figure 5-4 Effect of cement replacement by GGBS on the spread of UHPC

Prior research by the PIs has shown that UHPC mixtures with an 8 in (200 mm) spread are considered to be well-suited for the dispersion and casting of mixes with steel fibers. It can be seen from Figure 5-4 that partial replacement of 25% Portland cement with GGBS and 2% HRWR has approximately the same spread as the mix without any GGBS but with 4% HRWR. In other words, replacement of 25% of the Portland cement with GGBS led to a 50% reduction in the required amount of HRWR. This beneficial effect can be partly attributed to the low water absorption and the smooth and dense surface characteristics of the GGBS particles. In addition, when Portland cement is replaced on a mass basis, the paste content is increased because of its lower specific gravity, combined with enhanced cohesiveness. All these factors facilitate particle movement and

thus improve workability. Figure 5-4 shows that there are diminishing returns in terms of flowability when the replacement amount increases beyond 50%. This is particularly clear when the HRWR is 3%.

The air content of UHPC mixtures was measured in the fresh state using the unit weight method and characterized in the hardened state using the linear traverse method. The unit weight method is based on the following equation.

$$\boldsymbol{P_{air} = \frac{\rho_0 - \rho_a}{\rho_0} \times 100\%} \qquad \textbf{Equation 5.1}$$

where the ρ_0 and ρ_a are theoretical density and actual measured densities of the UHPC mixture, respectively.

The analysis of air void characteristics in fresh concrete and in hardened concrete revealed some significant differences. As listed in Table 5-2, the total air content in the hardened concrete seems about 1% lower than the fresh mix as computed by the unit weight method. This is attributed to the slight consolidation employed when making specimens for the linear traverse method, which likely removes some of the larger air bubbles. Regardless of the air content of the mixture in the fresh and hardened mixture, the total amount of air in the fresh and hardened concrete decreases from 5.8% to 4.8, and 4.7% to 3.2%, respectively, with the increase in the amount of replacement GGBS from 0 to 65%. For the fresh air content, it is noted that the addition of steel fibers reduces the air content (see Figure 5-5), which may be attributed to the unique geometry of fibers, which can break up big air bubbles thereby facilitating the de-airing process.

The distribution and content of air voids in concrete can affect durability. Since the liquid water in the voids increases in volume when it is freezes into ice, any unfrozen water is squeezed and discharged from the place where the ice initially formed. This liquid flow generates hydraulic

pressure in the pores, which often results in damage to the concrete. Powers and Willis [94] proposed a spacing factor which is an appropriate way to describe the air void structure. It gives the relationship between the air void content, specific surface and the spacing factor and is calculated as follows.

$$L = \begin{cases} \frac{P}{A} \times \frac{1}{S} & for\ \frac{P}{A} < 4.33 \\ \frac{3}{S}\left(1.4 \cdot \left(\frac{P}{A} + 1\right)^{1/3} - 1\right) & for\ \frac{P}{A} > 4.33 \end{cases} \qquad \textbf{Equation 5.2}$$

where P is the paste content of the mixture; A is the air content, and S is the specific surface in mm^{-1}. The air voids and their total specific surface area can be estimated from the average air void intercept or the chord length obtained from the linear traverse.

The hardened air content and spacing distance are listed in Table 5-2 and Figure 5-6 for UHPC specimens that include different amounts of GGBS. It can be seen from Table 5-2 that the hardened air content decreases from 4.8% to 3.0% as the GGBS replacement amount increases to 50%. The spacing factor is 681 μm while regular concrete has a spacing factor of 116 μm. These values are also consistent with values reported in literature [61]. The spacing factor here refers to the paste-void proximity; i.e. the fraction of paste within some distance of an air void. It provides an approximate representation of the air void structure in the cement paste. The physical reality is that the entrained air void is randomly distributed in the cement paste. In most cases, the inherent approximation of the Powers' spacing factor has been proven to be very good. When the distribution of the air void radius is skewed, or there are a disproportionate number of air voids with small or large radius, the average radius on which the Powers' spacing factor calculation is based does not accurately represent the air void structure in the cement paste.

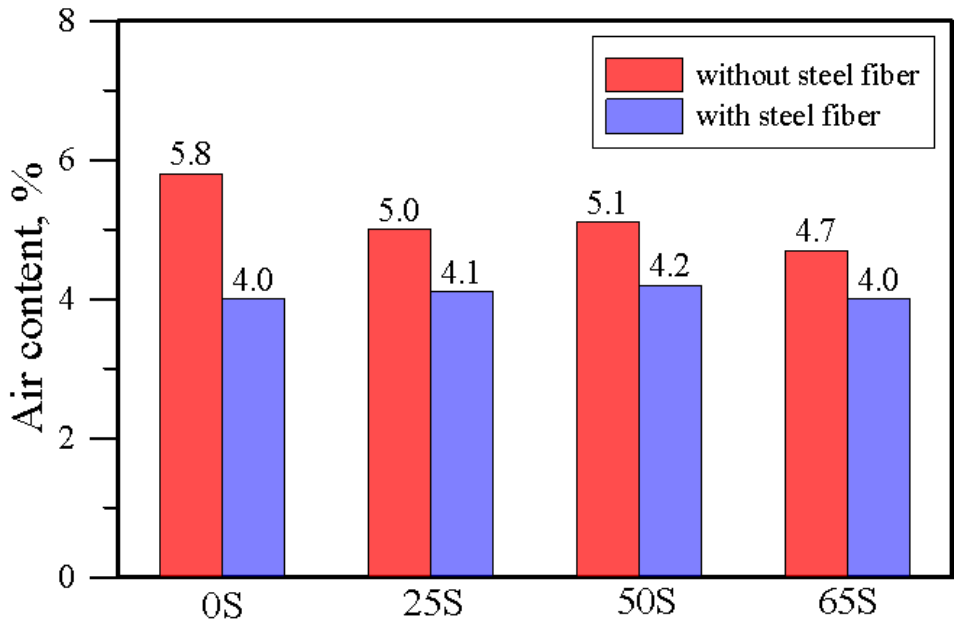

Figure 5-5 Effect of steel fiber addition on the fresh air content of UHPC mixes

The linear traverse method provides much more information regarding the size distribution of air voids, as seen Figure 5-7 and Figure 5-8. Almost half of the air voids had a size larger than 500 μm (a typical upper limit value for defining entrained air) with the majority concentrated between 500 and 1000 μm for non-air entrained UHPC mixes. In the case of a sufficiently air-entrained concrete, 75% of the air voids are less than 500 μm. Figure 5-7 shows a tendency of a change of air void size distribution due to increasing content of GGBS in cement, which is related to a decrease in small voids content. This result is inconsistent with the trend of the specific surface area given in Table 5-2. The reason is presumed to be that the calculation for the UHPC mixture has an inherent error in the computation of the specific surface area due to the small air voids. Meanwhile, unlike the typical entrapped air voids observed in ordinary concrete with an irregular shape, UHPC mixes, even though non-air entrained, have spherical air voids with a wide range of

size classes. This may be accounted for by the absence of coarse aggregate particles and the use of superplasticizer.

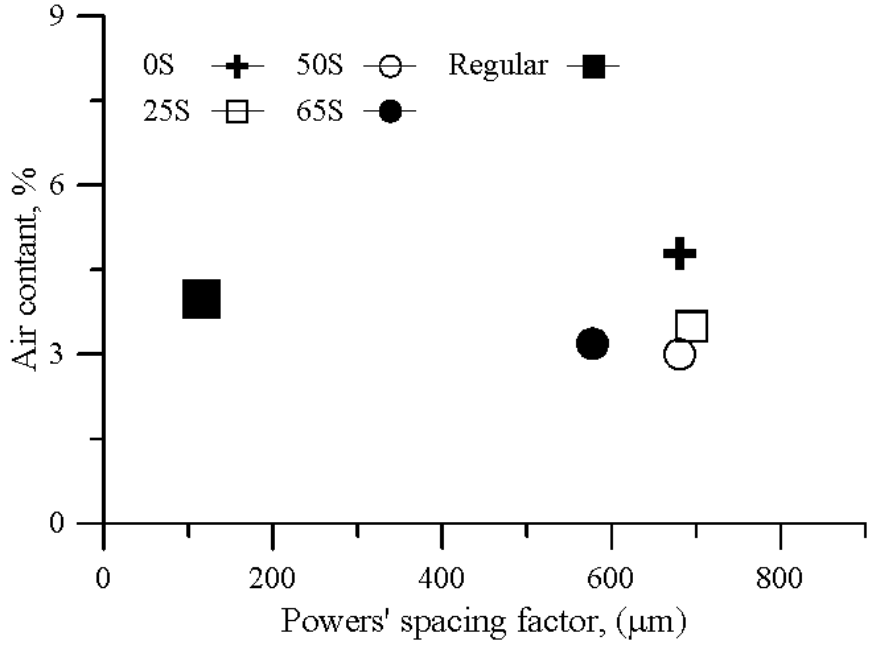

Figure 5-6 Air Content as a Function of Power's Spacing Factor

Table 5-2 Air content and void parameters for UHPC mixes

	Air content (%)				Powers' spacing factor, μm	specific surface, mm^{-1}	Paste content (%)
	Designed air content	Fresh air content		Hardened air content (linear traverse method)			
		W/O fibers	With fibers	Total			
0S	4.0	5.8	4.0	4.8	681	9.59	50.8
25S	4.0	5.0	4.1	3.5	695	10.87	51.3
50S	4.0	5.0	4.2	3.0	681	11.99	51.9
65S	4.0	4.7	4.0	3.2	577	13.70	52.2
Regular concrete	/	/		4.0	116	45.01	26.1

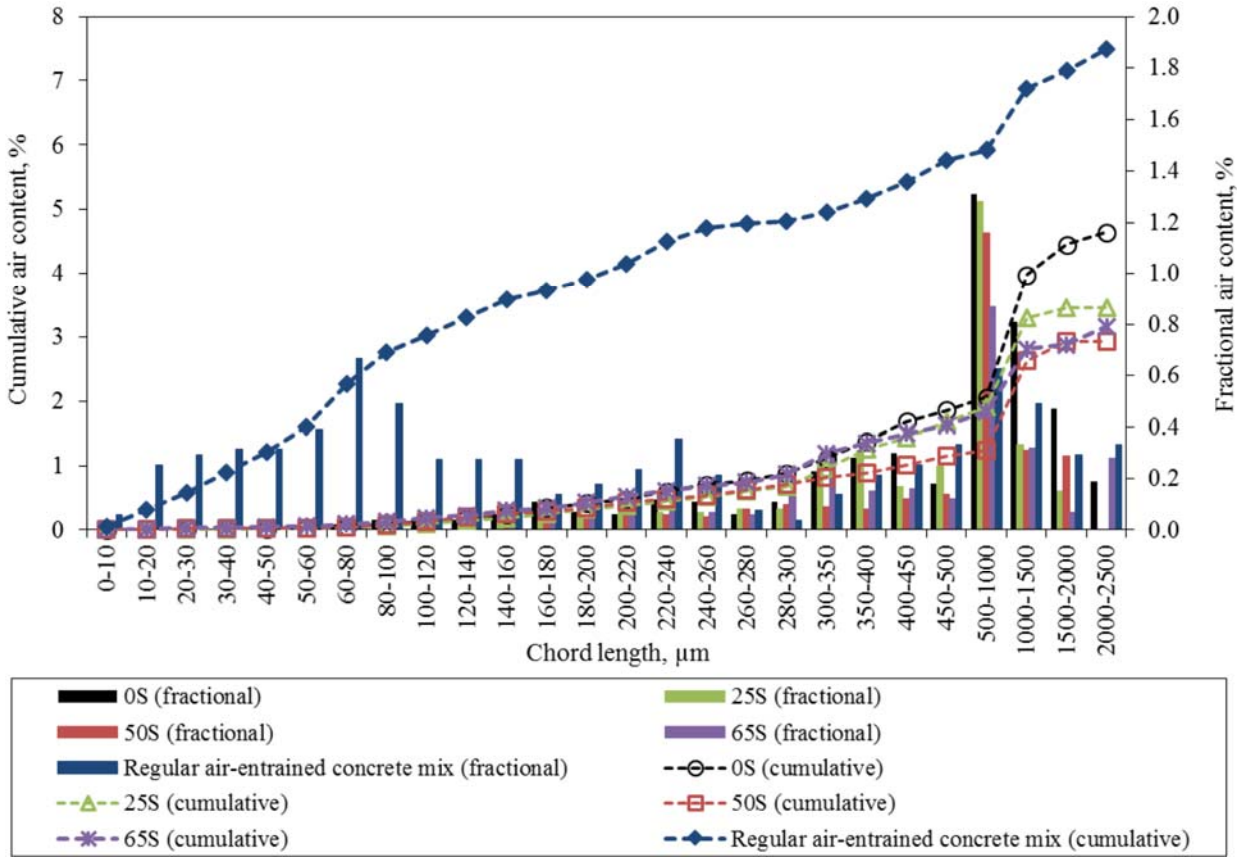

Figure 5-7 Air void size distribution based on the chord length from linear traverse method (air content of the regular air-entrained concrete is normalized to the paste content of UHPC mixes)

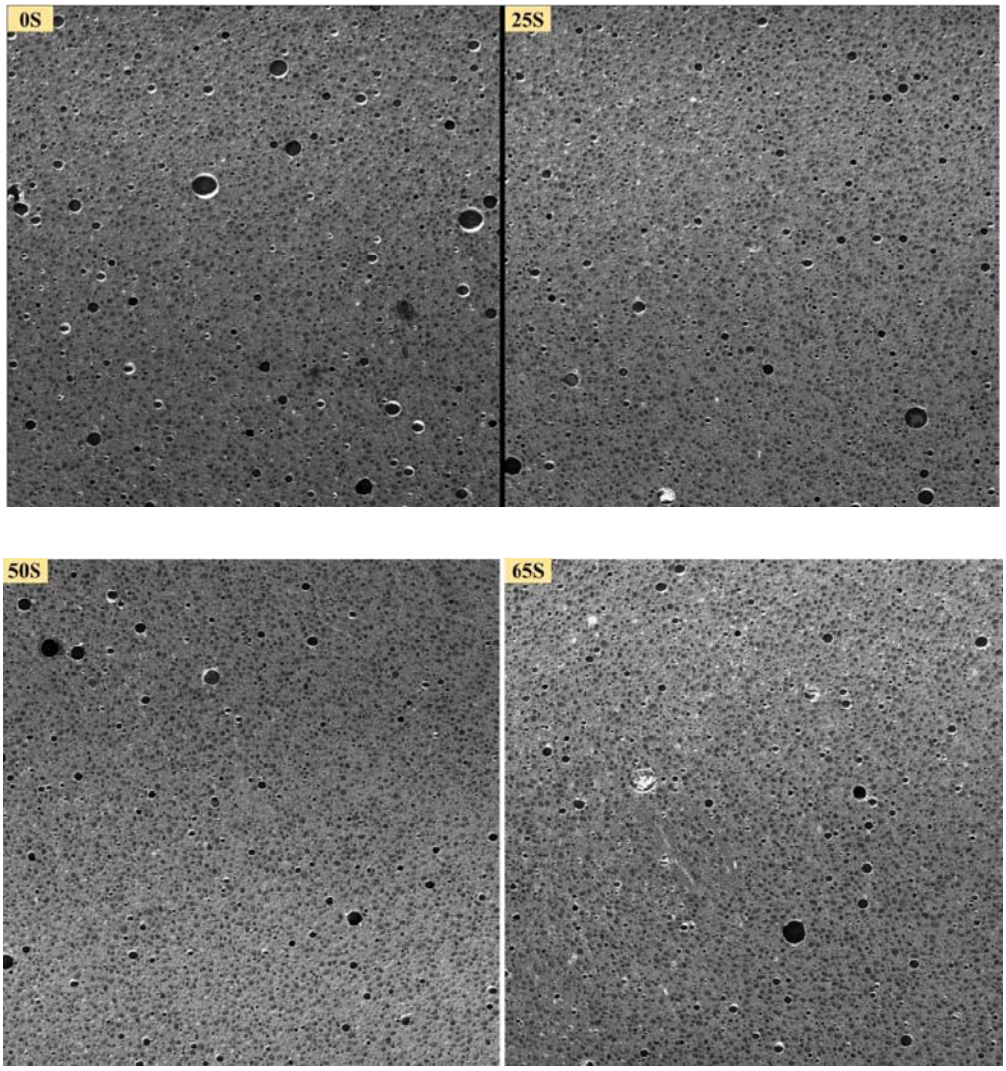

Figure 5-8 Air void profiles for the UHPC mixes with different GGBS contents

5.2.2. Hydration heat and degree of hydration

One major advantage of GGBS addition in concrete is the reduction of heat generation in the early age when young concrete is prone to cracking. This is clearly shown in Figure 5-9 where the temperature rise is suppressed in proportion to the degree of GGBS replacement. Close inspection of the initial temperature rise stage reveals that the replacement of Portland cement

slightly accelerates the initiation of temperature rise. This may be associated with the so-called "diluting effect" of GGBS since it acts almost as an inert filler as mentioned previously. This is equivalent to increasing the w/c ratio, which promotes the hydration of cement and thus heat liberation. However, this effect is not in proportion to the amount of slag cement present in the system with the 65% replacement level. In this case, the amount of cement is reduced to such an extent that the positive effect of the increased water availability for cement hydration is partially counterbalanced.

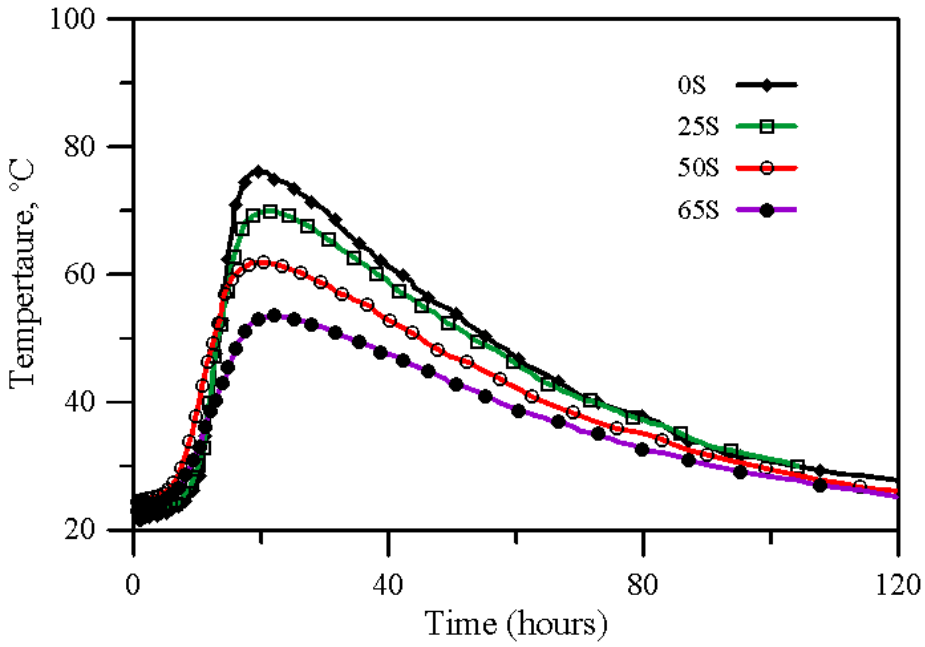

Figure 5-9 Temperature evolution in UHPC mixtures with different GGBS contents

Heat of hydration may also be used to observe the development of mechanical properties and the degree of hydration of the cementitious material. In general, the degree of hydration can be measured by X-ray diffraction analysis, SEM image analysis or by methods such as chemical

binding of water [85]. Compared to these complex test methods, Habel et al [95] proposed a simple model which was concluded from the results of the semi-adiabatic heat of hydration tests data. The degree of cement reaction is analyzed through the hyperbolic formulations of hydration heat change, and the relationship is expressed as

$$r(t) = \frac{Q(t)}{Q_{tot}} = \frac{k(t_{eq}-d)}{1+k(t_{eq}-d)} \qquad \textbf{Equation 5.3}$$

where $Q(t)$ is cumulated heat of hydration, and Q_{tot} is total heat of hydration, k is rate constant, t_{eq} is equivalent time and d is dormant period. This model is suitable for both conventional and slag cement concrete and has been successfully applied in UHPC [95]. It was assumed that the released heat is proportional to the hydration reaction, and the hyperbolic model of Equation 5.2 can be calculated and fitted from the experimental results of Figure 5-9. It is assumed that the strong heat release reaction begins after the dormant period. It can be observed from Figure 5-9 that the dormancy period for the mixtures content of different GGBS is around 6-11 hours. The fitted test results are shown in Figure 5-10. It can be seen from Figure 5-10 that the UHPC exhibited a strong increase in the degree of hydration reaction at an early stage. The degree of reaction on day 7 can reach r=0.72. Then on the 14th and 28th days, it reaches r=0.83 and r=0.91 respectively. In addition, it can also be observed from the figure that the hydration reaction rate slightly decreases with the increase of the GGBS content but that has no effect on the late strength. This trend is similar to the [95], although it is inconsistent with the conclusion of [85]-because the low water to cement ratio resulted in that a significant amount of cement in the UHPC formulation did not fully hydrate after 28 days. However, it is still a feasible qualitative way to observe the strength development trend of UHPC through Equation 5.2.

Hydration of GGBS alone is a very slow process requiring the break-down and dissolution of the glassy structure. Its reaction rate can be accelerated by the hydroxyl ions liberated during the hydration of Portland cement, which involves a two-stage reaction [96]. The initial reaction is with alkali hydroxide while the subsequent reaction is primarily with calcium hydroxide, the latter also being known as the pozzolanic reaction. This process consists of the consumption of a porous product (calcium hydroxide) and the precipitation of a dense product (calcium silicate hydrate), which leads to a more refined and condensed pore structure [97,98]. This explains the higher compressive strength in the later ages for the UHPC mixes with GGBS. However, the pozzolanic reaction lags behind cement hydration at the early hydration stage.

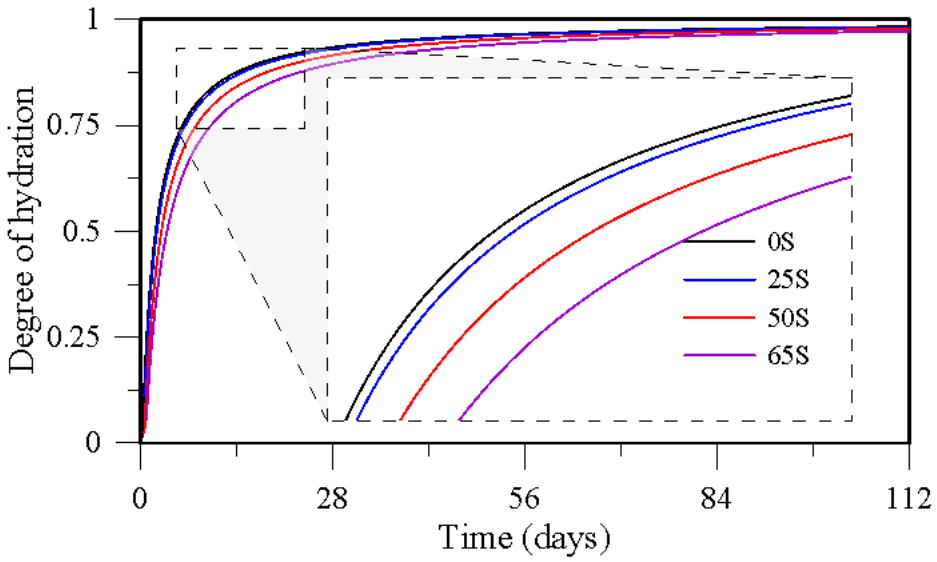

Figure 5-10 Evolution of the degree of hydration reaction with time in UHPC mixtures with different GGBS contents

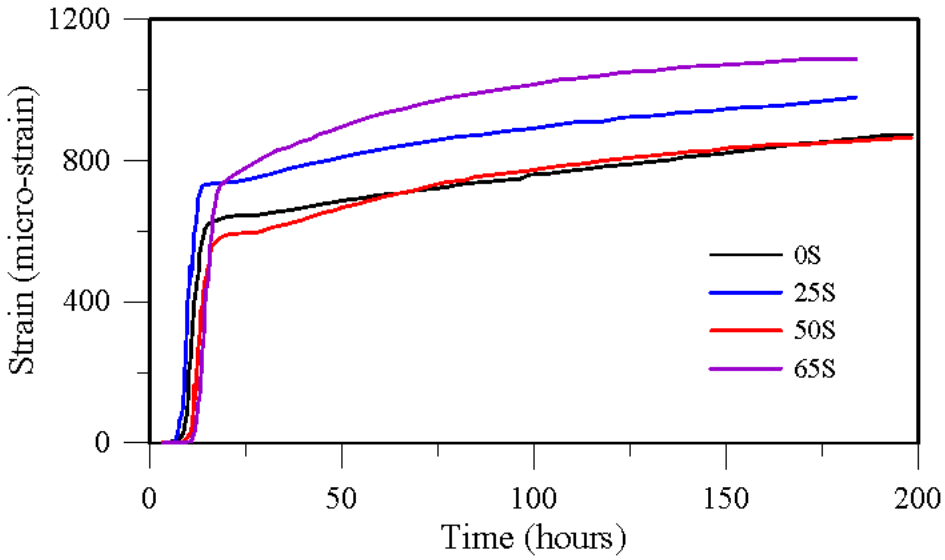

Figure 5-11 Shrinkage strain development of UHPC mixes with different GGBS contents

5.2.3. Autogenous shrinkage

Figure 5-11 shows the shrinkage strain development in UHPC mixes with different GGBS contents. The zero time on the x-axis characterizes the time when water was added during mixing. The UHPC shrinkage exhibits four distinctive stages: (I) the dormant period with almost zero shrinkage with varying lengths depending on the slag cement content; (II) the acceleration period with rapidly occurring shrinkage lasting around 7 hours; (III) a short-lived plateau period; (IV) the steady stage.

The dormant period is prolonged, compared with the regular cementitious system with a high w/c ratio, and its length shows good correlation to the initial setting time (Figure 5-12), before which the hydration reaction is limited. This may be a result of the excessive use of superplasticizer in UHPC [99-101]. The acceleration stage may be a result of the rapid chemical reaction of cementitious materials (primarily cement and silica fume) with water, as evidenced by the increase

in specimen temperature (Figure 5-13). It is currently hard to explain the existence of the short plateau observed in the 0S, 25S and 65S systems. What is more interesting is that its length corresponds well with that of the cooling stage on the temperature curve (Figure 5-13).

When the shrinkage strain is plotted for the steady state, it can be seen that GGBS exacerbates shrinkage (Figure 5-14). This suggests the pozzolanic reaction has occurred much earlier in UHPC.

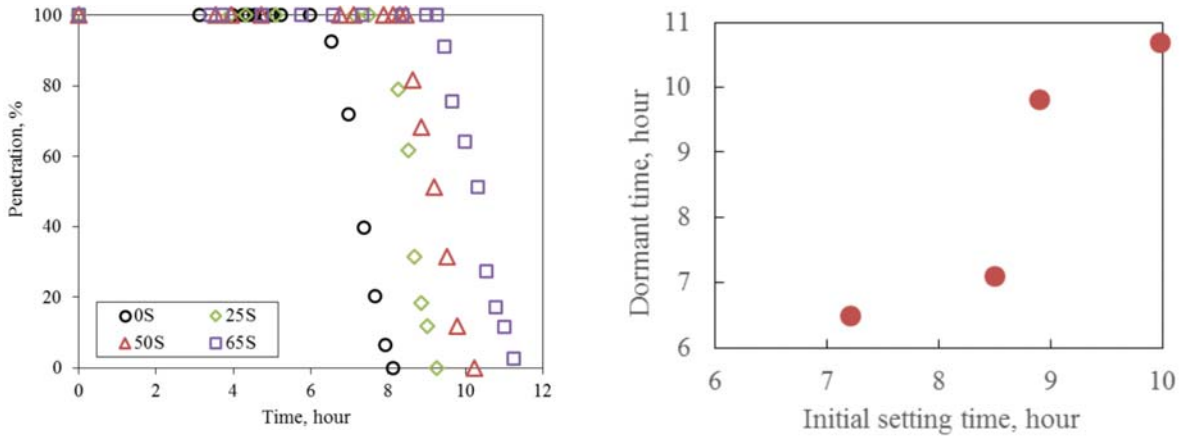

(a) (b)

Figure 5-12 (a) Penetration resistance of UHPC paste mixes and (b) correlation between dormant time and setting time

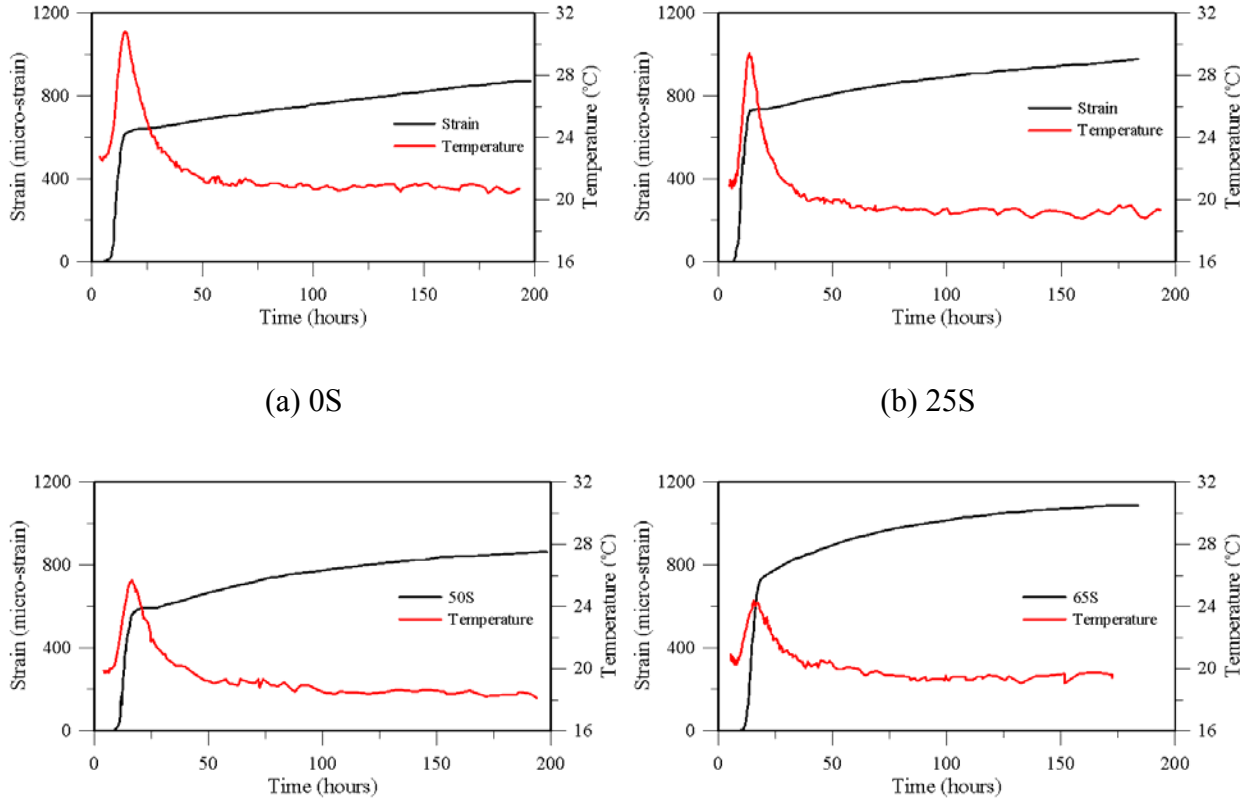

(a) 0S (b) 25S

(c) 50S (d) 65S

Figure 5-13 Simultaneous representation of temperature and strain evolution

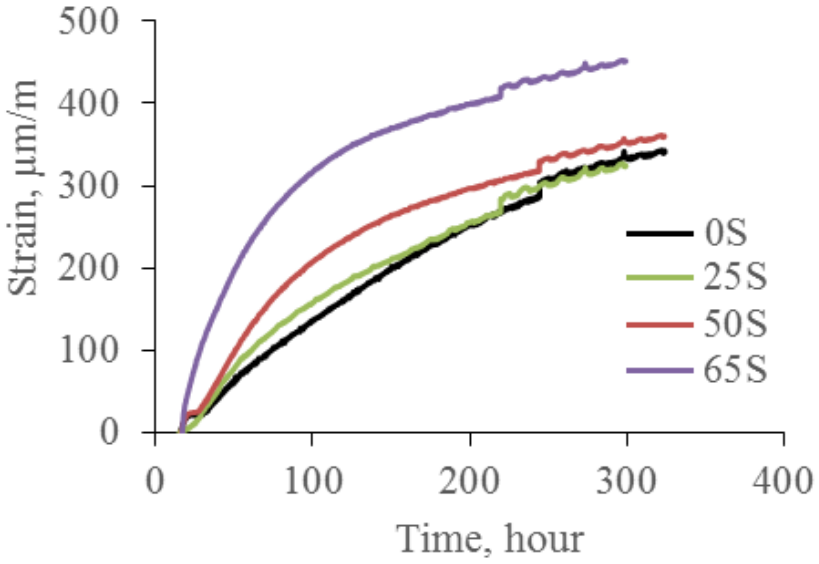

Figure 5-14 Shrinkage development in the steady state

5.2.4. Capillary absorption and F-T test

Concrete has the tendency to absorb water from the outside via primarily two mechanisms: capillary suction and diffusion [102]. The presence of moisture and the accompanying deleterious chemicals causes an array of durability-related issues, such as freeze-thaw deterioration, chloride ion-induced rebar corrosion and sulfate damage [103]. Thus, transported properties of concrete, especially the capillary absorption, has been proposed to evaluate durability in numerous studies [104-107].

The water absorption behavior before and during the F-T test is characterized by the moisture uptake of 70-mm thick (refer to Section 4.4.3) concrete specimens with the test surface immersed 0.2 inches (5-mm) in water and 3% salt solution, respectively. During pre-saturation at 20 °C, there is initially a rapid linear development with the square-root of time, a typical capillary suction process occurring in well-connected pores. This gradually tapers off and transitions into a

diffusion-controlled slow process. When moisture absorption is coupled with F-T exposure, the uptake is accelerated due to a "pumping effect" [108-110]. Nevertheless, the amount and rate of moisture absorption is much lower compared with regular normal and high strength concrete alike (Figure 5-15). Caution should be taken in the comparison between concrete mixes with a significant discrepancy in paste concrete, since moisture is imbibed mostly by the paste which is even truer in UHPC with high-quality silica sands. Thus, the moisture uptake is normalized with respect to the paste content in Figure 5-16. It can be seen that there is very limited absorption of UHPC mixes, even lower than a regular concrete with surface treatment. This serves as evidence for excellent durability.

Furthermore, the sorptivity, a parameter representing the suction rate, can be extracted from this linear segment (Figure 5-17). The mix with the highest slag cement replacement level (65S) also has the highest sorptivity value, compared with the other three mixes with no appreciable difference. A safe prediction can be made that the sorptivity of the 65S mix will be reduced if the specimens were tested at a further later age when more pozzolanic reaction was initiated.

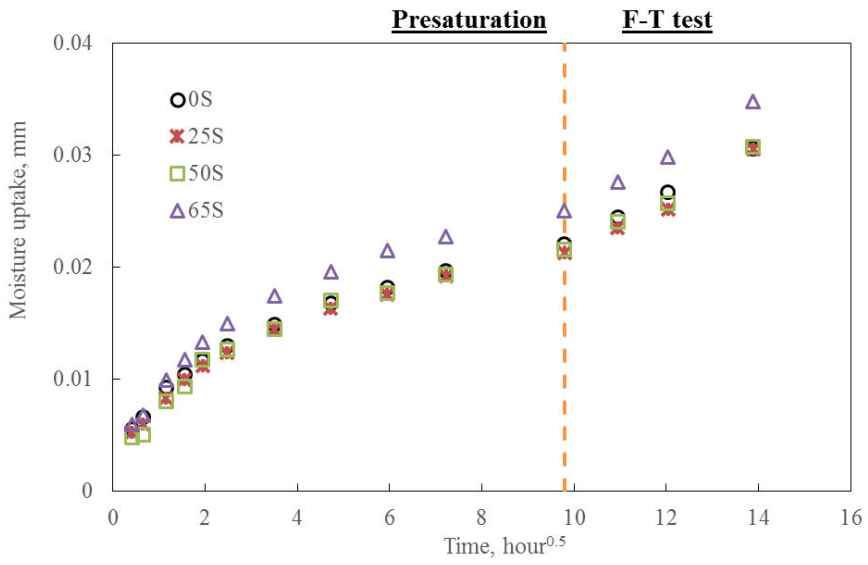

Figure 5-15 Moisture uptake curves of UHPC mixes

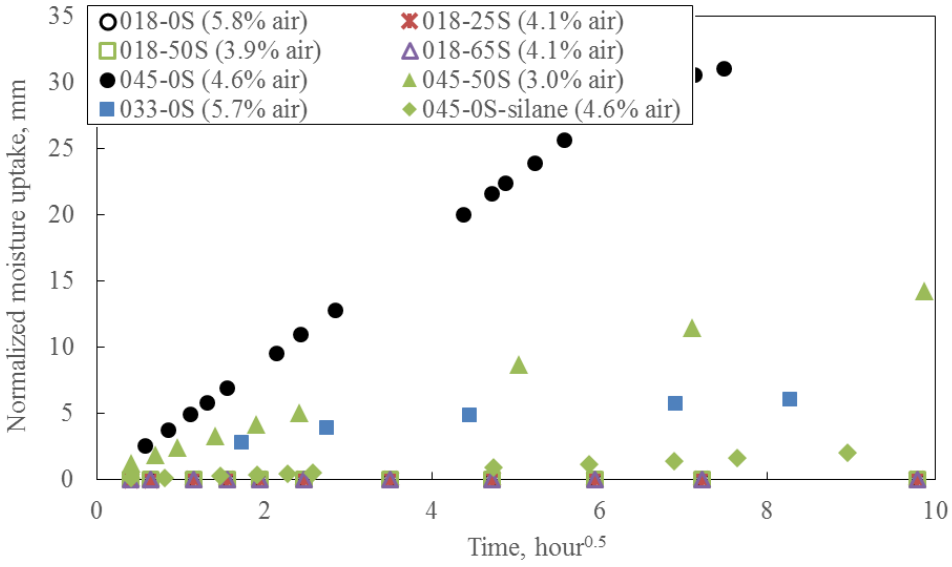

Figure 5-16 Normalized moisture uptake between different concrete mixes

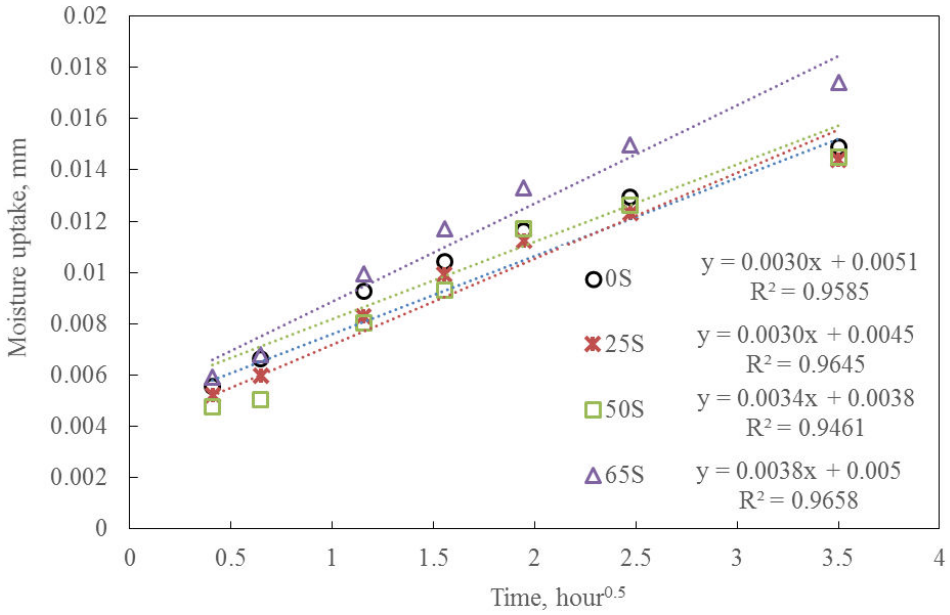

Figure 5-17 The capillary suction and associated sorptivity

5.2.5. Compressive strength development

The hardening process of UHPC is accompanied by an increase in the ability to resist mechanical load and the gradual densifying of the matrix. In the case of pre-selected components, there are still some minor factors that influence the development of mechanical properties. For example, partially replacing the cement with GGBS, as previously mentioned, despite the hydration reaction, can form hard calcium silicate hydrate. The reduced hydration rate of GGBS in concrete leads to a delayed strength development. Gupta [111] suggested that accelerating the development of UHPC hydration reaction and, therefore strength, can be achieved by using GGBS with a finer particle size. Variable fineness offers different specific surface areas for hydration reaction and influences the distribution of hydration products in the cementitious system which may eventually impact the strength and durability properties of UHPC.

The polycarboxylate based HRWR is used in UHPC to increase paste workability and its interaction with cement particles dispersion. In turn, there is a negative effects when the HRWR dose exceeds the optimum amount, i.e. it will result in a lower compressive strength. The reason can be explained by the segregation phenomenon, as shown in Figure 5-18. Due to the occurrence of segregation, the particles in the fresh UHPC paste and the steel fibers are no longer uniformly distributed. Therefore, some of the particles separate from the cement paste and cause a decrease in strength. In addition, [112,113] reported that when the HRWR dose was high, and the polymer surface coverage was higher, this meant that the effective layer thickness around the particles increased, resulting in a decrease in the maximum attraction between the particles.

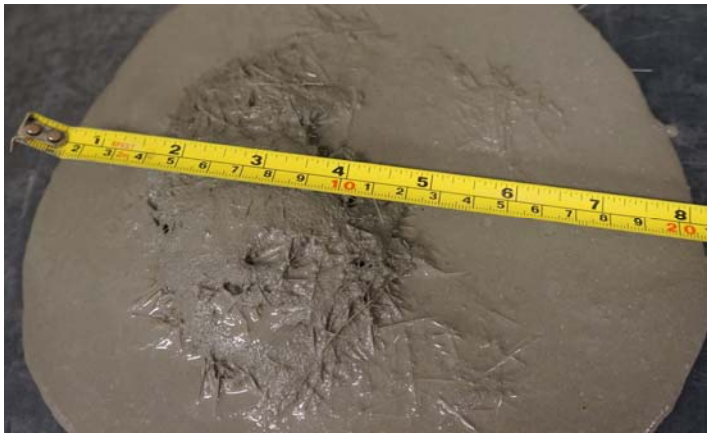

Figure 5-18 The segregation caused by high dose of HRWR

To study the effect of GGBS fineness on mechanical strength, two different grades of GGBS available in Michigan were employed: Grade 100 (G1) and Grade 120 (G2), which have specific surface areas of 551 m^2/kg and 572 m^2 /kg, respectively, and slag activity indices is 125% and 103% (as noted earlier). As noted earlier, the optimum dosage of HRWR is 2%-3% of the

weight of the cementitious material. Considering a spread of less than 8 inches (200 mm) after adding steel fibers, and taking into account the goal of field mixing, this section compares the results of varying the HRWR in the 2% to 3% range. To facilitate discussion, the naming scheme is X-H, in which X is the type of GGBS, such as G1 or G2, and H is the amount of H1 HRWR. For example, G1-2%HRWR indicates that G1 is used to partially replace cement, and the amount of H1 is 2%.

The strength of the two grades of GGBS specimens as a function of curing age are shown in Table 5-3 and Figure 5-19, which also reflects the effect of the dosage of HRWR. It can be seen from Figure 5-19 that UHPC gains compressive strength gradually with age. In Table 5-3, The compressive strength of G1-2%HRWR, G1-3%HRWR and G2-3%HRWR specimens at 28-days are 24.5 ksi (169.2 MPa), 23.1 ksi (159.0 MPa) and 21.1 ksi (146.1 MPa), respectively (refer to Table 5-3). These result indicate that compressive strength decreases when the dose of HRWR increases. For example, the compressive strength is reduced by 6% for G1-3%HRWR versus G1-3%HRWR. Opposite to the hypothesis, using finer GGBS product causes the compressive strength to decrease. For example, the compressive strength of G2-3%HRWR was reduced by 8.1% versus G1-3%HRWR. The cause of this phenomenon is unclear, presumably because the maximum attraction between the particles decreased due to the surface polymers. This restrains the hydration and consequently leads to a slower development of early-age strength of UHPC. For the Grade 120 GGBS, the phenomenon of promoting hydration due to a higher fineness was not observed in this test. Despite this, the 56-day compressive strength exceeds 25 ksi (172.4MPa).

The test results are compared with the model proposed by Wille et al. [114], which is an empirical equation describing UHPC strength development based on the 28-day compressive strength. The results show that the test strengths of 3-day, 7-day and 14-day are lower than the

empirical values. However, the compressive strength showed a significant increase at 56-day (Figure 5-19). The test values are 27.2 ksi (187.4 MPa), 25.6 ksi (176.4 MPa) and 25.7 ksi (177.5 MPa) for G1-2%HRWR, G1-3%HRWR and G2-3%HRWR, respectively. The values obtained from the empirical model are 26.1 ksi (179.6 MPa), 24.5 ksi (168.8 MPa), and 22.5 ksi (155.1 MPa). The increase in value is about 4% for G1 mixes. This trend, which is associated with degree of hydration, agrees with the data in Figure 5-10 where r=0.91 at 28-day and continues to rise to r=0.94 at 56-days.

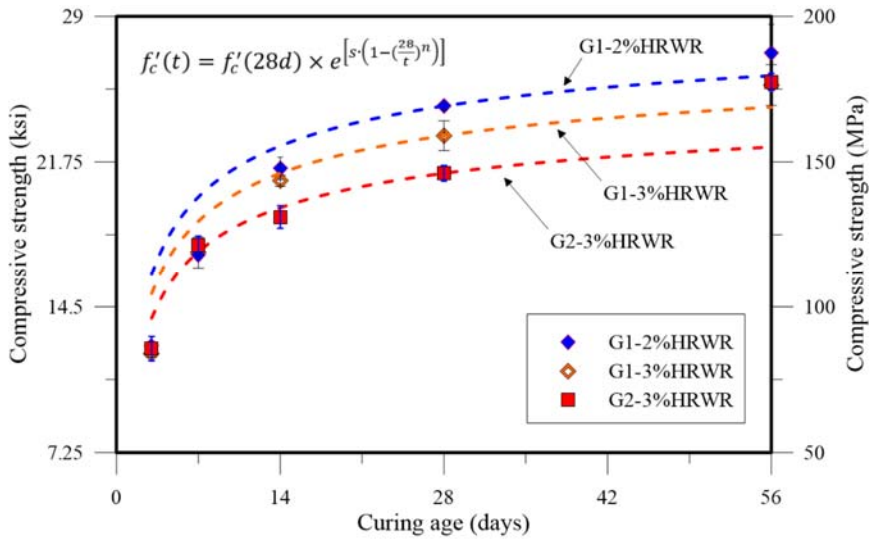

Figure 5-19 Effect of different grade of GGBS on the compressive strength of cube

Table 5-3 Performance of UHPC with different grades of GGBS

Matrix	Spread inch (mm)	HRWR	$^{w}/_{c}$	Average compressive strength ksi (MPa)				
				3 days	7 days	14 days	28 days	56 days
G1-2%HRWR	8.1 (205)	0.02	0.22	12.6 (86.5)	17.1 (118.2)	21.4 (147.8)	24.5 (169.2)	27.2 (187.4)
G1-3%HRWR	9.8 (248)	0.03	0.22	12.2 (83.9)	17.2 (118.8)	20.8 (143.5)	23.1 (159.0)	25.6 (176.4)
G2-3%HRWR	10.4 (264)	0.03	0.22	12.4 (85.6)	17.6 (121.5)	19.0 (131.1)	21.1 (146.1)	25.7 (177.5)

These test results imply that: (1) Wille's empirical model for estimating UHPC strength development is not suitable for UHPC where GGBS is used to partially replace cement. (2) Since UHPC with GGBS continues to gain strength significantly after 28 days, it could make sense to relax the 28-day strength-based acceptance criteria that are commonly used in industry and perhaps replace it with 56 day strength or some other suitable criterion. For example, a somewhat lower compressive strength at 28 days may be acceptable knowing that the strength will continue to rise substantially.

5.3. Compressive strength characteristics of UHPC

Compression test specimens are prepared and tested as outlined in Sections 4.3.1. The mixes are proportioned according to Table 5-1. The GGBS is selected as G1. The results of the test are shown in Table 5-4 and illustrated in Figure 5-20. The effect of cement type is shown in Figure 5-20 and can also be seen in Table 5-4 . The 14-days and 28-days compressive strengths are 20.9 ksi (143.6) and 22.5 ksi (155.3 MPa), 19.6 ksi (135.4 MPa) and 22.7 ksi (156.7 MPa), 20.2 ksi (139.0 MPa) and 23.1 ksi (159.5 MPa), respectively for cements LA, ST and LE. A review of the chemical composition and Blaine fineness of the three types of cement shows that they have the same amount of C_2S+C_3S, but the C_3A content is less than 8% for ST and LA, while the C_3A content for LE is 9.4%. In terms of Blaine fineness, the fineness of LE is slightly higher than LA and ST, which is 421 m^2/kg.

One of the critical performance indicators of UHPC is its flowability. Therefore, it is recommended to use a cement with a low C_3A content and moderate fineness. The reason for selecting cement with a low amount of C_3A is that the hydration process of C_3A is fast and the associated increase in the surface area of the particles and the demand for water to surround the particles during the mixing process leads to a higher viscosity [35,46]. On the other hand, higher Blaine values reduces workability. This is because the contact area between the cement particle and water increases with a decrease in the particle size of cement, causing a higher amount of demanded water to disperse and hydrate cement particles. The test results show that the three types of cement have a slight difference in chemical composition and fineness. The effect of these differences on the properties of fresh and hardened is negligible.

The effect of silica fumes on mechanical properties is shown in Figure 5-20. It can be seen from Figure 5-20 (a), which shows that when the HRWR is H1, the influence of the type of silica fume on the compressive strength is minor. For LA-EL-H1, LA-WM-H1, and LA-NC-H1, the 28-day compressive strengths are 22.5 ksi (155.3 MPa), 21.7 ksi (149.6 MPa), and 22.1 ksi (152.4 MPa), respectively. The variation is less than 3%. For the combination with H3 and NC, however, extremely low workability is manifested. As explained earlier, this is due to NC having a high carbon content (nearly 6%) and therefore needing more water to promote the fluidity of the paste.

As mentioned earlier, the WM had a high zirconium dioxide content, which caused it to exhibit better fluidity than its counterpart (see Figure 5-1) [69]. In terms of mechanical properties, mixes with WM develop the 14-day compressive strength rapidly. However, beyond that, the strength gain tends to stagnate. For example, the compressive strength of both LA-WM-H1 and LA-WM-H2 at 14-day is 21.1 ksi (145.3 MPa) but increases slightly to 21.7 ksi (149.6 MPa) and 22.1 ksi (152.3 MPa) at 28-day, respectively (Table 5-4). The reason for this phenomenon is unclear, but it is speculated that the high fluidity causes a precipitation of fibers, resulting in an uneven stress distribution within the specimens.

Nevertheless, with some exceptions, the 28-day compressive strength of all mixtures was above 21.7 ksi (150 MPa). Insufficient flowability results in a porous and inhomogeneous structure and poorly compacted samples. On the other hand, excessively high flowability may cause segregation of paste. The relationship between spread and compressive strength is presented in Figure 5-21. It appears from Figure 5-21 that a reasonable spread is between 7 in and 10 in.

Table 5-4 Compressive and tensile properties of UHPC

Name	Avg. compressive strength ksi (MPa)		first cracking strength σ_{cc}, ksi (MPa)	Post cracking strength σ_{pc}, ksi (MPa)	Strain capacity ε_{pc} (%)	Energy absorption capacity g, kcal/yd^3 (kJ/m^3)	Average fiber stress σ_{fpc} ksi (MPa)
	14 days	28 days					
LA-EL-H1	20.9 (143.6)	22.5 (155.3)	0.95 (6.6)	1.3 (9.2)	0.12	2.3 (12.7)	74.1 (511.1)
LA-EL- H2	19.4 (133.6)	22.8 (157.0)	0.97 (6.7)	1.2 (8.3)	0.11	1.1 (10.7)	66.9 (461.1)
LA-EL- H3	18.5 (127.3)	22.3 (154.0)	1.04 (7.2)	1.5 (10.1)	0.15	3.8 (21.2)	81.3 (561.1)
LA-WM- H1	21.1 (145.3)	21.7 (149.6)	0.95 (6.6)	1.3 (9.1)	0.11	2.4 (13.2)	73.3 (505.6)
LA-WM- H2	21.1 (145.6)	22.1 (152.3)	1.02 (7.0)	1.3 (9.2)	0.12	2.6 (14.3)	74.1 (511.1)
LA-WM- H3	19.1 (131.7)	23.1 (159.3)	1.03 (7.1)	1.4 (9.5)	0.13	3.3 (17.9)	76.5 (527.8)
LA-NC- H1	20.2 (139.4)	22.1 (152.4)	0.94 (6.5)	1.3 (9.1)	0.13	2.6 (14.1)	73.3 (505.6)
LA-NC- H2	18.3 (126.4)	21.5 (148.0)	0.94 (6.5)	1.5 (9.2)	0.08	1.9 (10.6)	74.1 (511.1)
LA-NC- H3	**Not Available**						
ST-EL- H1	19.6 (135.4)	22.7 (156.7)	1.07 (7.4)	1.5 (10.1)	0.17	4.0 (21.9)	81.3 (561.1)
ST-EL- H2	19.3 (133.1)	21.8 (150.4)	0.93 (6.4)	1.5 (10.1)	0.23	4.8 (26.6)	81.3 (561.1)
ST-EL- H3	18.2 (125.4)	21.7 (149.6)	0.93 (6.4)	1.4 (9.4)	0.12	2.9 (16.0)	75.7 (522.2)
ST-WM- H1	21.2 (146.4)	21.7 (149.5)	0.87 (6.0)	1.5 (10.0)	0.14	3.1 (17.3)	80.6 (555.6)
ST-WM- H2	20.4 (140.6)	22.9 (158.1)	0.81 (5.6)	1.3 (8.7)	0.22	3.5 (19.2)	70.1 (483.3)
ST-WM- H3	18.4 (126.7)	21.6 (149.3)	0.89 (6.1)	1.5 (10.2)	0.25	5.3 (29.2)	82.2 (566.7)
ST-NC- H1	19.9 (137.3)	22.0 (151.6)	0.78 (5.4)	1.3 (8.9)	0.16	2.5 (13.9)	71.7 (494.4)
ST-NC- H2	19.6 (134.9)	21.3 (146.8)	0.78 (5.4)	1.4 (9.7)	0.22	4.2 (23.2)	78.1 (538.9)
ST-NC- H3	**Not Available**						
LE-EL- H1	20.2 (139.0)	23.1 (159.4)	0.73 (5.0)	1.3 (9.2)	0.22	3.8 (20.8)	74.1 (511.1)
LE-EL- H2	19.4 (134.1)	24.1 (166.0)	1.10 (7.6)	1.4 (9.7)	0.13	4.7 (25.6)	78.1 (538.9)
LE-EL- H3	19.4 (133.6)	22.2 (153.2)	1.00 (6.9)	1.4 (9.9)	0.21	4.2 (23.1)	79.8 (550.0)
LE-WM- H1	19.6 (135.5)	21.7 (149.8)	1.18 (8.1)	1.4 (9.5)	0.12	3.2 (17.5)	76.5 (527.8)
LE-WM- H2	17.7 (121.8)	21.6 (149.1)	0.93 (6.4)	1.5 (10.3)	0.12	2.3 (12.4)	83.0 (572.2)
LE-WM- H3	19.2 (132.2)	22.3 (154.0)	1.04 (7.2)	1.5 (10.2)	0.13	3.5 (19.1)	82.2 (566.7)
LE-NC- H1	20.3 (19.5)	23.5 (161.8)	0.83 (5.7)	1.5 (10.1)	0.16	2.8 (15.3)	81.4 (561.1)
LE-NC- H2	19.4 (133.8)	21.9 (151.2)	1.19 (8.2)	1.4 (9.5)	0.07	2.0 (11.2)	76.5 (527.8)
LE-NC- H3	**Not Available**						

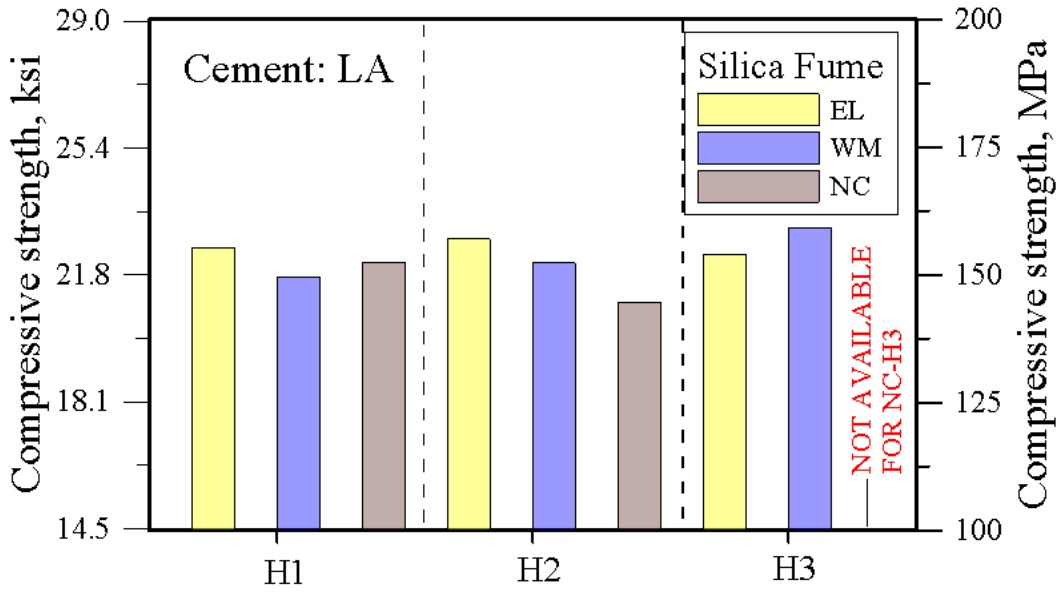
Cement: LA
Silica Fume
EL
WM
NC
NOT AVAILABLE FOR NC-H3
Compressive strength, ksi
Compressive strength, MPa
29.0
25.4
21.8
18.1
14.5
200
175
150
125
100
H1
H2
H3

(a)

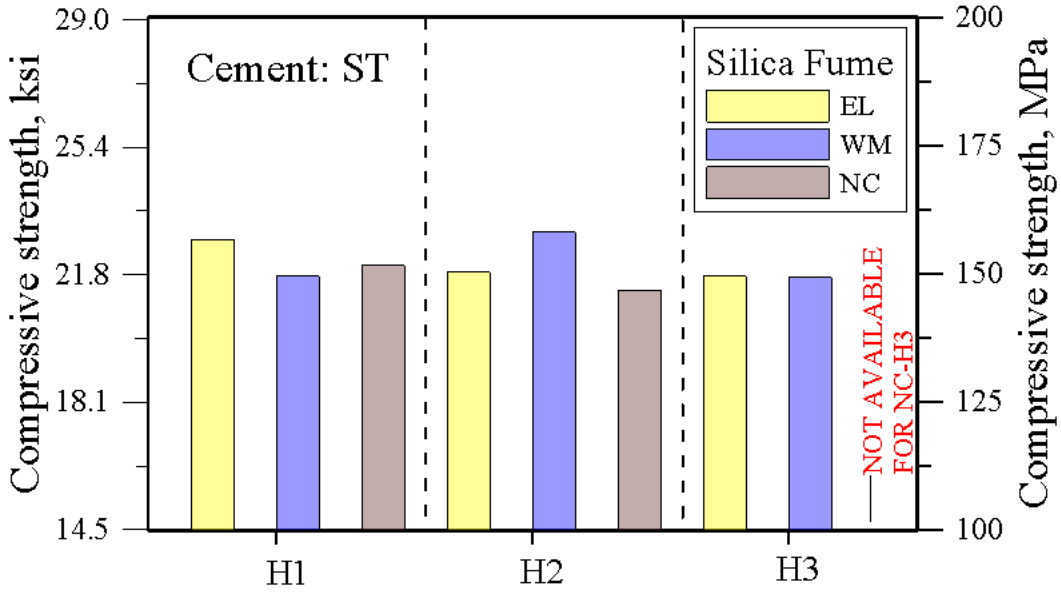
Cement: ST
Silica Fume
EL
WM
NC
NOT AVAILABLE FOR NC-H3
Compressive strength, ksi
Compressive strength, MPa
29.0
25.4
21.8
18.1
14.5
200
175
150
125
100
H1
H2
H3

(b)

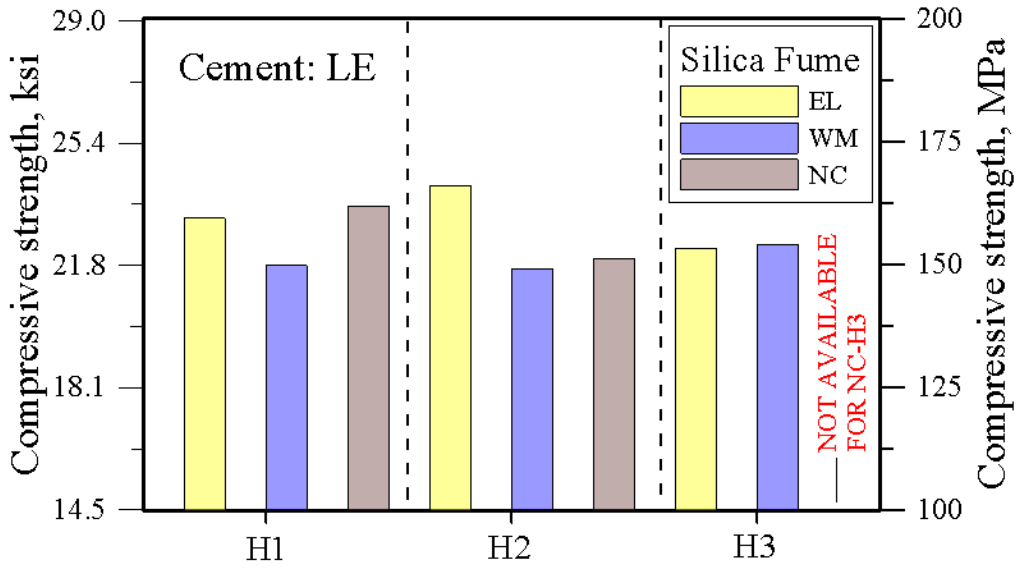

(c)

Figure 5-20 Effects of different combinations on compressive strength

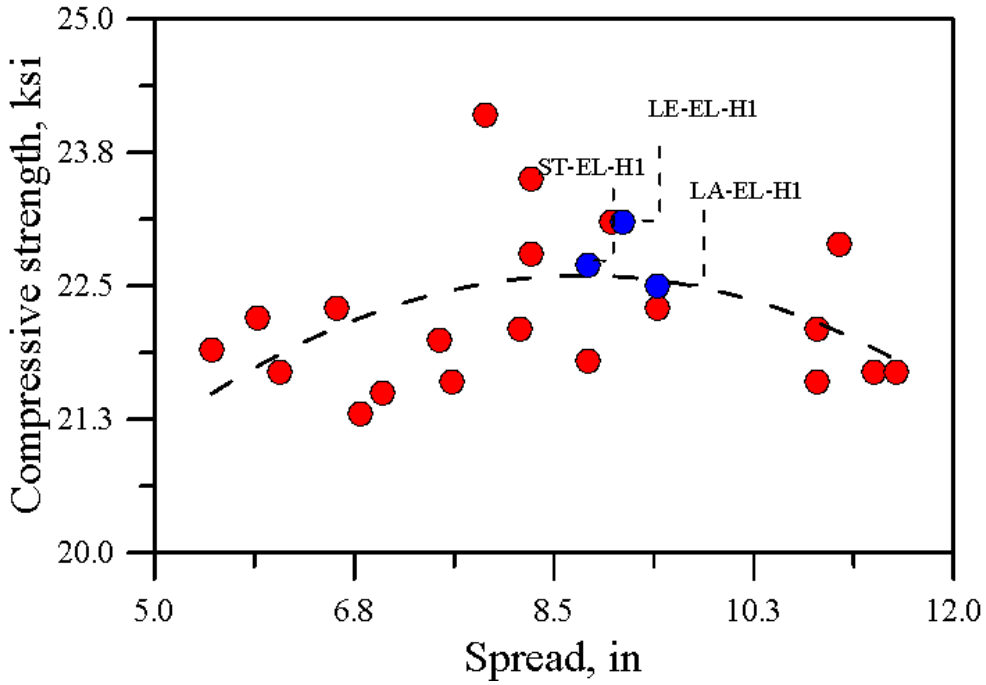

Figure 5-21 Relationship between compressive strength and spread

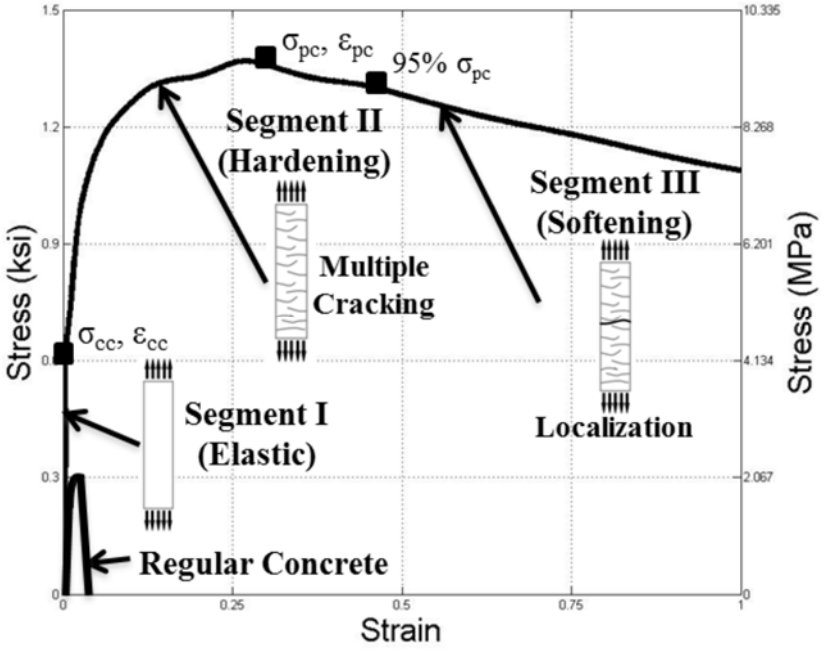

Figure 5-22 Typical Tensile Strain Response in UHPC [115]

5.4. Tensile behavior of UHPC

The typical tensile stress-strain curve for UHPC is shown in Figure 5-22. Following the definitions in Naaman [116], the material is strain hardening because the post-cracking strength (tensile strength) is more than the initial cracking stress. The idealized tensile response splits the tensile behavior into three parts. The first part is elastic response, which continues up until the specimen develops an initial crack, known as the first cracking strength point (σ_{cc}, ε_{cc}) in Figure 5-22. Following this, the material then exhibits strain hardening up until its peak point (σ_{pc}, ε_{pc}). The strain hardening behavior of part II is typically characterized by multiple crack development in the gauge length of the specimen. Following the strain-hardening region, the material then begins to exhibit crack localization (part III). To facilitate discussion, the following parameters are determined: post cracking strength (tensile strength), σ_{pc}, strain capacity, ε_{pc}, energy absorption

capacity, g, and the average stress in the fibers, σ_{fpc}. The energy absorption capacity is the area under the stress-strain curve until a softening trend occurs and the stress drops to $\sigma_u = 0.95\,\sigma_{pc}$. The average stress in fibers, σ_{fpc} represents the average tensile stress in the fibers at peak tensile stress in the composite. It is calculated based on the following equation.

$$\boldsymbol{\sigma_{fpc} = \frac{\sigma_{pc}}{\phi \cdot V_f}} \qquad \textbf{Equation 5.4}$$

where ϕ is an orientation factor, taken 0.9 for all series because most of the fibers are aligned in the load direction due to the casting method employed as proposed in [1].

Tension test specimens were prepared and tested as outlined in Sections 4.3.2 and documented in Appendix A. The mixes were proportioned according to Table 5-3. The GGBS was selected as G1 whereas 2% by volume steel fibers were used. The results of the test are shown in Table 5-4 and illustrated in Figure 5-23 through Figure 5-26. It can be seen from the stress-strain relationships in Appendix A that all mixtures exhibited strain hardening behavior. Another key observation is that the peak tensile strength of all mixtures exceeded 1.2 ksi, fulfilling the minimum requirement for field-cast UHPC as noted in [22]. All mixtures showed little variation and no clear trend between the types of cement, silica fume, and HRWR emerged.

Figure 5-24 and Table 5-4 summarize the strain capacity values for each series. Strain capacity is characterized by ε_{pc}, which ranged from 0.11 to 0.25. These values are a little less than observed in previous testing [5]. The lower strain capacity is attributed to the use of shorter steel fibers (0.5 inches (13 mm) in length in this work) versus the longer fibers previously used (0.75 inches (19 mm)). The use of shorter fibers reduces the capacity to better develop multiple cracking and promotes early stress softening. The deleterious effect of shorter fibers is also manifested in lower energy absorption characteristics (Figure 5-25). The energy absorption values range from

10.7 kJ/m^3 to 29.2 kJ/m^3. According to the classification scheme proposed by Naaman and Reinhardt [116], the UHPC mixes studied in this work can still be classified as tensile strain hardening. The average fiber tensile stress for all series is shown in Figure 5-26.

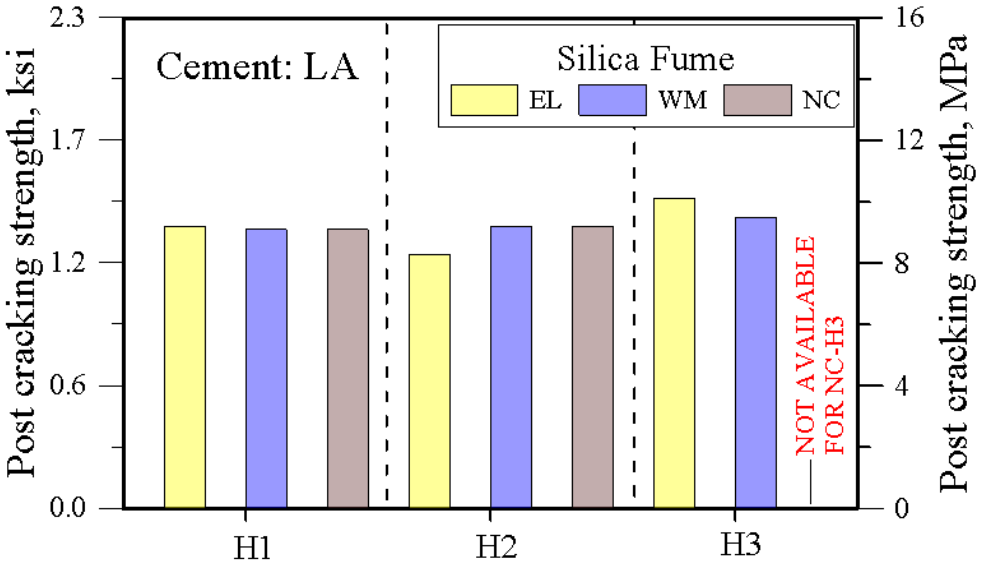

(a)

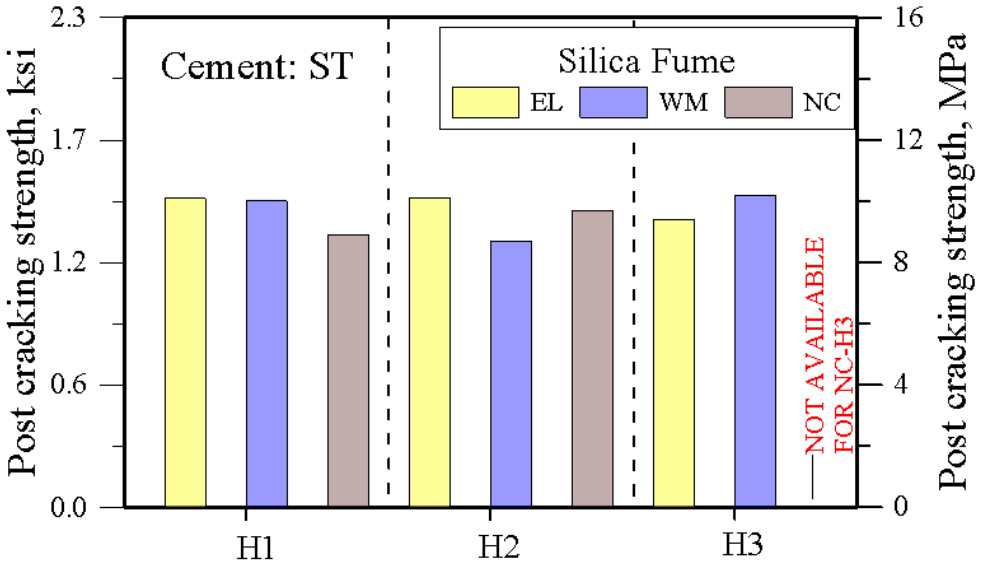

(b)

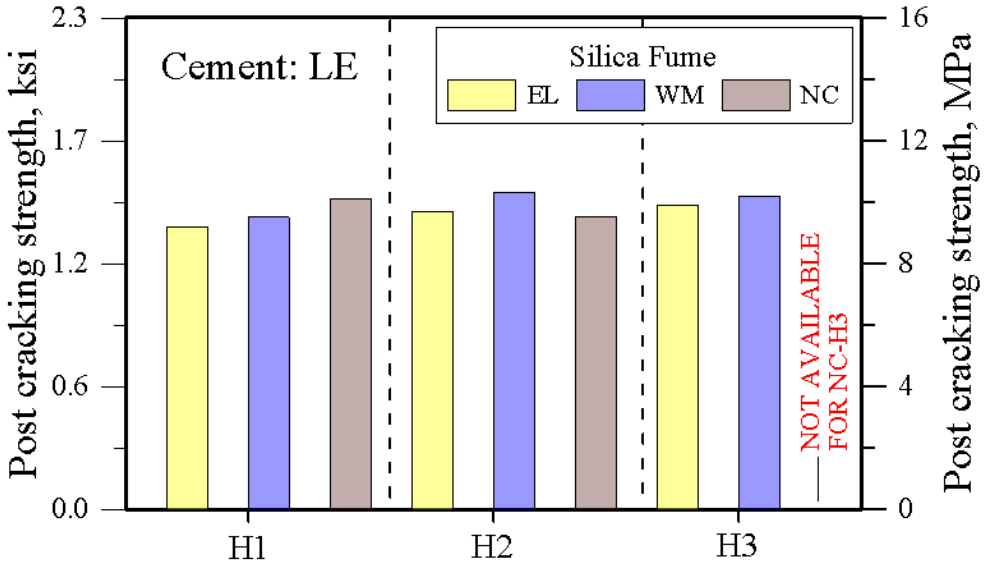

(c)

Figure 5-23 Effects of the different variables on post-cracking strength

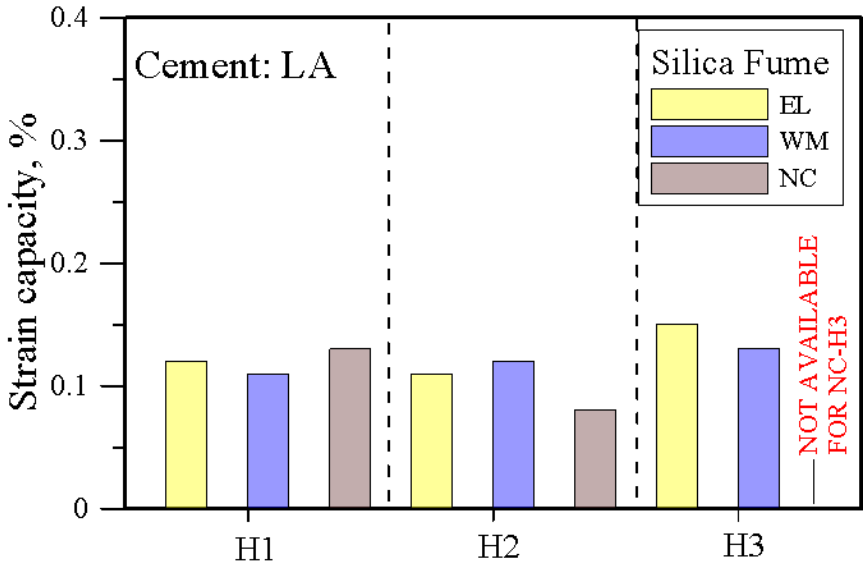

(a)

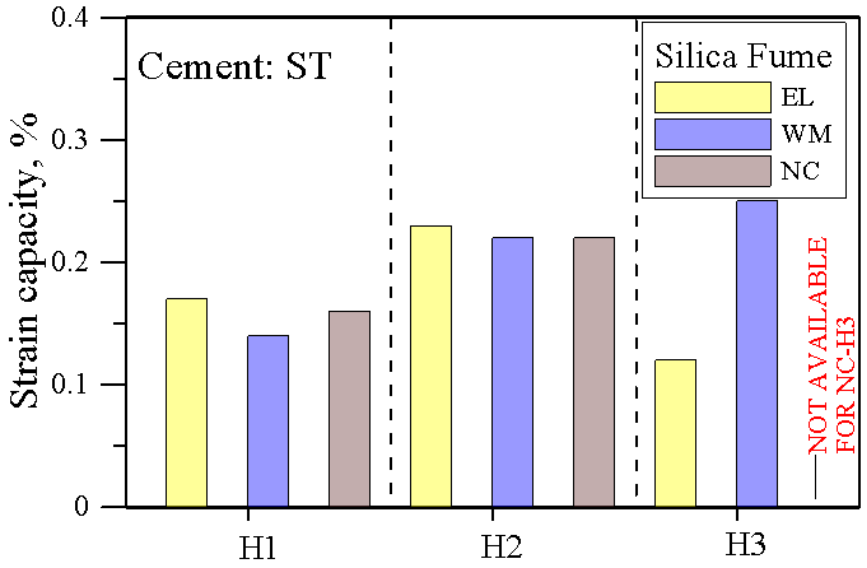

(b)

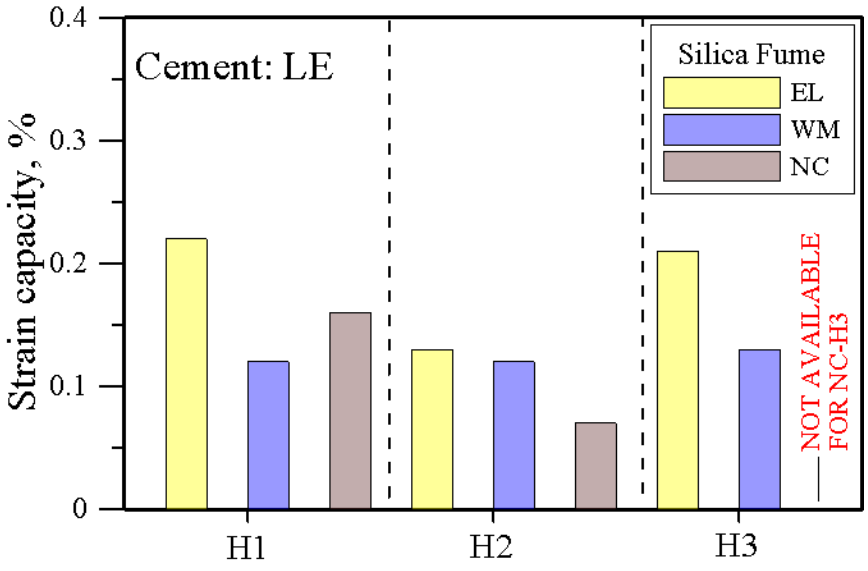

(c)

Figure 5-24 Effects of different variables on strain capacity

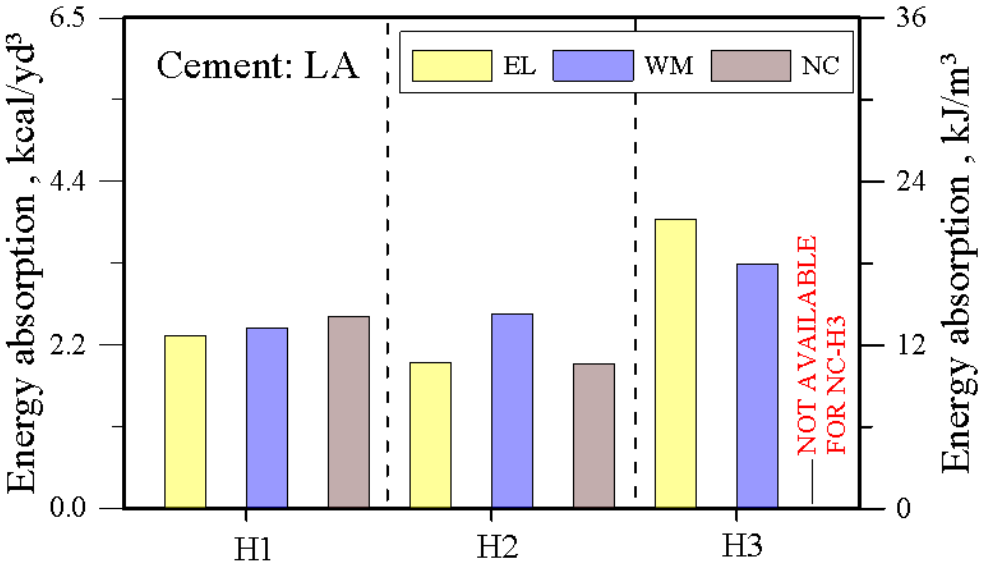
Cement: LA
EL
WM
NC
Energy absorption , kcal/yd³
Energy absorption , kJ/m³
6.5
4.4
2.2
0.0
36
24
12
0
NOT AVAILABLE
FOR NC-H3
H1
H2
H3

(a)

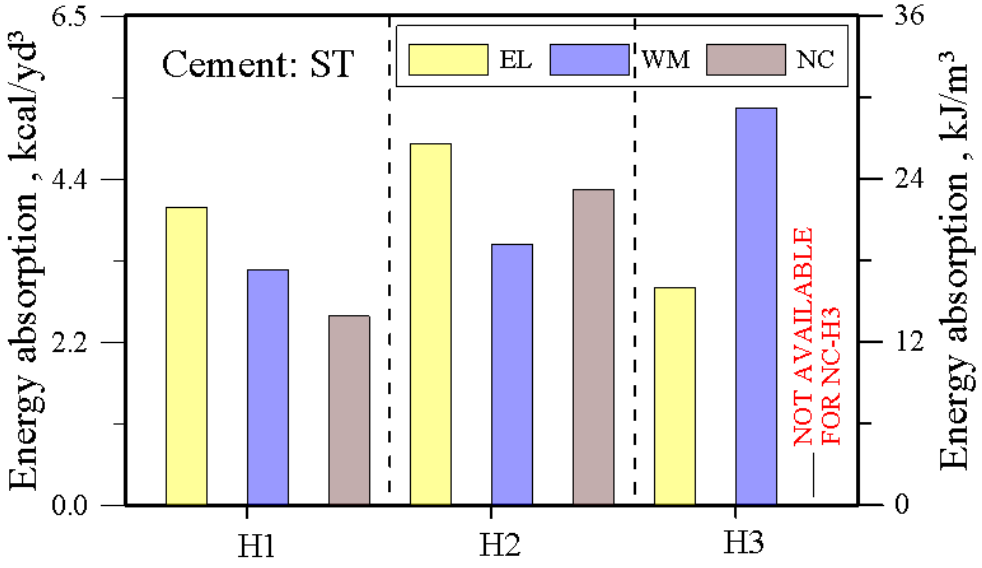
Cement: ST
EL
WM
NC
Energy absorption , kcal/yd³
Energy absorption , kJ/m³
6.5
4.4
2.2
0.0
36
24
12
0
NOT AVAILABLE
FOR NC-H3
H1
H2
H3

(b)

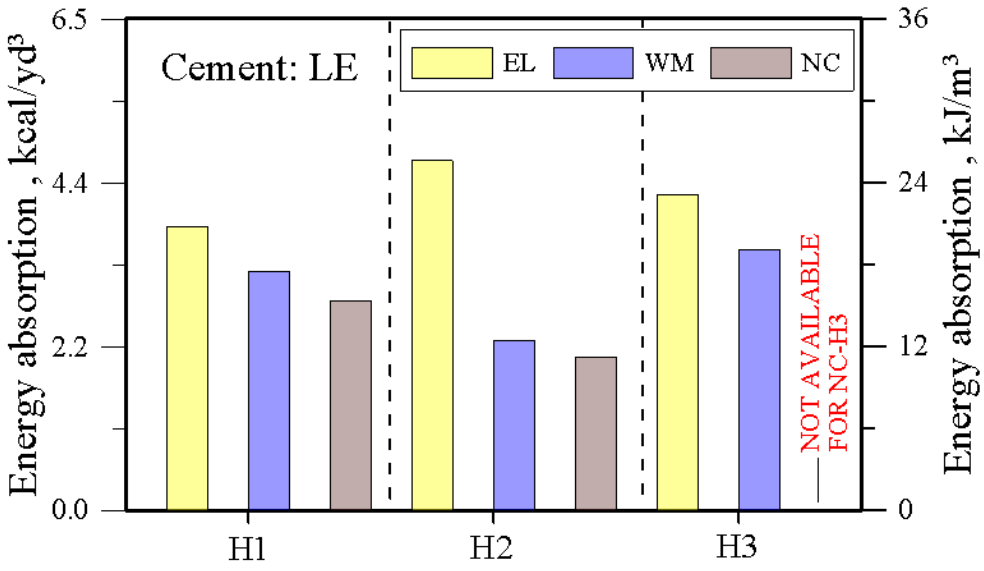

(c)

Figure 5-25 Effects of different variables on energy absorption capacity

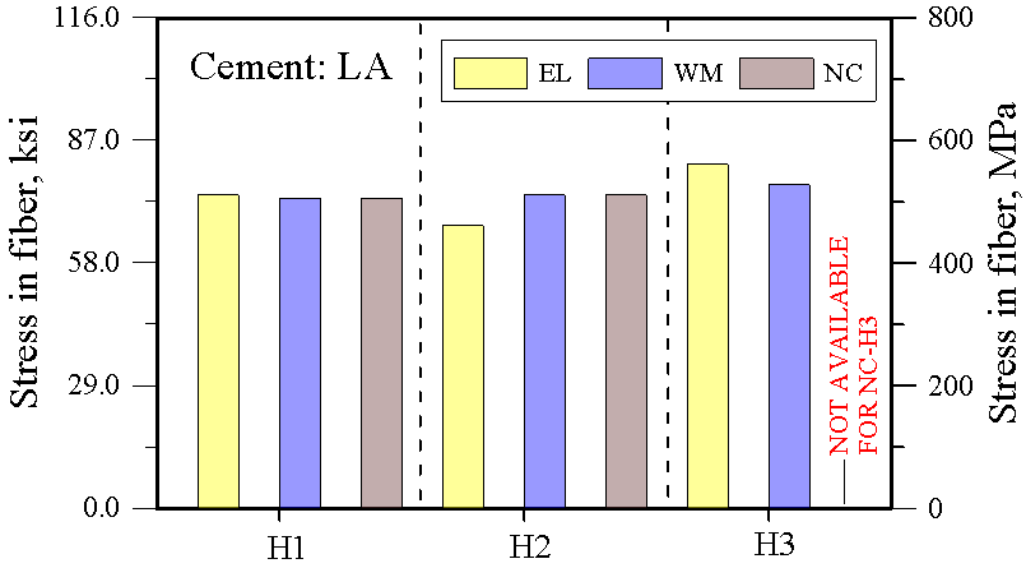

(a)

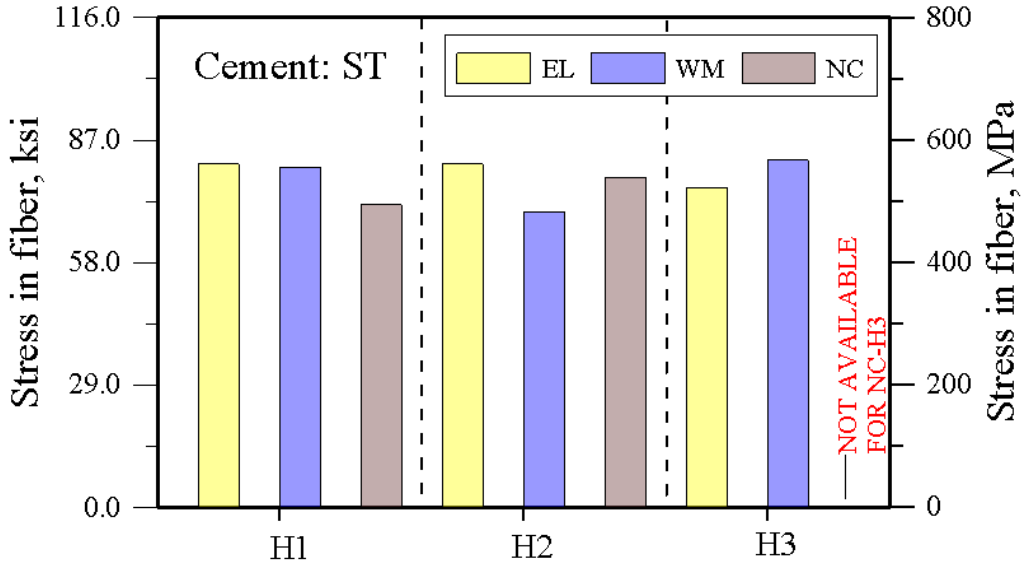

(b)

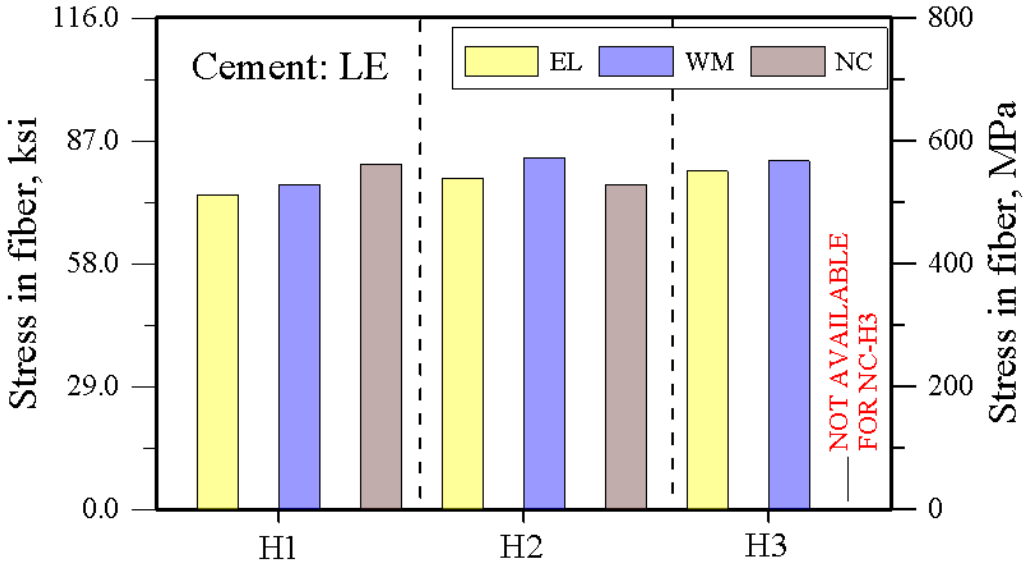

(c)

Figure 5-26 Effects of different variables on average fiber stress

5.5. Effect of fiber characteristics

Mixture ST-EL-H1 was selected to further study the effect of fiber characteristics on UHPC performance. The mix has a good set of workability and mechanical characteristics. The mix turned over within 3 minutes and had a spread of 8.8 in (223 mm). Its compressive and tensile strengths were 22.7 ksi (156.7 MPa) and 1.5 ksi (10.1 MPa), respectively.

The experimental variables were fiber length (0.5 in (13 mm) versus 0.75 in (19 mm)), fiber material (steel versus polymer), and fiber dosage (a volume fraction of 2% versus 1.5%). The properties of the mixes selected for study are shown in Table 5-5. The naming scheme follows the previous one, except that the fiber type and dosage are appended. In Table 5-5, F19 implies 19 mm fiber while F13 refers to 0.5 in (13 mm) fibers, PF (refer to Table 3-5) are polymeric fibers, while the numbers 1.5% and 2.0% refer to the fiber dosage.

The test results for all mixes are shown in Table 5-5 and Figure 5-27. Mix ST-EL-H1-F19-2.0% had a 28-day compressive strength of 23.2 ksi (160.4 MPa) whereas ST-EL-H1-F19-1.5% had a strength of 22.1ksi (152.6MPa). The reduction of 5% is attributed to the lower fiber dosage. A similar slight drop can be seen in ST-EL-H1-F13-2.0% versus ST-EL-H1-F13-1.5%, where the 28 day compressive strength drops from 22.7 ksi (156.7 MPa) to 22.3 ksi (154.2 MPa). The effect of aspect ratio of the fiber does not seem to play a significant role in the compressive strength.

The polymeric fibers (at both dosages) caused almost complete loss of fluidity during mixing. In addition, the 28 day compressive strength is substantially lower than for steel fibers, i.e. 14.8 ksi (106.3 MPa) for ST-EL-H1-PF-2.0% versus 23.2 ksi (160.4 MPa) for ST-EL-H1-F19-2.0%. Clearly, the polymeric fibers selected are not suitable for UHPC.

The post-cracking strengths of ST-EL-H1-F19-2.0% and ST-EL-H1-F13-2.0% are 1.8 ksi (12.6 MPa) and 1.5 ksi (10.1 MPa), respectively. The corresponding strain capacities are 0.5% and 0.17%. As previously discussed, fibers with higher aspect ratios are beneficial for redistribution of stresses after first cracking and promote multiple crack development. These results are also reflected the energy absorption characteristics (61.8 kJ versus 21.9 kJ, respectively). The bonding force is typically related to half the length of the fiber in the composite.

The results pertaining to fiber dosage are mixed. For example, ST-EL-H1-F19-1.5% has the same peak tensile strength (1.8 ksi (12.1 MPa)) as ST-EL-H1-F19-2%. However, mix ST-EL -H1-F13-1.5% had a peak tensile strength that was lower than ST-EL-H1-F13-2.0% (1.1 ksi (7.5 MPa) versus 1.5 ksi (10.1 MPa)).

Table 5-5 Effect of fiber effect on mechanical properties of UHPC

Name	Avg. compressive strength ksi (MPa)		Post cracking strength σ_{pc}, ksi (MPa)	Strain capacity ε_{pc} (%)	Energy absorption capacity g, kcal/yd^3 (kJ/m^3)	Stress in the fibers σ_{fpc} ksi (MPa)
	14 days	28 days				
ST-EL-H1-F19-2.0%	19.0 (131.2)	23.2 (160.4)	1.8 (12.6)	0.50	11.2 (61.8)	101.5 (700.0)
ST-EL-H1-F19-1.5%	19.1 (132.0)	22.1 (152.6)	1.8 (12.1)	0.34	8.9 (48.7)	130.0 (896.3)
ST-EL-H1-F13-2.0%	19.6 (135.0)	22.7 (156.7)	1.5 (10.1)	0.17	4.0 (21.9)	81.3 (561.1)
ST-EL-H1-F13-1.5%	19.4 (134.0)	22.3 (154.2)	1.1 (7.5)	0.15	3.8 (20.7)	80.6 (555.6)
ST-EL-H1-PF-2.0%	12.2 (84.3)	14.8 (102.0)	--	--	--	--
ST-EL-H1-PF-1.5%	13.3 (91.9)	15.4 (106.3)	--	--	--	--

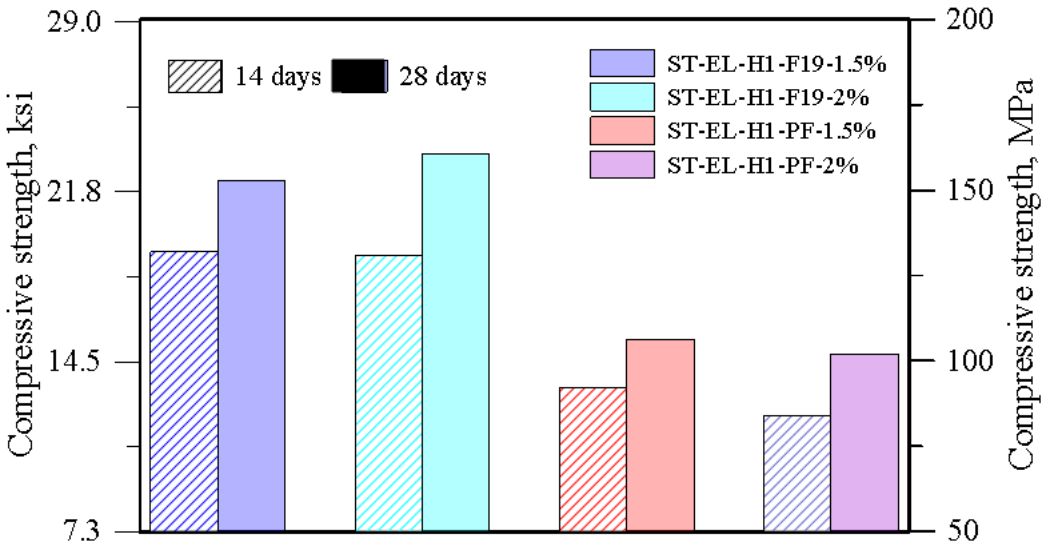

Figure 5-27 Effect of fiber type, length and dosage on mechanical properties of UHPC

5.6. Durability

Unlike regular concrete, which has a large and continuous pore structure, UHPC's dense matrix can provide exceptional durability [5], extend the life of the structure, reduce maintenance costs, and help achieve a more sustainable infrastructure. To evaluate the durability of the non-proprietary UHPC, the properties of several mixtures are investigated by evaluating the presence and distribution of air voids, the ingress of chlorides, and the material's resistance to freeze-thaw cycling. The main experimental variables are the type of silica fume and the amount of superplasticizer. The proportion of the mixture is shown in Table 5-1, three types of silica fumes were studied, which were Elkem-955 (EL(955)), Elkem-965 (EL(965)), and Norchem (NC). In addition, for the EL(965) blend, three different H1 (ViscoCrete 2100 from Sika Inc.) dosages were used: 1.35%, 2% and 3% by weight of the cement, respectively. The previous naming scheme is

employed except that the HRWR dosage is appended. For example, EL(955)-H1-3.0% indicates that Elkem 955 silica fume is used and that HRWR for H1 is 3.0%.

5.6.1. Analysis of air void distribution

Table 5-6 and Figure 5-28 to Figure 5-30 summarize the air void analysis results for UHPC samples by the ASTM C457 modified point count method and linear transverse method. As discussed in Section 4.4.1, the linear traverse method counts the number of voids along a single line, while the point count method determines the number of voids within an area. Figure 5-28 shows the air content measured using these two methods. As can be seen from the figure, there is good agreement between the two methods.

The entrapped air content in the fresh and hardened UHPC mixture can be reduced when a suitable dose of HRWR is used. Typical air content ranges from 0.3 to 6% by volume of the mixture, depending on the composition of the UHPC [35]. In this study, the results from the figure show that the air content for different UHPCs ranges from 4.5% to 6.2%. The type of silica fume does not seem to affect the air content. For example, the air content for EL(955)-H1-3.0%, EL(965)-H1-3.0%, and NC-H1-3.0% varies in a tight range from 4.5% and 4.8%, respectively. The trapped air is larger than 1 mm in size, and the contents are 1.4%, 0.8%, and 0.5%, respectively. For EL(965)-H1-1.35%, less workability leads to more entrapped air which cannot escape from the paste because of the high viscosity of the mixture. Poor workability also leads to a higher content of air in the cavities and pores of the capillaries which have a significant impact on the durability properties. Figure 5-29 shows the air void distribution on the surface of the specimen for EL(965)-H1-1.35% where significant entrapped air bubbles can be seen.

The Powers' spacing factor is the most important indicator of the durability of the cement paste in terms of freezing and thawing resistance. For ordinary concrete, the maximum value of the spacing factor for moderate exposure to concrete is typically 0.20 mm. Although this indicator may not be suitable for determining an appropriate measure of freeze-thaw resistance in UHPC, considering the Powers' spacing factor essentially estimates the mean thickness of the paste fraction surrounding the air void under the assumption that all the voids are monosized spheres located at the center of a cube. The volume of an array of such cubes packed together, along with the inclusive air voids, is equal to the combined volume of air and paste in the concrete [94]. Since the specific surface is an indicator of the average void size on the matrix surface, the Powers' spacing factor hence give an approximation of how close the air voids are to each other. In essence, a larger value indicates lower resistance to freeze-thaw.

Information on the air void size distribution as measured by the linear traverse method is shown in Figure 5-30. It is well-known that the dose of HRWR affects the workability of the paste, and a proper addition of HRWR results in better compaction and reduced air void size. According to the test results, the most common air void size (in all mixes) is between 500-1000 μm. If this is defined as the upper limit of the entrained air void, it can be seen that the distribution of finer air voids is almost identical in all mixtures and the cumulative air void content ranges from 3.2% to 4.4% (see Table 5-6). In addition, it can be seen from the Table 5-6 and Figure 5-30 that EL(965)-H1-1.35% has a relatively high amount of entrapped air content (> 1 mm) of 2.3%. Poor workability leads to more entrapped air during mixing and casting which cannot escape from the paste.

Table 5-6 Air void analysis results for different mixes

Mixture	Modified Point Count Method			Linear Traverse				
	Paste	Total Air	Total Agg.	Total air	Entrained air	Entrapped air	Powers' spacing Factor	Specific Surface
	%	%	%	%	%	% > (1 mm)	mm	1/mm
EL(955)-H1-3.0%	57.5	4.8	37.9	4.5	3.2	1.4	0.644	11.19
EL(965)-H1-1.35%	56.5	7.1	36.5	6.2	4.0	2.3	0.590	10.35
EL(965)-H1-2.0%	48.3	4.9	46.9	4.9	3.5	1.4	0.677	9.44
EL(965)-H1-3.0%	46.8	4.5	48.8	4.5	3.7	0.8	0.583	11.34
NC-H1-3.0%	60.2	4.3	35.5	4.8	4.4	0.5	0.547	12.82

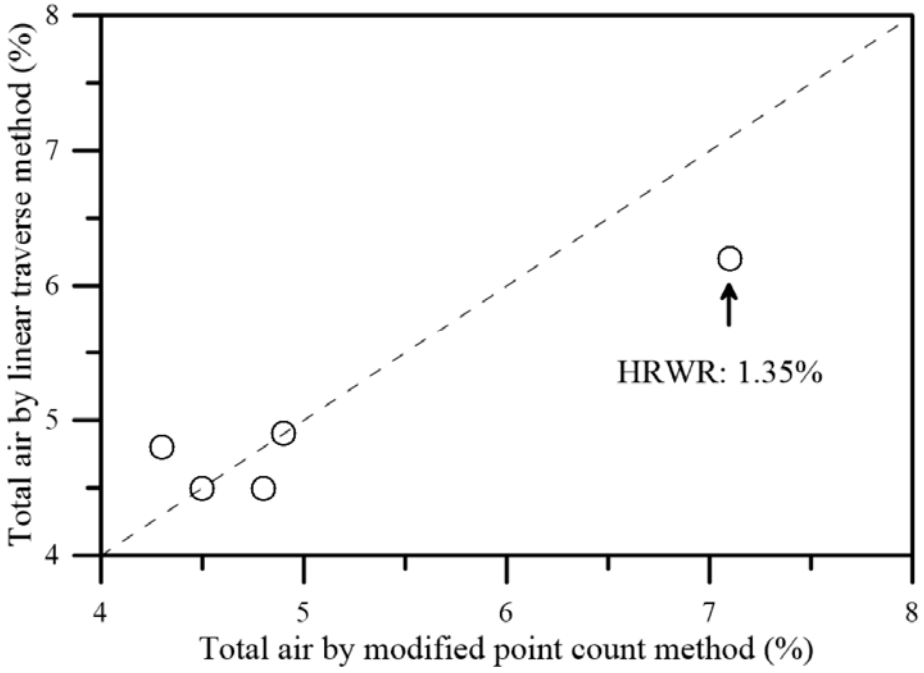

Figure 5-28 Comparison between modified point count method and linear traverse test method

EL:965-H1-1.35% EL:965-H1-2% EL:965-H1-3%

Figure 5-29 Air void profiles for the UHPC mixes with different HRWR contents

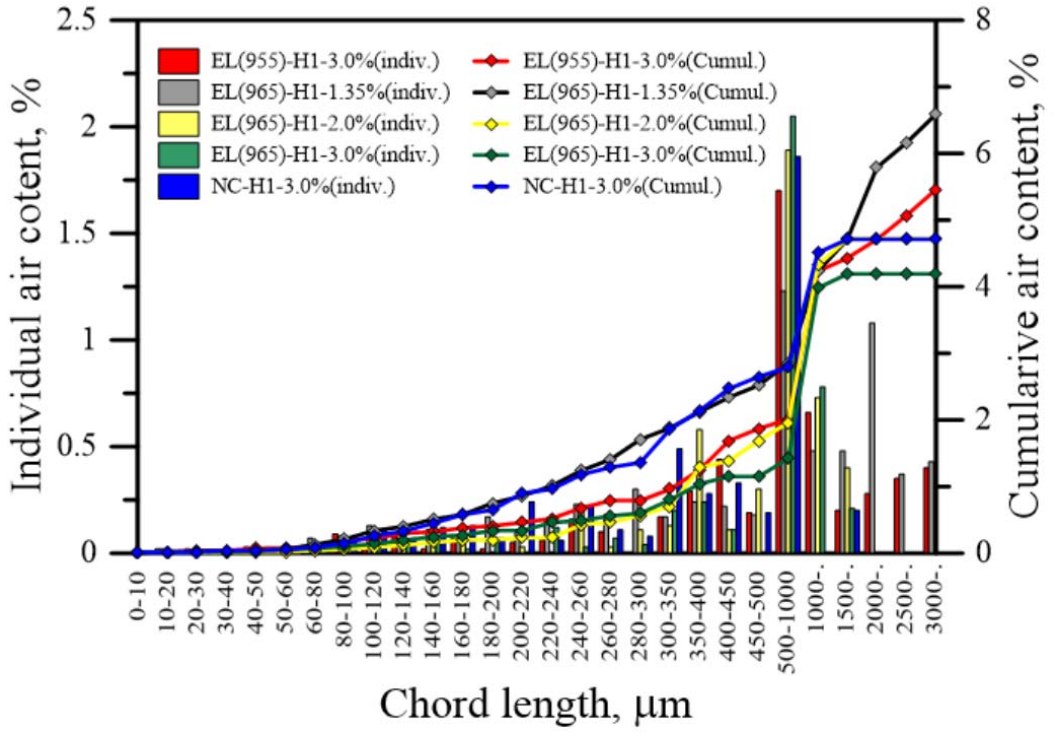

Figure 5-30 Air void size distribution based on the chord length from linear traverse method

5.6.2. Chloride penetration resistance test results

The ASTM C1202 test methodology is used to determine the chloride penetration resistance of UHPC (see Section 4.4.2). All tests were conducted after 28-days of water curing. After curing, the specimens were removed from the water and excess water blotted off. The specimens were then sealed in an airtight can in order to keep the specimen in an environment with 95 % relative humidity. Each specimen was then mounted on the voltage cell and rubber gaskets and sealants were used to seal the specimen-cell and its boundary to avoid liquid outflow.

Chloride penetration measures the coulombs passed through a vacuum saturated cylinder exposed to a current for 6 hours. During the test, the temperature ranged between 70 °F (20 °C) to 80 °F (25 °C). The current was read and recorded every 30 min. The UHPC mixtures used in this test did not contain steel fibers; since these fibers are not interconnected within the mixture, they are not expected to affect the results of this test.

The RCPT results for all UHPC mixes are shown in Figure 5-31. The total charge passed for EL(955)-H1-3%, EL(965)-H1-1.35%, EL(965)-H1-2.0%, EL(965)-H1-3.0%, and NC-H1-3.0% is 26.5 Coulombs, 22.0 Coulombs, 33.0 Coulombs, 31.0 Coulombs, and 38.5 Coulombs, respectively. It can be seen from these results that all UHPC specimens showed a very low chloride ion penetrability, well below 100 Coulombs. According to ASTM C1202, the test demonstrates that the UHPCs considered has low chloride ion penetration at 28-days, which could be classified as negligible. This is in contrast to regular concrete with a water-cement ratio of 0.35, which passes 2290.0 Coulombs and regular concrete with a water-cement ratio of 0.4, which passes 5445.0 Coulombs.

It is not surprising for UHPC to have extremely low or negligible chloride ion penetration characteristics. As discussed in [5], partial replacement of cement by GGBS provides the best resistance to chloride ion permeability. This is believed to be due to the use of a lower water-cement ratio, the high dispersion in voids and the refinement of the pore structure characteristic of UHPC. Also, the GGBS acts as a filler material and yields a significant reduction in the total charge passed.

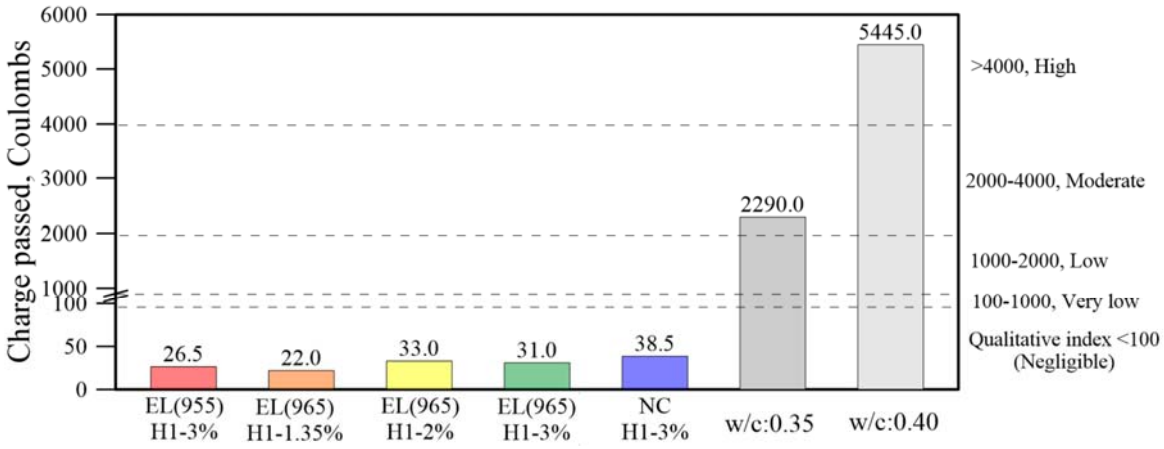

Figure 5-31 Total charge passed for UHPC and regular concrete

5.6.3. Freeze-thaw (F-T) resistance of UHPC

The specimens were subjected to fast freeze-thaw testing in 3% sodium chloride (NaCl) salt solution. The change in mass and relative dynamic elastic modulus were measured during the test. Before the F-T test, the water absorption behavior is characterized by the moisture uptake of 2.8 in (70-mm) thick specimens with the test surface immersed 0.2 in(5-mm) in a 3% salt and water solution. The test results are shown in Figure 5-32. It can be seen from this figure, there is initially a rapid development with the square-root of time during the pre-saturation stage, which is due to the typical capillary suction process occurring in well-connected pores. This gradually

tapers off and transitions into a diffusion-controlled slow process. The whole process takes about 250 hours, which is obviously longer than regular concrete. In addition, Figure 5-32 shows that all mixes tested had a very low water uptake percent, lower than 0.4% for all the mixes, while regular concrete will absorb more moisture, approximately 1% [117]. This means that lower capillary porosity absorbs a small amount of water and is less prone to saturation, translating into higher resistance to freeze-thaw cycles and chloride and sulfate penetration.

An additional behavior that occurs during the freeze-thaw cycle is mass change, the specimens lose mass as surface scaling occurs. The total amount of surface scaling after 96 cycles of freeze-thaw is as shown in Figure 5-33. The figure indicates a very slight scaling for all mixes and their range varies from 84 to 142 g/m^2. Studies have concluded that the mass loss due to surface scaling in UHPC is well below the limiting values (1000–1500 g/m^2) [36,118].

The relative dynamic modulus (RDM) provides a reliable measure for evaluating internal frost damage, and is calculated as follows

$$\boldsymbol{RDM\%} = \frac{\boldsymbol{n_c^2}}{\boldsymbol{n^2}} \times \mathbf{100} \qquad \textbf{Equation 5.5}$$

where c is the number of cycles of freezing and thawing, n_c is the resonant frequency after c cycles, and n is the initial resonant frequency (at zero cycles). The RDM result are shows in Figure 5-34. The RDM values of the specimens did not show an obvious drop during the freeze-thaw cycles and they always varied from 97 to 100 % of the initial value. This can be attributed to the optimal particle packing density in UHPC, which can strongly decrease the void connectivity within the concrete matrix; therefore, although scaling damage existed, the RDM value did not show a clear change, indicating no internal damage.

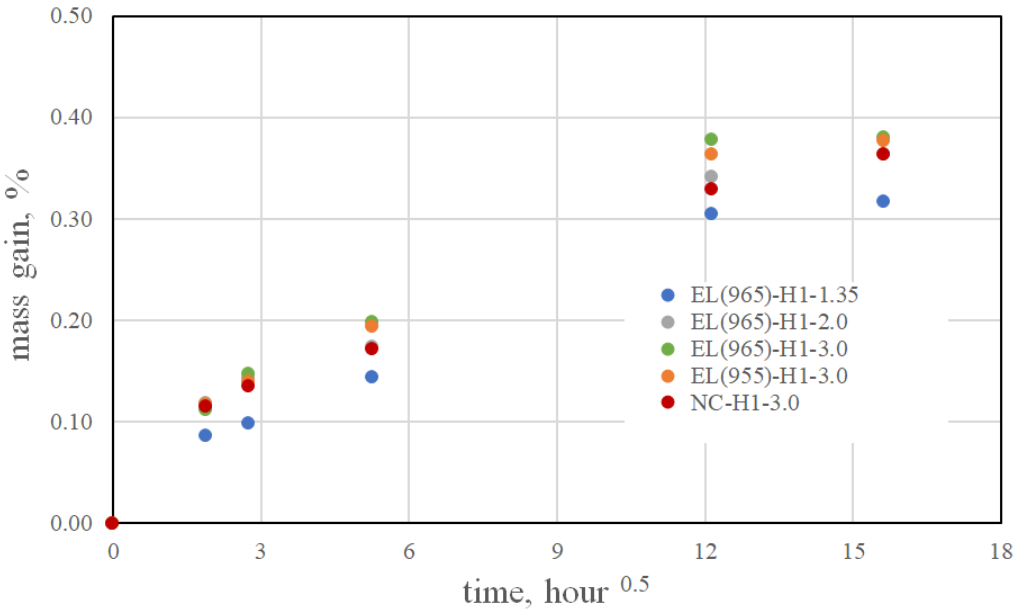

Figure 5-32 Moisture uptake curves of UHPC

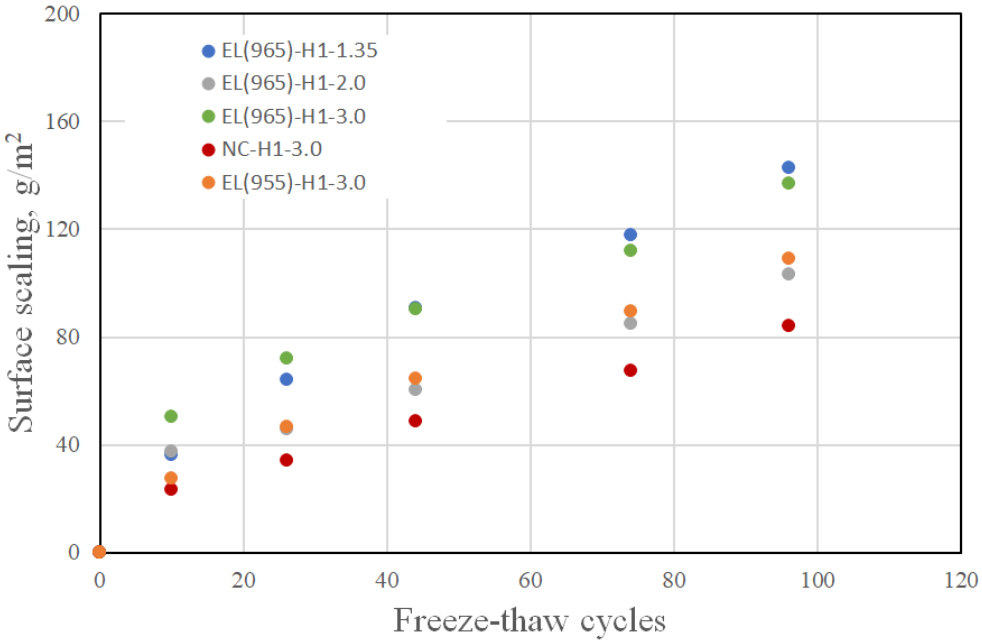

Figure 5-33 Evolution of the surface scaling for UHPC

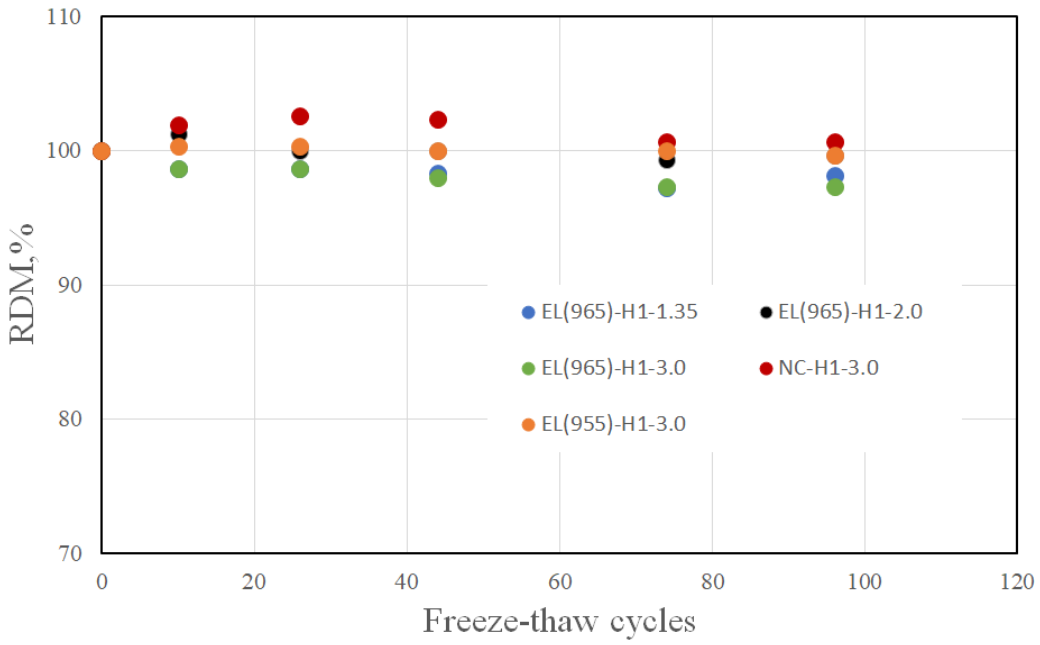

Figure 5-34 Effects of freeze-thaw cycling on the relative dynamic modulus of UHPC

6. SCALING UP TO FIELD IMPLEMENTATION

6.1. Introduction

This chapter outlines efforts undertaken to achieve a successful field application using the developed UHPC mixes. Four variants of the mixes discussed in Chapter 5 are considered candidates for field application. The experimental variables are the amount of superplasticizer and fiber length. Due to the sensitivity of mixing to the composition of silica fume, especially the carbon content and the activity of cement, larger dosages of HRWR are explored to ensure suitable workability for field applications. Three different doses of HRWR (i.e. 2.0%, 3.0%, and 3.5%) are considered. Also, two different fiber lengths (0.5 inch [13mm] and 0.75 inch [19 mm]) are considered. The mix proportions by weight are shown in Table 6-1 and the specific materials used are discussed later on.

Table 6-1 Field mix proportions (by weight)

No	w/c	Ordinary Portland Cement Type I	GGBS	Silica Fume	HRWR (%)	Silica Sand		Steel Fiber	
						Sand A	Sand B	Length inch (mm)	V_f (%)
1	0.22	0.5	0.5	0.25	2	0.30	1.21	0.75 (19)	2.0
2					2		1.21	0.5 (13)	2.0
3					3		1.21	0.5 (13)	2.0
4					3.5		1.20	0.5 (13)	2.0

6.2. Laboratory trial batches

Laboratory mixing was done as outlined earlier in Section 4.1. After mixing was completed, the rheology of the UHPC mix was assessed by measuring spread as outlined in Section 4.2.1. The

compressive strength is obtained from cubes tested as outlined in Section 4.3.1 while tensile strength is obtained using coupons tested as indicated in 4.3.2. Table 6-2 summarizes the properties of the four trial mixes. Table 6-2 clearly confirms the beneficial effects of the longer steel fibers, where Mix 1 (with 0.75 inch [19 mm] fibers) has a larger strain at peak tensile stress than the other mixes with 0.5 inch (13 mm) fibers and a larger peak tensile strength, e.g. 1.87 ksi (12.9 MPa) versus 1.38 ksi (9.5 MPa) for Mix 3. The longer fibers also lead to a slightly higher compressive strength than the shorter fibers, e.g. Mix 1's 28 day strength is 25.5 ksi (175.7 MPa) versus 24.6 ksi (169.2 MPa) for Mix 2. These results are consistent with the results outlined in Chapter 5.

As also seen in Chapter 5, the 28 day compressive strength decreases with increasing amount of superplasticizer, e.g. the 28 day strength of mix 2 drops from 24.5 ksi (169.2 MPa) to 22.0 ksi (151.9 MPa) for mix 4, a 10% drop (Table 6-2). This is true also for tensile strength. The effects of using GGBS are also evident, where the strength keeps rising substantially beyond 28 days, where an additional 2.5-2.9 ksi (17-20 MPa) strength is gained by 56 days. Synthesizing all the results, it is clear that Mix 3 provides a good compromise between flowability and strength and was selected for the field pour.

Table 6-3 shows the amount and cost per cubic yard (in 2017 dollars) of the main components of Mix 3. It also lists specific materials used and other alternative materials that were explored. It is important to note that not all combinations of materials yielded good results. For example, the Norchem silica fume had a high carbon content and could only be mixed successfully with the Sika HRWR and not the other two candidates.

Table 6-2 Mechanical properties of laboratory and field batches

No	Spread *inch* (mm)	Compressive strength *ksi* (MPa)				Tensile strength *ksi* (MPa)	Strain at peak tensile stress (%)
		7-d	14-d	28-d	56-d		
1	8.4 (214)	17.6 (121.3)	21.6 (149.1)	25.5 (175.7)	28.5 (196.2)	1.87 (12.9)	0.41
2	8.4 (215)	17.1 (118.2)	21.4 (147.8)	24.6 (169.2)	27.2 (187.4)	1.6 (11.1)	0.17
3	9.3 (235)	17.2 (118.8)	20.8 (143.5)	23.1 (159.0)	25.6 (176.4)	1.4 (9.5)	0.18
4	9.4 (238)	16.4 (113.4)	19.9 (137.1)	22.0 (151.9)	---*	1.4 (9.6)	0.14
Field mix	9.4 (238)	15.8 (108.9)	18.4 (127.0)	21.5 (148.1)	---*	1.2 (8.3)	0.13

*Specimens not tested. Not enough were made due to an oversight.

Table 6-3 Cost per component of Mix 3 in 2017 dollars

Component	Quantity per Cubic Yard of UHPC (lb)	Cost per yard (% of total)	Trade Name or Supplier	Alternate Trade Names or Suppliers*
Portland Type I	650	$44.4 (5.0%)	St. Mary	Lafarge, Lehigh
GGBS	650	$38.5 (4.3%)	St. Mary Grade 100	Lafarge (Grade 100 or 120)
Silica Fume	327	$71.7 (8%)	Elkem Microsilica 955	Norchem, Washington Mill
HRWR	39.2	$56.5 (6.3%)	*Sika* ViscoCrete®-*2100*	Euclid Chemical: Plasto 6400, GCP Applied Technologies: ADVA® Cast 575
Sand A	395	$10.7 (1.2%)	US Silica F75	Fairmount Santrol
Sand B	1580	$42.9 (4.8%)	US Silica F12	Fairmount Santrol
Steel Fibers	265	$628 (70.4%)	Nycon	Bekaert
Total cost		$892.7		

*The majority, but not all combinations, of these materials resulted in a successful mix

6.3. Field demonstration of UHPC application

UHPC was utilized on a bridge repair project located on Kilgore Road over the Pine River (Structure No. 10091), Kenockee Township, MI. The location of the project is shown in Figure 6-1 (a). The bridge is 44.7 feet long and 21.4 feet wide (Figure 6-1(b)). The repair effort using UHPC entailed replacing the joints connecting the reinforced concrete slabs, i.e. a closure pour (Figure 6-2(a)).

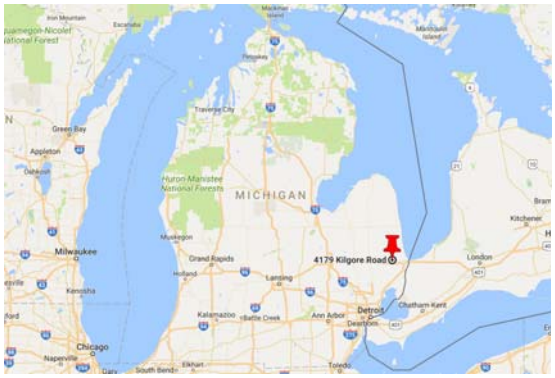

(a) Location of UHPC deployment in the State of Michigan

(b) Bridge site

Figure 6-1 Bridge repair plan and site

(a)

(b)

Figure 6-2 (a) Closure pour and (b) transportation of UPHC to pour location

6.3.1. Mixing equipment

Mixing was carried out by a Michigan-based contractor employing the mix protocol used in the lab and accomplished using two Mortarman 360 MBP pan mixers with a capacity of 8 cubic feet. Each mix was limited to 5.5 cubic feet because higher mix loads led to mixing difficulties in preliminary field mix experiments. The material's viscosity increases dramatically at turnover and the mixer's engine was noted to labor noticeably at higher mix loads and even stall. Once

successfully mixed, the material was discharged from the mixer into wheelbarrows for transportation to the pour location. The UHPC was then poured into hoppers, which directed the flow of UHPC into the joints (Figure 6-2 (b)). The hoppers were eventually deemed not useful and abandoned about half way into the pour. The flowability of UHPC requires well-constructed formwork to eliminate leakage. Threaded rods and nuts were used to ensure that the bottom formwork did not leak (Figure 6-2 (a)).

6.3.2. Mixing process

Construction took place on a hot summer day. The temperature was forecast to range from 73 °F to 89 °F. The high temperature prompted concerns about water evaporation during mixing. Since UHPC uses a small w/c ratio, loss due to evaporation could result in a degradation in the fresh and hardened properties of UHPC. The ambient temperatures during a few batches are summarized in Table 6-4 along with the measured mix temperatures. The latter are generally higher than the former due to the mixing energy imparted to the mix and heat of hydration.

Table 6-4 shows that, in general, the turn over time is substantially less than that observed with the Hobart mixer in the lab. It is not clear why that is the case, especially because the field mixer is slower than the lab mixer. However, it is possible that the field mixing attachments are more effective than the lab mixer in inducing shear into the mix. The general trend of faster turnover time with larger mixer was actually observed in the lab when larger mixers were employed in the pilot study, although not to the extent seen in the field mix. Two other observations are evident from Table 6-4. First, turnover time increases somewhat with ambient and mix temperatures, and second, the spread drops significantly as the mix temperature increases.

Table 6-4 UHPC fresh test results

Batch	Turnover Time	Ambient Temperature (˚F)	Mixture Temperature (˚F)	Spread inch (mm)
1	1’30”	75	80	9.4 (238)
3	2’05”	77	95	7.9 (200)
4	2’30”	78	86	9.1 (231)
7	2’45”	80	85	8.7 (220)

The first batch was mixed at an ambient temperature of 75 ˚F. The mix temperature peaked at 80 ˚F and the spread was 9.4 in (238 mm). The ambient temperature for the 2nd batch was 77 ˚F, but the mix temperature rose to 95 ˚F. The increased mix temperature caused a marked reduction in spread, decreasing to 7.9 inch (200 mm) from 9.4 inch (238 mm) for the first batch.

To address the adverse effects of high mix temperature and with the knowledge that the temperature would rise as the day progressed, cubed ice was added as a replacement for some of the mix water as recommended in [5]. On site experimentation showed that a 40% replacement yielded good results and kept the mix temperature to below ~ 85˚F, which seems to be a point beyond which the spread drops quickly. Figure 6-3 shows the steps of the field mixing process.

(a) Addition of ingredients

(b) Dry mix

(c) Addition of liquid with cubed ice

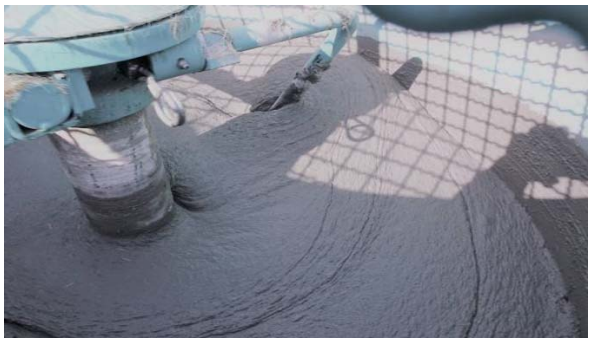

(d) Mix dispersion and homogenization

(e) Addition of steel fibers

(f) Flow test on UHPC

Figure 6-3 Field mixing process

6.3.3. Casting process

UHPC was cast at a rate that did not allow it to flow too far during placement in order to minimize preferential alignment of the fibers in the direction of flow. This was done by starting

the casting process at one end of the joint and proceeding to the other end at a speed comparable to the flow speed of the fresh mix. The forms can be coated or pre-wet to ensure that they do not absorb water. The latter route was selected as the more practical solution. The surface of existing concrete and the rebars were also pre-wet to prevent the mix from losing water to the dry surfaces (Figure 6-4 (a)). Once casting was carried out, top forms were added to promote expulsion of trapped air and reduce surface dehydration (Figure 6-4 (b)).

(a) Pre-wetting and placement (b) Top forms after placement

Figure 6-4 Casting of UHPC into the longitudinal connection

6.3.4. Post-curing inspection

After the formwork was stripped (1 day after construction day), the top surface of the UHPC joints was seen to have some small holes and shrinkage cracks (Figure 6-5). These defects are attributed to two factors: 1) dehydration of the top layer associated with the extremely hot weather during construction day, and 2) entrapped air rising during curing. Nevertheless, a close examination showed that the underlying material is sound.

(a) Poured UHPC connection

(b) Shrinkage cracks on the surface

Figure 6-5 Field cast result

6.3.5. Comparison between lab and field properties

Cubes and coupons were made during field mixing in order to compare field properties to lab values. As with the lab program, cube testing of the field mix was done according to ASTM C109. As shown in Table 6-2, the 7-days, 14-days, and 28-days compressive strengths are 15.8 ksi (108.9 MPa), 18.4 ksi (127.0 MPa), and 21.5 ksi (148.1 MPa). The tensile strength is 1.2 ksi (8.3 Mpa), also shown in Table 6-2.

The 28-day compressive strength of the field mix is 1.5 ksi (10 MPa) less than the lab one. The tensile properties of the field mix are also lower than those the lab one. For example, the tensile strength is 1.2 ksi (8.3 MPa), which is less than 1.3 ksi (9.3 MPa) for the lab mix. The strain at peak tensile stress is 0.13%, which is less than that seen in the lab mix (0.18%). Two hypotheses are advocated to help explain this discrepancy. The first is that it is possible that the hot weather caused mix water to evaporate rapidly, thereby compromising hydration. The second is that the mixer, while efficient at turning over the mix quickly, did not achieve uniform enough mixing causing incomplete dispersal of the mix constituents. In spite of these relatively small

discrepancies, the field mix hardened properties do not differ too much from their corresponding lab mix values.

6.4. A note about cost

To satisfy the requirements of the Michigan Department of Transportation, the material utilized in this project used constituent components that were available on the open US market. At $2.37 per pound, the steel fibers, in particular, were the most expensive component (refer to Table 6-3 for cost and percentage of total cost). Fiber costs will likely drop with increasing demand. At present, several suppliers outside of the United States produce steel fibers at a reduced unit cost. For example, a recent web search showed multiple Chinese suppliers offering high strength steel fibers for $0.30 per pound. Using these suppliers, and assuming that the fiber quality is similar to the US products, will dramatically reduce the current cost of a non-proprietary UPHC mix per cubic yard to $344 from $892.7 (Table 6-3). Another cost reducing step is to decrease the amount of steel fibers from 2% to 1.5% by volume. Research documented in [1] showed that this lower level of fiber dosage still yields a material with good short term and long term properties. However, even with a reduced cost, UHPC is still a relatively expensive material, although its extremely high durability has the potential to significantly reduce life cycle costs. Research is needed to fully evaluate the long term benefits, which are likely considerable.

6.5. Summary and conclusions

This chapter reported on a field construction project using a non-proprietary blend of UHPC. The properties of the material as mixed in the lab were first discussed and then the field

pour project was described. Then, the properties of the field mixed materials were compared to those seen in the lab and the cost of the UPHC discussed.

Casting UHPC on a warm day led to two complications: 1) a reduction in the spread (flowability) because the excessive temperature compromised the effectiveness of the HRWR, and 2) the potential for evaporation of water during mixing and placement. To address the former, it was recommended that about 40% of the mix water should be replaced with ice. Substantially hotter days will require greater ice quantities, which can be ascertained by trial and error. The objective is to cool the mix to less than 85 ^{o}F to ensure effectiveness of the superplasticizer. The latter issue can only be resolved by speeding up the mixing and placing processes.

The 28 day compressive strength of the field-mixed material is 21.5 ksi (148.1 MPa), which is about 1% less than the 21.7 ksi (150 MPa) needed to define the material as UHPC. However, the 28 days strength is misleading in this case because the material continues to gain substantial strength due to the use of GGBS. To address this issue, it seems reasonable to specify an acceptance limit for UHPC that includes a tolerance. For example, a limit of 20.3 ksi (140 MPa) at 28-days or with the caveat that the material reaches 21.7 ksi (150 MPa) at 56 days. FHWA recommends a limit of 21 ksi (145 MPa) at 28-days.

7. SUMMARY, MAJOR CONCLUSIONS AND FUTURE RESEARCH

7.1. Summary

The objective of this project was to systematically investigate the characteristics of non-proprietary UHPC, while considering cost optimization, feasibility of field construction, and providing relevant information for the development of a special provision for field use of UHPC. The specific research objectives were: 1) Understand why an earlier UHPC mix did not scale up for field application; 2) Conduct further optimization studies of fibers and cementitious components, to determine the range of material properties that will lead to a successful larger scale mix regardless of potential sources of key ingredients; 3) Provide material properties for engineering design and specifications; and 4) Demonstrate constructability of the mix on large scale closure pours in a field environment.

The first phase of the work examined the fresh, short-term and long-term properties of UHPC. These tests were conducted to develop the knowledge required to control the quality of the non-proprietary UHPC developed in this project. Next, to ensure that the non-proprietary UHPC investigated in this study is truly generic, its components were sourced from multiple vendors. In particular, the ordinary Portland Type I cement, silicon fume, and high range water reducer used in this research were each obtained from three different suppliers to study the effect of material sources on UHPC performance. Another test variable was the slag activity level of GGBS (two levels considered) and the impact of GGBS content on UHPC properties. In particular, a key question that was explored was how much cement can be replaced by GGBS. Tests conducted included workability, hydration heat, autogenous shrinkage, freeze-thaw, rapid chloride

penetration and air void distribution. Steel fibers with two different aspect ratios were also investigated and the possibility of replacing steel fibers with polyethylene fibers was also explored.

7.2. Why field-mixing failed in the previous project

A previous project funded by MDOT developed a generic, cost-optimized UHPC mix (named MI-UHPC) that performed exceptionally well in the lab but could not be mixed during field trials. The results of this project shed light on the reasons why the field-mixing process failed in the previous project.

The lab mix used in the previous project employed 900W silica fume, an undensified product from Elkem, Incorporated, with a 0.6% carbon content. The field mix employed PCA-DSF, a densified silica fume from Premiere TM Concrete Admixture Company that had a carbon content of almost 10%. The fact that the silica fume in the field mix was densified posed an additional challenge for the mixer as it tried to deagglomerate the material and sufficiently disperse it during dry mixing. The high carbon content was another issue and likely more important problem. Research in this project showed that increasing the carbon content will increase the demand for water, which could impede mixing unless a sufficient amount of HRWR is added. In the previous project, the amount of HRWR used was too low (at 1.35% by weight of the cement) to permit mixing. The research in this report suggests that mixing of generic UHPC is feasible as long as a sufficient amount of HRWR is provided and the mixer has sufficient capacity to turn over the mix.

7.3. Major Conclusions

The following conclusions can be made based on the investigations in this work:

- Field efforts to mix generic UHPC in an earlier project failed for four key reasons: 1) the silica fume used in the field had a high carbon content, which drove up water demand, 2) the dosage of the high range water reducer (HRWR) was too low to compensate for the higher water demand, making mixing more difficult, 3) the silica fume was a densified product that posed an additional challenge for the mixer as it tried to deagglomerate the material and sufficiently disperse it during dry mixing, and 4) the field mixer did not have sufficient capacity to induce turnover in the wet mix, compromising the mixing process.
- Results from this research project showed that generic UHPC can be successfully mixed using components sourced from a variety of suppliers as long as a proper HRWR dose is selected. An appropriate HRWR dosage can be identified through field trial batches in order to achieve a mix that meets the required performance criteria and can be mixed in the field.
- The proposed mixing protocol reduces the burden on field mixers, allowing for larger mix loads in the field.
- With few exceptions, the 28-day compressive strength and peak tensile strength of all mixtures (sourced from the various suppliers considered in this work) were higher than 21.7 ksi (150 MPa) and 1.2 ksi (8.3 MPa), respectively, fulfilling the minimum requirement for field-cast UHPC. This means that truly generic UHPC is feasible to produce. Proposed Special Provisions for making generic UHPC are provided in Appendix C.
- One of the critical performance indicators of UHPC is its flowability. Insufficient flowability can result in porous and inhomogeneous structures as well as poorly packed samples. On the other hand, excessive workability may result in the segregation of the paste. A reasonable spread is between 7 in and 12 in.

- Polycarboxylate-based HRWR was used in UHPC to increase the workability of the paste. The test results showed that there was a mild, inverse relationship between HRWR dose and compressive strength of UHPC. It is speculated that this adverse effect is due to the increase in polymer surface coverage and effective layer thickness around the UHPC particles. In order to balance the fresh and hardened properties of UHPC, a dosage of HRWR of between 1.5% and 3% by weight of cement is suggested.
- Testing showed that the HRWR dosage has a minor effect on the void distribution and content of UHPC. All UHPC formulations tested had excellent resistance to freeze-thaw and chloride ion penetration.
- Partial replacement of cement by GGBS can improve the workability of UHPC paste, lead to favorable self-consolidating characteristics and reduce air voids and porosity. The tests results showed the total amount of air void in the concrete decreases with the increase in the amount of replacement GGBS, which is beneficial for the durability of UHPC. An optimal replacement value of 50% by weight is recommended based on the test results.
- The test data showed that the aspect ratio of the steel fibers seems to play a relatively minor role in the compressive strength of UPHC. However, a higher aspect ratio is beneficial for redistribution of stresses after first cracking under tensile load and promotes multiple crack development, which enhances energy absorption characteristics.
- Reducing the steel fiber volume fraction from 2% to 1.5% also has a mild effect on the compressive strength (a 5% reduction was observed).
- High levels of carbon content in the silica fume can cause the demand for water to increase during mixing, making mixing more difficult. Although successful mixing can still be achieved by increasing the HRWR dosage, the increase in HRWR usage can cause a mild

reduction in the material's hardened performance, as noted in earlier conclusions. To maximize the chances for successful mixing, it is best to use silica fumes with low carbon content. It is recommended that the percentage of carbon be 2% or less in the silica fume used. The silica fume should also be of the undensified type to facilitate dispersal during dry mixing.

- Field application of non-proprietary UHPC was successfully achieved for the Kilgore Road Bridge Restoration Project on the Pine River in Kenockee, Michigan. Key lessons learned during the field operation include:
    - Mixing during warm days can cause the mix to become too hot, adversely affecting the effectiveness of the high range water reducer and significantly decreasing the workability of mix. The adverse effects of high temperatures can be alleviated by replacing some of the mix water with cube ice or the casting process can be done at night. Field experiments showed that 40% replacement yielded good results, but the actual replacement amount depends on how hot the mix becomes. It is recommended that the mix should not exceed 85 degrees F.
    - The 28-day compressive strength of the field-mixed material was about 1% less than that required to define the material as UHPC. However, in this case, the 28-day strength is misleading because the material continues to gain substantial strength due to the use of GGBS. To solve this problem, it is necessary to specify acceptance limits for UHPC that include appropriate tolerances at 28 days provided that the full strength is reached later on, say by

56 days. For example, a compressive strength of 20 ksi at 28 days may be acceptable, provided 21.7 ksi is eventually reached at 56 days.

7.4. Commercial Potential of UHPC

The non-proprietary UHPC mixes developed in this work have strong potential for use in structures that will be significantly more durable than currently possible with conventional materials. The note in El-Tawil et al. [5] about cost is still valid as of the writing of this report:

> "The current cost of a cubic yard of the nonproprietary UHPC developed in this work is … roughly 5x the present cost of regular concrete. Using [overseas supplier for the steel fibers] … will reduce the current cost of UHPC (including fibers) to $325 per cubic yard, which is only about twice the cost of regular concrete. For an initial increase in material cost compared to regular concrete, whether 2x or even 5x, the benefits of UHPC can be substantial compared to traditional concrete products … With durability that boasts virtually no deterioration after 60+ cycles of freeze-thaw and almost no chloride penetration, UHPC structures will have extremely low maintenance requirements, and therefore costs, for lifespans that are substantially longer than currently possible."

The unique characteristics of UHPC explored in this research open up new applications, such as super-thin, very light, extremely durable, and ultra-long span structures,

and offer an opportunity to build the next generation of infrastructure that is significantly more robust, resilient and sustainable.

8. REFERENCES

[1]. Wille, K., El-Tawil, S. and Naaman, A.E. (2014), "Properties of Strain Hardening Ultra High Performance Fiber Reinforced Concrete (UHP-FRC) under Direct Tensile Loading," Journal of Cement and Concrete Composites, Elsevier, 48, pp. 53-66, doi:10.1016/j.cemconcomp.2013.12.015

[2]. Graybeal, Benjamin A. "Field-Cast UHPC Connections for Modular Bridge Deck Elements." FHWA-HRT-11-022 48.6 (2014): n. pag. FHWA. Web.

[3]. Wille, Kay, and Antoinne Naaman. "Pullout Behavior of High-Strength Steel Fibers Embedded in Ultra-High-Performance Concrete." ACI Materials Journal MJ 109.4 (2012): n. pag. Web.

[4]. Wille, Kay, Antoine E. Naaman, Sherif El-Tawil, and Gustavo J. Parra-Montesinos. "Ultra-high Performance Concrete and Fiber Reinforced Concrete: Achieving Strength and Ductility without Heat Curing." Mater Struct Materials and Structures 45.3 (2011): 309-24. Web.

[5]. El-Tawil, S., Alkaysi, M., Naaman, A.E., Hansen, W. and Liu, Z. (2016), Development, Characterization and Applications of a Non Proprietary Ultra High Performance Concrete for Highway Bridges, Michigan Department of Transportation, Lansing, MI. Report No. RC-1637.

[6]. Alkaysi, M., El-Tawil, S. (2016). Effects of Variations in the Mix Constituents of Ultra High Performance Concrete (UHPC) on Cost and Performance. Materials and Structures, 49(10), 4185-4200.

[7]. Kim, D-J., Wille, K., Naaman, A. E. and El-Tawil, S. (2011), "Strength Dependent Tensile Behavior of Strain Hardening Fiber Reinforced Concrete," Proceedings of HPFRCC6, H. W. Reinhardt and G. Parra Editors, Ann Arbor, MI.

[8]. Kim, D-J, Naaman, A. E. and El-Tawil, S. (2010a), "High Performance Fiber Reinforced Cement Composites With Innovative Slip Hardening Twisted Steel Fibers" International Journal of Concrete Structures and Materials, Korean Concrete Institute, ISSN: 1976-0485, 3(2), pp. 119 – 126; DOI 10.4334/IJCSM.2009.3.2.119.

[9]. Kim, D-J, El-Tawil, S., Sirijaroonchai, K. and Naaman, A. E. (2010b), "Numerical Simulation of the Split Hopkinson Pressure Bar Test Technique for Concrete Under Compression," International Journal of Impact Engineering, 37(2), Pages 141-149.

[10]. Kim, D-J., Naaman, A.E. and El-Tawil, S. (2010c), "Correlation between Tensile and Bending Behavior of FRC Composites with Scale Effect," Proceedings of FraMCoS-7, 7th International Conference on Fracture Mechanics of Concrete and Concrete Structures, May 23-28, 2010, Jeju Island, South Korea

[11]. Kim, D-J, Naaman, A. E. and El-Tawil, S. (2008a), "Comparative Flexural Behavior of Four Fiber Reinforced Cementitious Composites," Journal of Cement and Concrete Composites, Elsevier, Vol. 30, November 2008, pp.917-928.

[12]. Kim, D-J, El-Tawil, S. and Naaman, A. E. (2008b), "Rate-Dependent Tensile Behavior of High Performance Fiber Reinforced Cementitious Composites," Materials and Structures, RILEM, ISSN 1359-5997 (in print), 1871-6873 (online).

[13]. Kim, D-J, El-Tawil, S. and Naaman, A. E. (2008c), "Loading Rate Effect on Pullout Behavior of Deformed Fibers," ACI Materials Journal, 105(6), November-December 2008, pp.576-584

[14]. Kim, D-J, Naaman, A. E. and El-Tawil, S. (2008d), "High Tensile Strength Strain-Hardening FRC Composites with Less Than 2% Fiber Content," Proceedings of the Second International Symposium on Ultra High Performance Concrete, March 05 - 07, 2008, Kassel, Germany.

[15]. Kim, D-J, El-Tawil, S. and Naaman, A. E. (2007), "Correlation between Single Fiber Pullout and Tensile Response of FRC Composites with High Strength Steel Fibers," Proceedings of HPFRCC5, H. W. Reinhardt and A.E. Naaman Editors, July 10-13, Mainz, Germany.

[16]. Pyo, Sukhoon, Kay Wille, Sherif El-Tawil, and Antoine E. Naaman. "Strain Rate Dependent Properties of Ultra High Performance Fiber Reinforced Concrete (UHP-FRC) under Tension." Cement and Concrete Composites 56 (2015a): 15-24. Web.

[17]. Pyo, S., El-Tawil, S. (2015b), "Capturing the Strain Hardening and Softening Responses of Cementitious Composites Subjected to Impact Loading," Journal of Construction and

Building Materials, Elsevier, 81(15), April 2015, pp. 276–283, doi:10.1016/j.conbuildmat.2015.02.028.

[18]. Pyo, S. and El-Tawil, S. (2013a), "Crack velocity-dependent dynamic tensile behavior of concrete", International Journal of Impact Engineering, V55, pp. 63-70, http://dx.doi.org/10.1016/ j.ijimpeng.2013.01.003.

[19]. Pyo, S. and El-Tawil, S. (2013b), "Dynamic Fracture Mechanics Based DIF Models for Concrete under Tensile Loading," 2013 Conference of the ASCE Engineering Mechanics Institute, August 4 – 7, 2013, Northwestern University, Evanston, IL

[20]. Pyo, S., El-Tawil, S. and Naaman, A.E. (2013c), "Parametric Study of a New Impact Testing System for Ultrahigh Performance Concrete in Tension," 2013 Conference of the ASCE Engineering Mechanics Institute, August 4 – 7, 2013, Northwestern University, Evanston, IL

[21]. Hansen, L., and Jensen, B. (1999). A New Building System Using Joints of Ultra High-Strength Fibre Reinforced Concrete, Innovation in Concrete Structures: Design and Construction, pp. 543-552.

[22]. Graybeal, B. (2014). Design and Construction of Field-Cast UHPC Connections, FHWA Publication No. FHWA-HRT-14-084, Turner-Fairbank Highway Research Center, Federal Highway Administration, McLean, VA.

[23]. Wille, K., Kim, D., and Naaman, A.E., "Strain-Hardening UHP-FRC With Low Fiber Contents," Materials and Structures, Vol. 44, No. 3, 2011, pp. 583–598

[24]. Wille, K., Naaman, A.E., and El-Tawil, S., "Optimizing Ultra-High-Performance Fiber Reinforced Concrete," Concrete International, Vol. 33, No. 9, September 2011, pp. 35–41

[25]. Pyo, Sukhoon, Sherif El-Tawil, and Antoine E. Naaman. "Direct tensile behavior of ultra high performance fiber reinforced concrete (UHP-FRC) at high strain rates." Cement and Concrete Research 88 (2016): 144-156.

[26]. Alkaysi, Mo, et al. "Effects of silica powder and cement type on durability of ultra high performance concrete (UHPC)." Cement and Concrete Composites 66 (2016): 47-56.

[27]. Birchall, J. D., A. J. Howard, and K. Kendall. "Flexural strength and porosity of cements." Nature 289.5796 (1981): 388.

[28]. Bache, Hans Henrik. "Densified cement/ultra-fine particle based materials." the second international conference on superplasticizers in concrete, 1981. 1981.

[29]. Bache, Hans H. "Compact reinforced composite." U.S. Patent No. 4,979,992. 25 Dec. 1990.

[30]. Lankard, David R., and Jeffrey K. Newell. "Preparation of highly reinforced steel fiber reinforced concrete composites." Special Publication 81 (1984): 287-306.

[31]. Svermova, L., and P. J. M. Bartos. "Development of in-situ SIFCON for connections in pre-cast concrete and seismic resistant structures'." 27 th Conference on Our World in Concrete & Structures, Singapore (August 2002). 2002.

[32]. Richard, Pierre, and Marcel H. Cheyrezy. "Reactive powder concretes with high ductility and 200-800 MPa compressive strength." Special Publication 144 (1994): 507-518.

[33]. Richard, Pierre, and Marcel Cheyrezy. "Composition of reactive powder concretes." Cement and concrete research 25.7 (1995): 1501-1511.

[34]. de Larrard, François, and Thierry Sedran. "Optimization of ultra-high-performance concrete by the use of a packing model." Cement and Concrete Research 24.6 (1994): 997-1009.

[35]. Wille, Kay, Antoine E. Naaman, and Gustavo J. Parra-Montesinos. "Ultra-High Performance Concrete with Compressive Strength Exceeding 150 MPa (22 ksi): A Simpler Way." ACI Materials Journal 108.1 (2011).

[36]. Schmidt, Michael, and Ekkehard Fehling. "Ultra-high-performance concrete: research, development and application in Europe." ACI Special publication 228 (2005): 51-78.

[37]. Graybeal, B. A. "UHPC in the US highway transportation system." Proceedings of the Second International Symposium on Ultra High Performance Concrete, Kassel, Germany. 2008.

[38]. Graybeal. "Ultra-High Performance Concrete: A State-Of-The-Art Report for The Bridge Community." Chapters 6-7 - , June 2013 - FHWA-HRT-13-060. N.p., n.d. Web. 06 Dec. 2014

[39]. El-Tawil, Sherif, Yuh-Shiou Tai, and John A. Belcher II. "Field Application of Nonproprietary Ultra-High-Performance Concrete." Concrete International 40.1 (2018): 36-42.

[40]. Haber, Zachary B., Jose F. Munoz, and Benjamin A. Graybeal. Field Testing of an Ultra-High Performance Concrete Overlay. No. FHWA-HRT-17-096. 2017.

[41]. Azreen, N. M., Rashid, R. S., Haniza, M., Voo, Y. L., & Amran, Y. M. (2018). Radiation shielding of ultra-high-performance concrete with silica sand, amang and lead glass. Construction and Building Materials, 172, 370-377.

[42]. Voo, Y. L., Poon, W. K., & Foster, S. J. (2010). Shear strength of steel fiber-reinforced ultrahigh-performance concrete beams without stirrups. Journal of structural engineering, 136(11), 1393-1400.

[43]. Voo, Y. L., and S. J. Foster. "MALAYSIA FIRST ULTRA-HIGH PERFORMANCE CONCRETE PRESTRESSED MOTORWAY BRIDGE: EXPERIMENTAL VERIFICATION."

[44]. Tayeh, B. A., Bakar, B. A., Johari, M. M., & Voo, Y. L. (2012). Mechanical and permeability properties of the interface between normal concrete substrate and ultra high performance fiber concrete overlay. Construction and building materials, 36, 538-548.

[45]. Wille, Kay, and Christopher Boisvert-Cotulio. "Material efficiency in the design of ultra-high performance concrete." Construction and Building Materials 86 (2015): 33-43.

[46]. Sakai, Etsuo, et al. "Influence of superplasticizers on the fluidity of cements with different amount of aluminate phase." Second International Symposium on Ultra High Performance Concrete. 2008.

[47]. ASTM C150/C150M-18 Standard Specification for Portland Cement, ASTM International, West Conshohocken, PA, 2018, https://doi.org/10.1520/C0150_C0150M-18

[48]. Deeb, Rola, Akbar Ghanbari, and Bhushan Lai Karihaloo. "Development of self-compacting high and ultra high performance concretes with and without steel fibres." Cement and concrete composites 34.2 (2012): 185-190.

[49]. El-Dieb, Amr S. "Mechanical, durability and microstructural characteristics of ultra-high-strength self-compacting concrete incorporating steel fibers." Materials & Design 30.10 (2009): 4286-4292.

[50]. Li, P. P., Q. L. Yu, and H. J. H. Brouwers. "Effect of coarse basalt aggregates on the properties of Ultra-high Performance Concrete (UHPC)." Construction and Building Materials 170 (2018): 649-659.

[51]. Kozul, Rozalija, and David Darwin. Effects of Aggregate type, size, and content on concrete strength and Fracture Energy. University of Kansas Center for Research, Inc., 1997.

[52]. Ma, Jianxin, et al. "Comparative investigations on ultra-high performance concrete with and without coarse aggregates." Proceedings of international symposium on ultra high performance concrete, Germany. 2004.

[53]. Orgass, Marko, and Yvette Klug. "Fibre reinforced ultra-high strength concretes." Proceedings of the International Symposium on Ultra High Performance Concrete, Kassel, Germany. 2004.

[54]. Yoo, Doo-Yeol, and Nemkumar Banthia. "Mechanical properties of ultra-high-performance fiber-reinforced concrete: A review." Cement and Concrete Composites 73 (2016): 267-280.

[55]. Chan, Yin-Wen, and Shu-Hsien Chu. "Effect of silica fume on steel fiber bond characteristics in reactive powder concrete." Cement and Concrete Research 34.7 (2004): 1167-1172.

[56]. Song, Ha-Won, and Velu Saraswathy. "Studies on the corrosion resistance of reinforced steel in concrete with ground granulated blast-furnace slag—an overview." Journal of Hazardous Materials138.2 (2006): 226-233.

[57]. Halit Yazıci, et al. "Mechanical properties of reactive powder concrete containing high volumes of ground granulated blast furnace slag." Cement and Concrete Composites 32.8 (2010): 639-648.

[58]. Oner, A., and S. Akyuz. "An experimental study on optimum usage of GGBS for the compressive strength of concrete." Cement and Concrete Composites 29.6 (2007): 505-514.

[59]. Li, P. P., Q. L. Yu, and H. J. H. Brouwers. "Effect of PCE-type superplasticizer on early-age behaviour of ultra-high performance concrete (UHPC)." Construction and Building Materials 153 (2017): 740-750.

[60]. Hirschi, Thomas, and Franz Wombacher. "Influence of different superplasticizers on UHPC." Proceedings of the Second International Symposium on Ultra High Performance Concrete, Kassel University Press, Kassel. 2008.

[61]. Graybeal, Benjamin A. Material property characterization of ultra-high performance concrete. No. FHWA-HRT-06-103. 2006.

[62]. Tue, N. V., Ma, J., & Orgass, M. (2008). Influence of addition method of superplasticizer on the properties of fresh UHPC. In Proceedings of Second International Symposium on Ultra High Performance Concrete, University of Kassel, Germany (pp. 93-100).

[63]. Dils, Jeroen, Geert De Schutter, and Veerle Boel. "Influence of mixing procedure and mixer type on fresh and hardened properties of concrete: a review." Materials and structures 45.11 (2012): 1673-1683.

[64]. Hiremath, Parameshwar N., and Subhash C. Yaragal. "Influence of mixing method, speed and duration on the fresh and hardened properties of Reactive Powder Concrete." Construction and Building Materials 141 (2017): 271-288.

[65]. Hale, W. Micah, and Andrew M. Tackett. Examining the Effects of Mixer Type and Temperature on the Properties of Ultra-high Performance Concrete. No. MBTC DOT 3012. 2010.

[66]. Dils, Jeroen, V. Boel, and G. De Schutter. "Vacuum mixing technology to improve the mechanical properties of ultra-high performance concrete." Materials and Structures 48.11 (2015): 3485-3501.

[67]. ASTM C109/C109M-16a Standard Test Method for Compressive Strength of Hydraulic Cement Mortars (Using 2-in. or [50-mm] Cube Specimens), ASTM International, West Conshohocken, PA, 2016

[68]. ASTM C989/C989M-18, Standard Specification for Slag Cement for Use in Concrete and Mortars, ASTM

[69]. Shin, Hyun-Oh, Doo-Yeol Yoo, and Joo-Ha Lee. "Development of 300 MPa ultra-high-strength mortar through a special curing regime." Construction and Building Materials 171 (2018): 312-320.

[70]. Andreasen, A. H. M. "Über die Beziehung zwischen Kornabstufung und Zwischenraum in Produkten aus losen Körnern (mit einigen Experimenten)." Kolloid-Zeitschrift 50.3 (1930): 217-228.

[71]. Funk, James E., and Dennis R. Dinger. Predictive process control of crowded particulate suspensions: applied to ceramic manufacturing. Springer Science & Business Media, 2013.

[72]. Brouwers, H. J. H., and H. J. Radix. "Self-compacting concrete: theoretical and experimental study." Cement and Concrete Research 35.11 (2005): 2116-2136.

[73]. Hüsken, Götz, and H. J. H. Brouwers. "A new mix design concept for earth-moist concrete: A theoretical and experimental study." Cement and Concrete Research 38.10 (2008): 1246-1259.

[74]. Hunger, Martin. An integral design concept for ecological self-compacting concrete. University of Technology, 2010.

[75]. Long, G., Wang, X., & Xie, Y. (2002). Very-high-performance concrete with ultrafine powders. Cement and concrete research, 32(4), 601-605.

[76]. Tafraoui, Ahmed, et al. "Metakaolin in the formulation of UHPC." Construction and Building Materials 23.2 (2009): 669-674.

[77]. Abdulkareem, Omar M., et al. "Mixture design and early age investigations of more sustainable UHPC." Construction and Building Materials 163 (2018): 235-246.

[78]. Ferdosian, Iman, and Aires Camões. "Effective low-energy mixing procedure to develop high-fluidity cementitious pastes." Matéria (Rio de Janeiro) 21.1 (2016): 11-17.

[79]. ASTM C230 / C230M-14, Standard Specification for Flow Table for Use in Tests of Hydraulic Cement, ASTM International, West Conshohocken, PA, 2014

[80]. ASTM C1856/C1856M-17 Standard Practice for Fabricating and Testing Specimens of Ultra-High Performance Concrete, ASTM International, West Conshohocken, PA, 2017

[81]. ASTM C1437-15 Standard Test Method for Flow of Hydraulic Cement Mortar, ASTM International, West Conshohocken, PA, 2015

[82]. ASTM C191-13 Standard Test Methods for Time of Setting of Hydraulic Cement by Vicat Needle, ASTM International, West Conshohocken, PA, 2013

[83]. H. Yazıcı, H. Yiğiter, A.Ş. Karabulut, B. Baradan, "Utilization of fly ash and ground granulated blast furnace slag as an alternative silica source in reactive powder concrete," Fuel, 87 (12) (2008), pp. 2401-2407

[84]. Ghafari, E., Ghahari, S. A., Costa, H., Júlio, E., Portugal, A., & Durães, L. (2016). Effect of supplementary cementitious materials on autogenous shrinkage of ultra-high performance concrete. Construction and Building Materials, 127, 43-48.

[85]. Korpa, A., T. Kowald, and R. Trettin. "Phase development in normal and ultra high performance cementitious systems by quantitative X-ray analysis and thermoanalytical methods." *Cement and Concrete Research* 39.2 (2009): 69-76.

[86]. AASHTO, T. "132-87 Standard Method of Test for Tensile Strength of Hydraulic Cement Mortars." American Association of State and Highway Transportation Officials (2009).

[87]. ASTM C457/C457M-16 Standard Test Method for Microscopical Determination of Parameters of the Air-Void System in Hardened Concrete, ASTM International, West Conshohocken, PA, 2016,

[88]. ASTM C1202-17a Standard Test Method for Electrical Indication of Concrete's Ability to Resist Chloride Ion Penetration, ASTM International, West Conshohocken, PA, 2017

[89]. Jianyong, Li, and Tian Pei. "Effect of slag and silica fume on mechanical properties of high strength concrete." Cement and Concrete Research 27.6 (1997): 833-837.

[90]. Olorunsogo, Folarin T., and Peter J. Wainwright. "Effect of GGBFS particle-size distribution on mortar compressive strength." Journal of materials in civil engineering 10.3 (1998): 180-187.

[91]. Nath, Pradip, and Prabir Kumar Sarker. "Effect of GGBFS on setting, workability and early strength properties of fly ash geopolymer concrete cured in ambient condition." Construction and Building materials 66 (2014): 163-171.

[92]. Li, Guoxin, et al. "Ground granulated blast furnace slag effect on the durability of ternary cementitious system exposed to combined attack of chloride and sulfate." Construction and Building Materials158 (2018): 640-648.

[93]. Yalçınkaya, Çağlar. "Effects of ambient temperature and relative humidity on early-age shrinkage of UHPC with high-volume mineral admixtures." Construction and Building Materials144 (2017): 252-259.

[94]. Powers, Treval Clifford, and T. F. Willis. "The air requirement of frost resistant concrete." Highway Research Board Proceedings. Vol. 29. 1950.

[95]. Habel, Katrin, et al. "Development of the mechanical properties of an ultra-high performance fiber reinforced concrete (UHPFRC)." Cement and Concrete Research 36.7 (2006): 1362-1370.

[96]. Roy, D. M. "Hydration, structure, and properties of blast furnace slag cements, mortars, and concrete." Journal Proceedings. Vol. 79. No. 6. 1982.

[97]. Manmohan, D., and P. K. Mehta. "Influence of pozzolanic, slag, and chemical admixtures on pore size distribution and permeability of hardened cement pastes." Cement, Concrete and Aggregates 3.1 (1981): 63-67.

[98]. Bakker, Robert FM. "Permeability of blended cement concretes." Special Publication 79 (1983): 589-606.

[99]. Yu, R., P. Spiesz, and H. J. H. Brouwers. "Effect of nano-silica on the hydration and microstructure development of Ultra-High Performance Concrete (UHPC) with a low binder amount." Construction and Building Materials 65 (2014): 140-150.

[100]. Wang, Xiao-Yong. "Properties prediction of ultra high performance concrete using blended cement hydration model." Construction and Building Materials 64 (2014): 1-10.

[101]. Morin, V., et al. "Superplasticizer effects on setting and structuration mechanisms of ultrahigh-performance concrete." Cement and concrete research 31.1 (2001): 63-71.

[102]. Martys, Nicos S., and Chiara F. Ferraris. "Capillary transport in mortars and concrete." Cement and Concrete Research 27.5 (1997): 747-760.

[103]. Kropp, J. "Relations between transport characteristics and durability. RILEM, 1995." Performance Criteria for Concrete Durability.

[104]. Kropp, J. "Relations between transport characteristics and durability. RILEM, 1995." Performance Criteria for Concrete Durability.

[105]. Chidiac, S. E., and D. K. Panesar. "Sorptivity of concrete as an indicator of laboratory freeze-thaw scaling performance." Proceedings of the International Réunion International des Laboratoire et Experts des Matériaux, systèmes de constructions et ouvrages (RILEM) Workshop on performance based evaluation and indicators for concrete durability. Madrid, Spain. 2006.

[106]. Gagné, Richard, et al. "Study of the relationship between scaling resistance and sorptivity of concrete." Canadian Journal of Civil Engineering38.11 (2011): 1238-1248.

[107]. Li, Wenting, et al. "Water absorption and critical degree of saturation relating to freeze-thaw damage in concrete pavement joints." Journal of Materials in Civil Engineering 24.3 (2011): 299-307.

[108]. Setzer, M. J. "Action of frost and deicing chemicals: basic phenomena and testing." Freeze—thaw durability of concrete (1976): 3-21.

[109]. Jacobsen, Stefan. "Liquid uptake mechanisms in wet freeze/thaw: review and modelling." RILEM Proceedings PRO. Vol. 25. 2002.

[110]. Sandström, Tomas, et al. "The influence of temperature on water absorption in concrete during freezing." Nordic Concrete Research 45.1 (2012): 45-58.

[111]. Gupta, Souradeep. "Effect of content and fineness of slag as high volume cement replacement on strength and durability of ultra-high performance mortar." Journal of Building Materials and Structures 3.2 (2016): 43-54.

[112]. Lowke, Dirk, et al. "Effect of cement on superplasticizer adsorption, yield stress, thixotropy and segregation resistance." Design, production and placement of self-consolidating concrete. Springer, Dordrecht, 2010. 91-101.

[113]. Han, Virak, Soty Ros, and Hiroshi Shima. "Effects of sand content, superplasticizer dosage, and mixing time on compressive strength of mortar." ACI Materials Journal 110.1 (2013): 23.

[114]. Wille, K., and C. Boisvert-Cotulio. "Development of non-proprietary ultra-high performance concrete for use in the highway bridge sector." Report No. PB2013-110587, National Technical Information Service, Springfield, VA (2013).

[115]. Alkaysi, Mouhamed. "Strength and Durability of Ultra-High Performance Concrete Materials and Structures." (2016).

[116]. Naaman, A. E., and H. W. Reinhardt. "Proposed classification of HPFRC composites based on their tensile response." Materials and structures 39.5 (2006): 547-555.

[117]. Liu, Zhichao. "Frost Deterioration in Concrete Due to Deicing Salt Exposure: Mechanism, Mitigation and Conceptual Surface Scaling Model." (2014).

[118]. Bonneau, Olivier, et al. "Mechanical properties and durability of two industrial reactive powder concretes." Materials Journal 94.4 (1997): 286-290.

9. APPENDIX A – STRESS-STRAIN PLOTS FOR ALL UHPC MIXES

This appendix lists the stress-strain plots for all tensile tests conducted on UHPC coupons. For each set of tensile tests, at least 3 specimen tensile plots are averaged in order to produce a single tensile response curve. The plots are averaged at each point along the strain range. The result is then processed through a moving average filter to account for minute changes due to the sensitivity of the equipment. See Section 3.3.1 for further details.

9.1. LA CEMENT MIXES

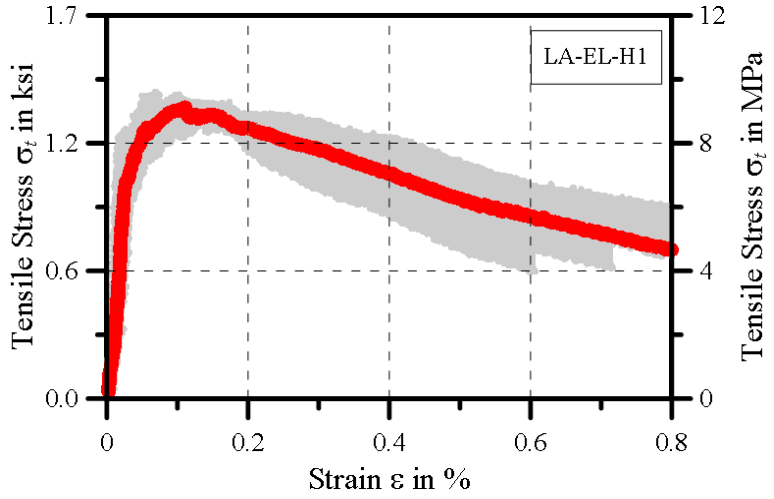

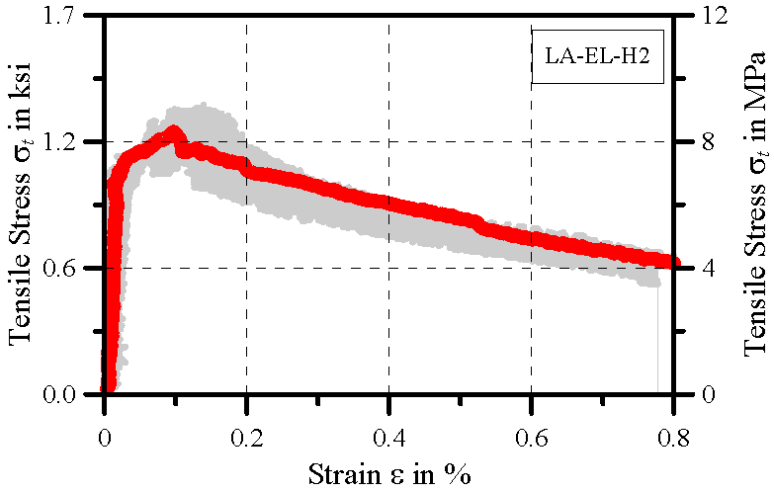

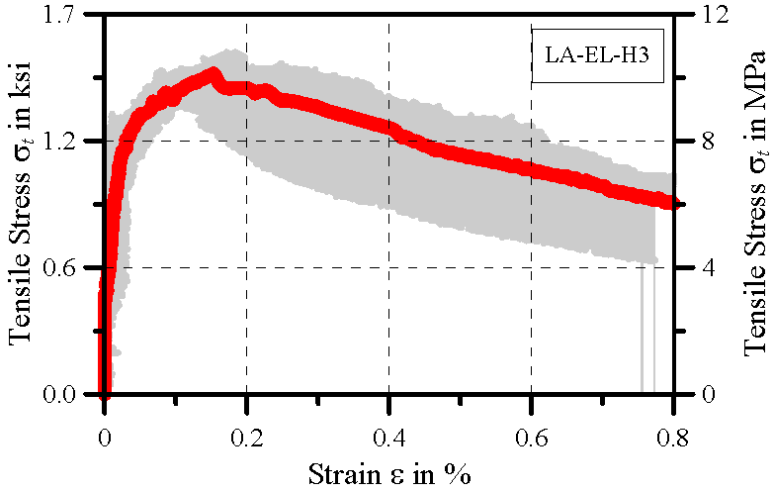

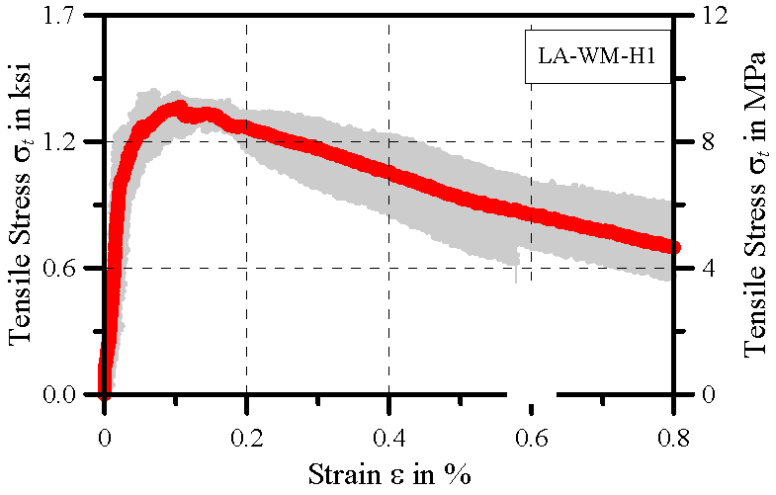
LA-WM-H1
Tensile Stress σ_t in ksi
Tensile Stress σ_t in MPa
Strain ε in %
1.7
1.2
0.6
0.0
12
8
4
0
0
0.2
0.4
0.6
0.8

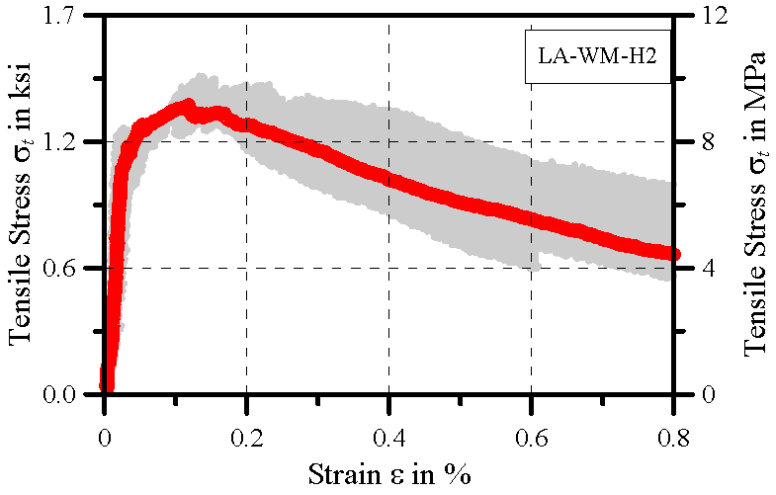
LA-WM-H2
Tensile Stress σ_t in ksi
Tensile Stress σ_t in MPa
Strain ε in %
1.7
1.2
0.6
0.0
12
8
4
0
0
0.2
0.4
0.6
0.8

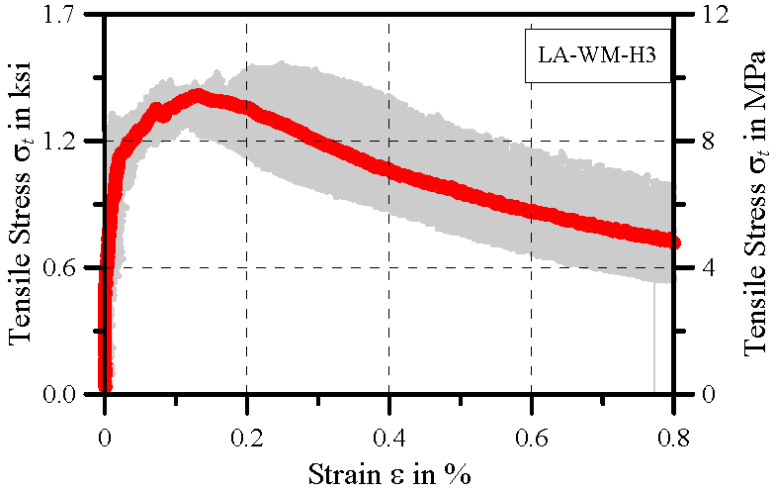
LA-WM-H3
Tensile Stress σ_t in ksi
Tensile Stress σ_t in MPa
Strain ε in %
1.7
1.2
0.6
0.0
12
8
4
0
0
0.2
0.4
0.6
0.8

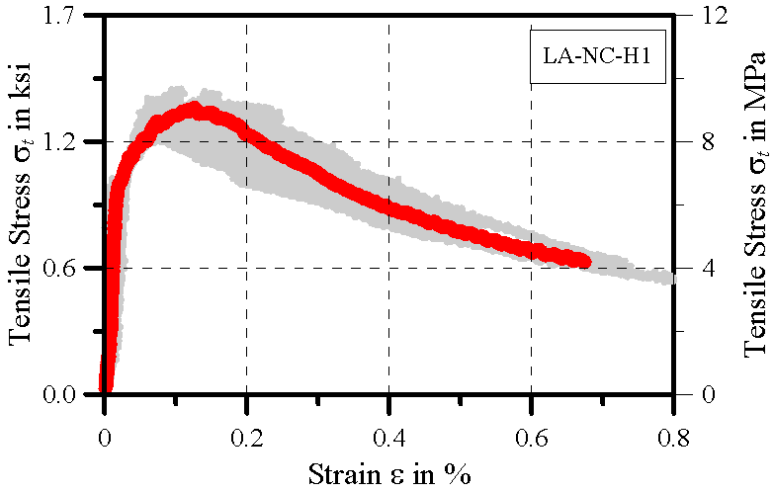
LA-NC-H1
Tensile Stress σ_t in ksi
Tensile Stress σ_t in MPa
Strain ε in %
1.7
1.2
0.6
0.0
12
8
4
0
0
0.2
0.4
0.6
0.8

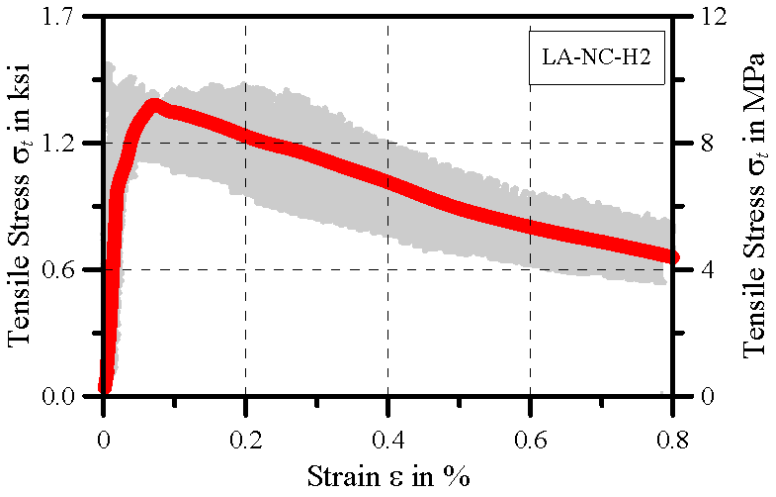
LA-NC-H2
Tensile Stress σ_t in ksi
Tensile Stress σ_t in MPa
Strain ε in %
1.7
1.2
0.6
0.0
12
8
4
0
0
0.2
0.4
0.6
0.8

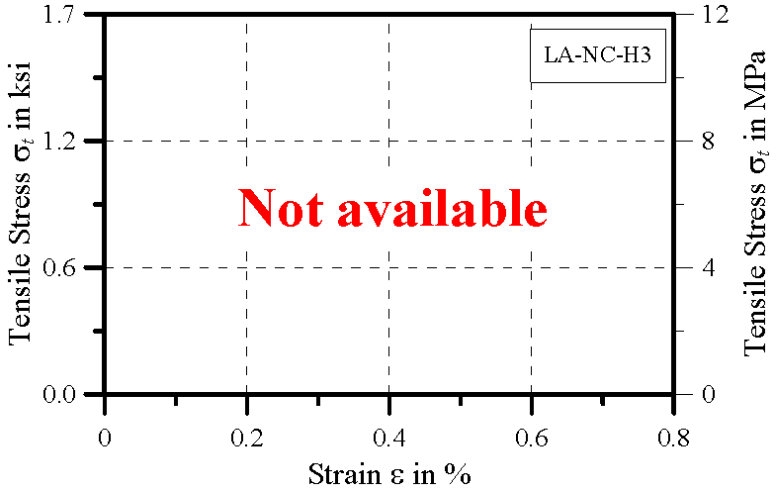
LA-NC-H3
Not available
Tensile Stress σ_t in ksi
Tensile Stress σ_t in MPa
Strain ε in %
1.7
1.2
0.6
0.0
12
8
4
0
0
0.2
0.4
0.6
0.8

9.2. ST CEMENT MIXES

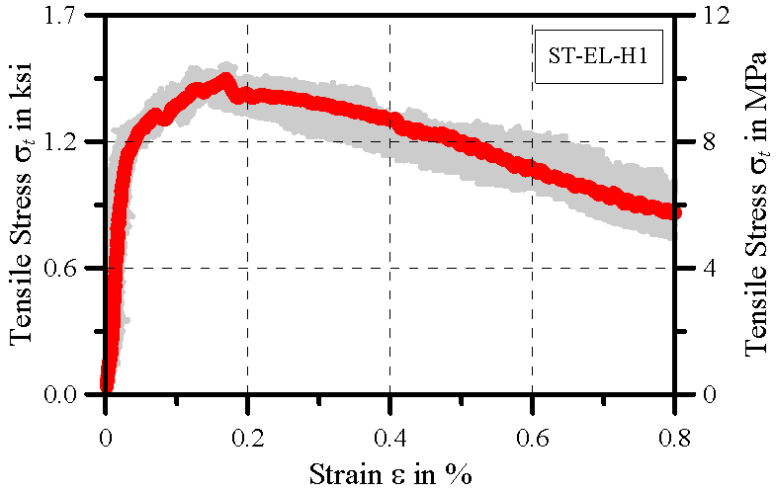

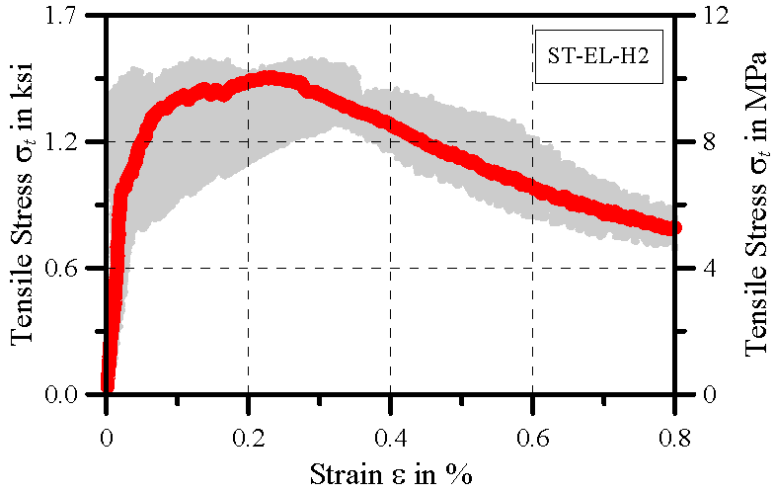

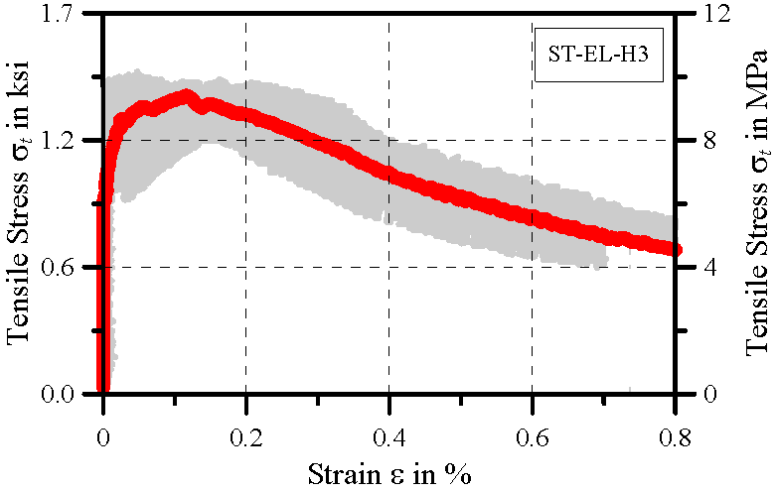

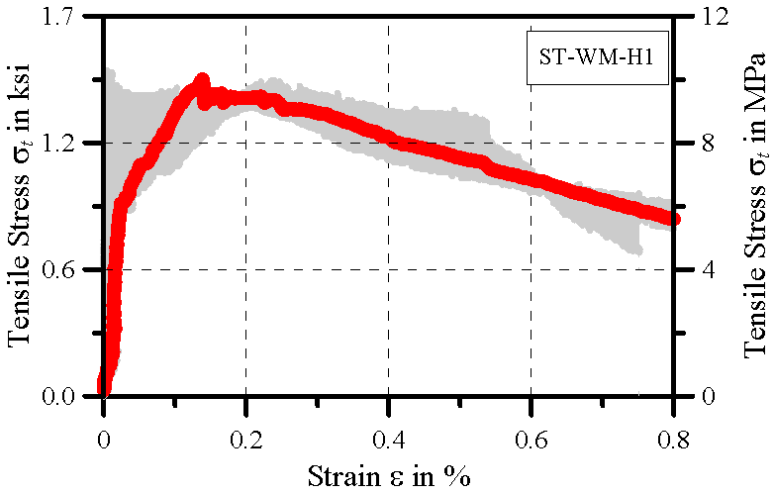
ST-WM-H1
Tensile Stress σ_t in ksi
Tensile Stress σ_t in MPa
Strain ε in %
1.7
1.2
0.6
0.0
12
8
4
0
0
0.2
0.4
0.6
0.8

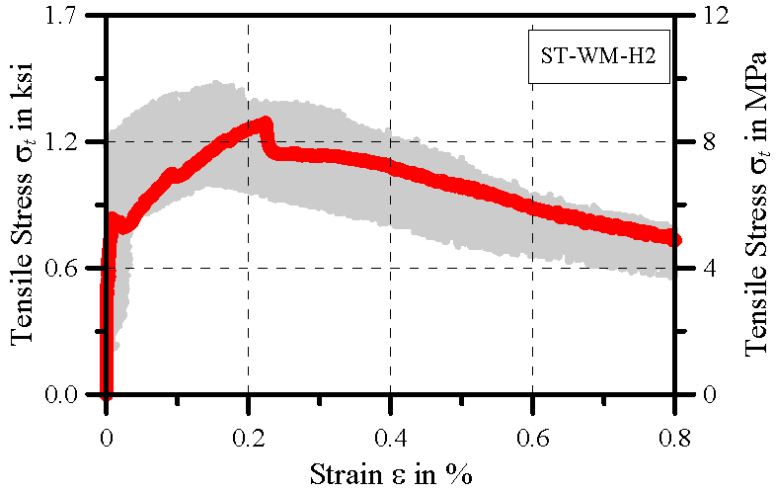
ST-WM-H2
Tensile Stress σ_t in ksi
Tensile Stress σ_t in MPa
Strain ε in %
1.7
1.2
0.6
0.0
12
8
4
0
0
0.2
0.4
0.6
0.8

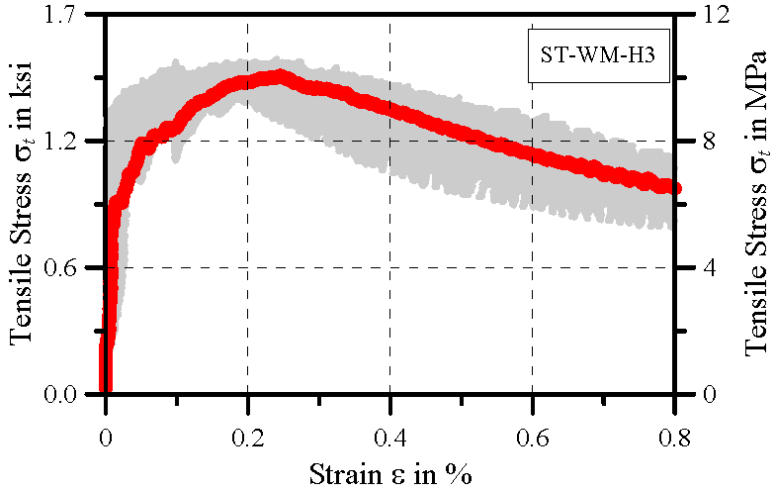
ST-WM-H3
Tensile Stress σ_t in ksi
Tensile Stress σ_t in MPa
Strain ε in %
1.7
1.2
0.6
0.0
12
8
4
0
0
0.2
0.4
0.6
0.8

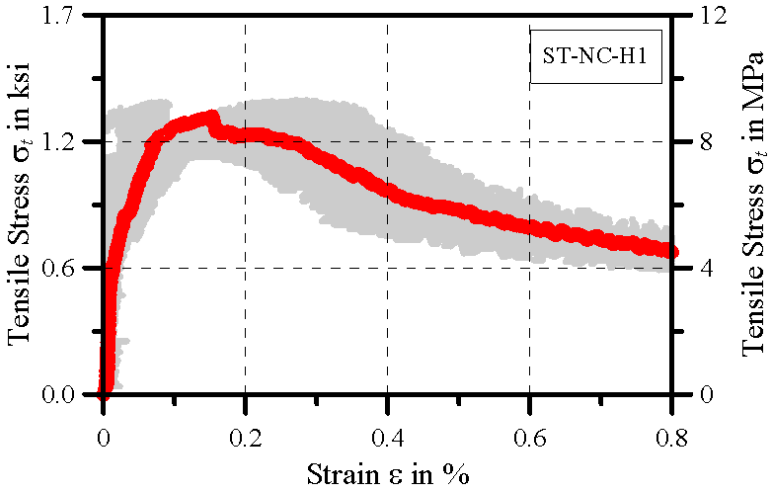
ST-NC-H1
Tensile Stress σ_t in ksi
Tensile Stress σ_t in MPa
Strain ε in %
1.7
1.2
0.6
0.0
12
8
4
0
0
0.2
0.4
0.6
0.8

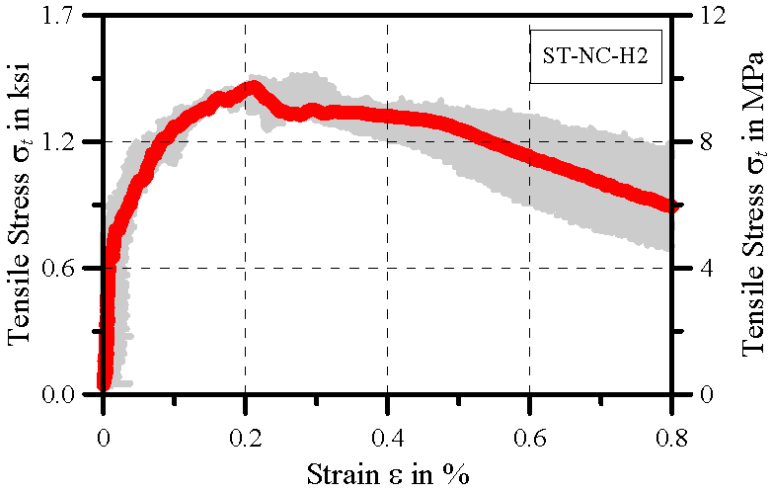
ST-NC-H2
Tensile Stress σ_t in ksi
Tensile Stress σ_t in MPa
Strain ε in %
1.7
1.2
0.6
0.0
12
8
4
0
0
0.2
0.4
0.6
0.8

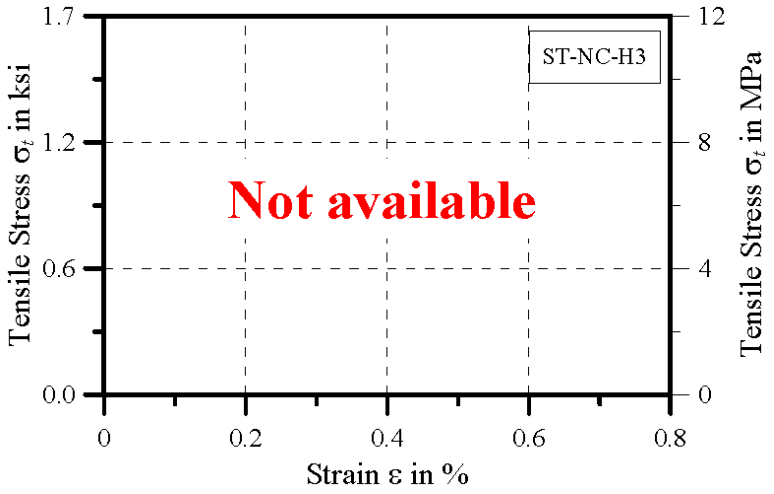
ST-NC-H3
Not available
Tensile Stress σ_t in ksi
Tensile Stress σ_t in MPa
Strain ε in %
1.7
1.2
0.6
0.0
12
8
4
0
0
0.2
0.4
0.6
0.8

9.3. LE CEMENT MIXES

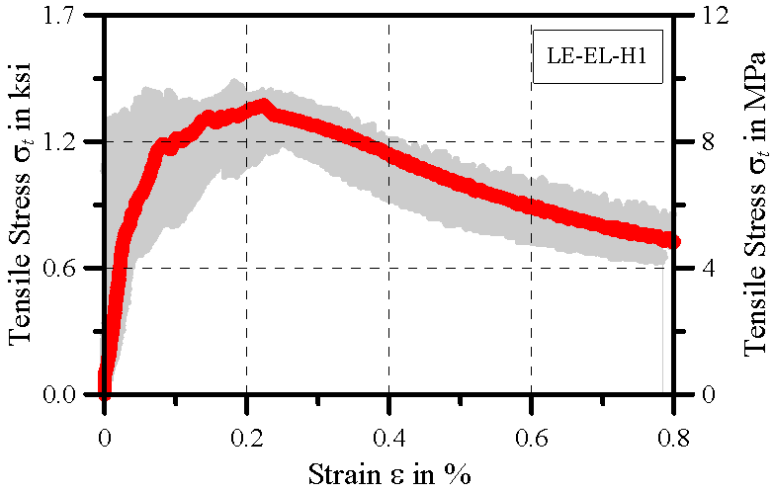

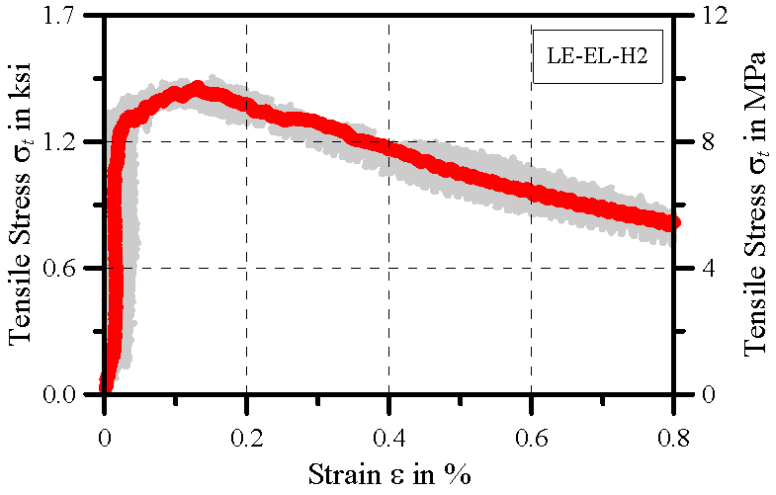

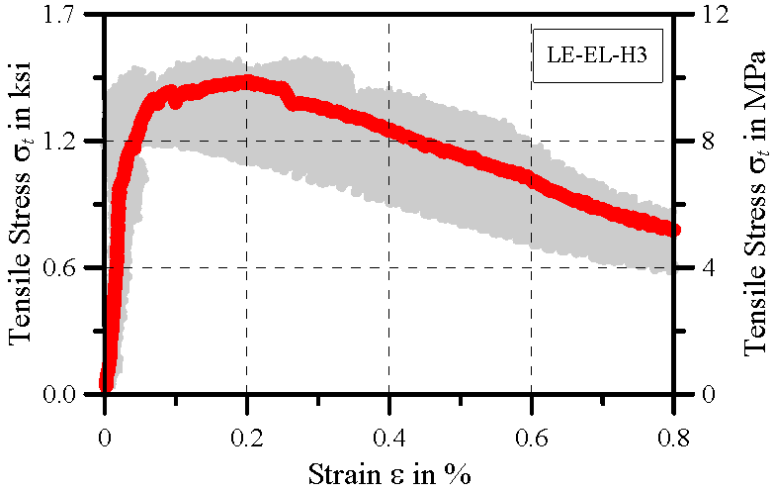

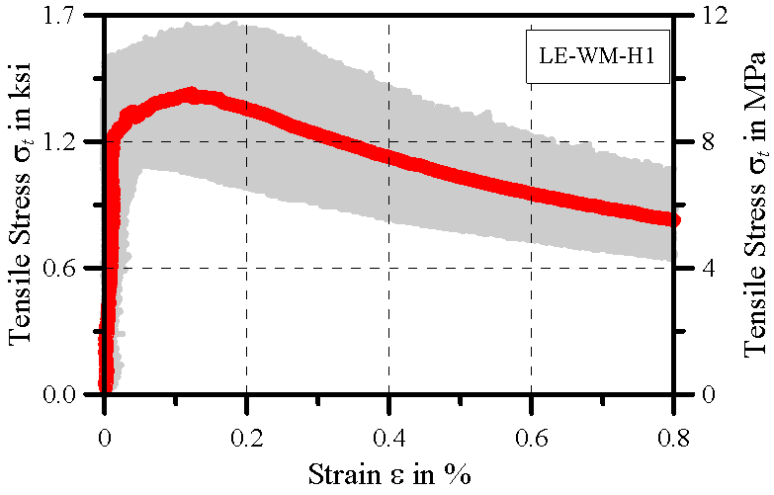
LE-WM-H1
Tensile Stress σ_t in ksi
Tensile Stress σ_t in MPa
Strain ε in %
1.7
1.2
0.6
0.0
12
8
4
0
0
0.2
0.4
0.6
0.8

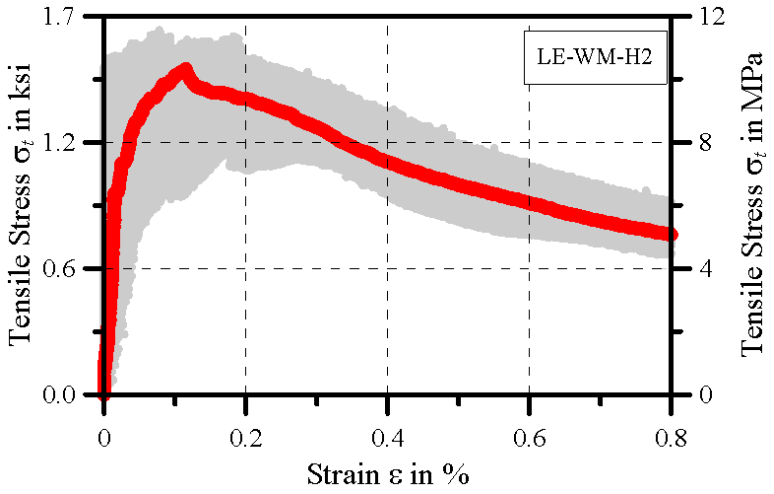
LE-WM-H2
Tensile Stress σ_t in ksi
Tensile Stress σ_t in MPa
Strain ε in %
1.7
1.2
0.6
0.0
12
8
4
0
0
0.2
0.4
0.6
0.8

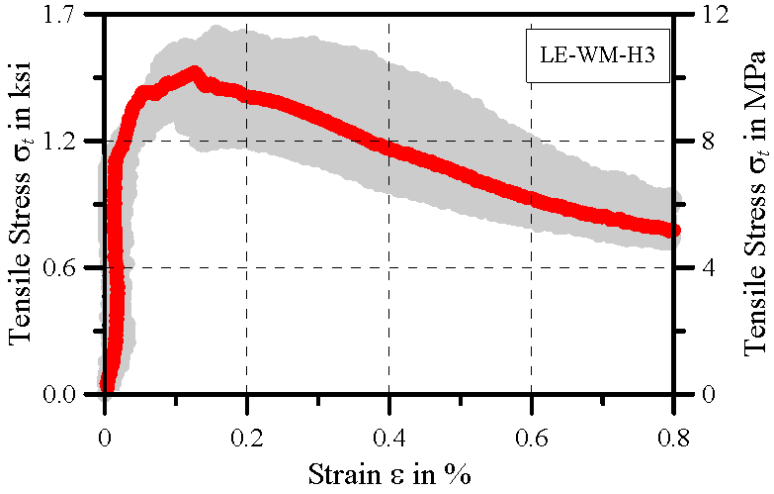
LE-WM-H3
Tensile Stress σ_t in ksi
Tensile Stress σ_t in MPa
Strain ε in %
1.7
1.2
0.6
0.0
12
8
4
0
0
0.2
0.4
0.6
0.8

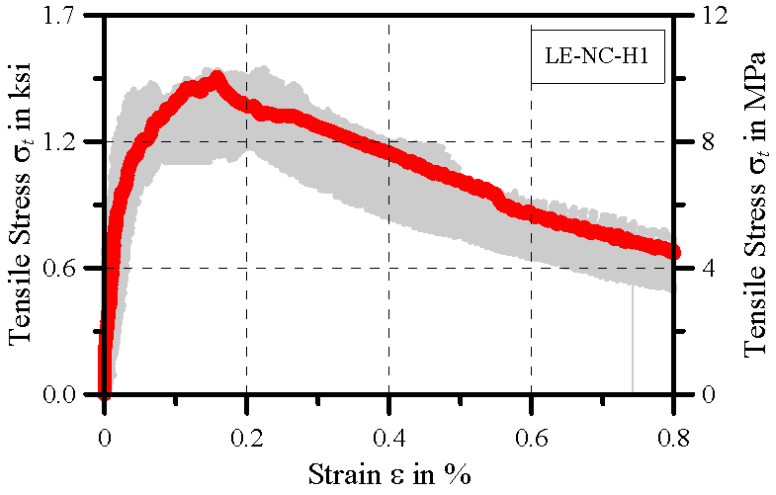
LE-NC-H1
Tensile Stress σ_t in ksi
Tensile Stress σ_t in MPa
Strain ε in %
1.7
1.2
0.6
0.0
12
8
4
0
0
0.2
0.4
0.6
0.8

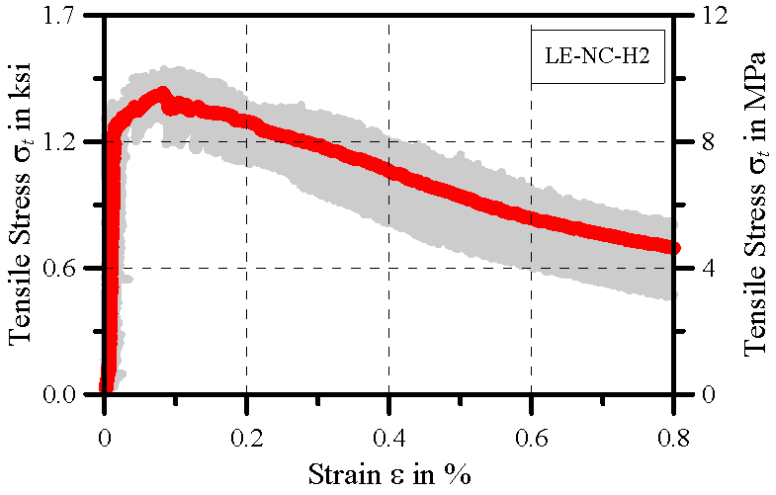
LE-NC-H2
Tensile Stress σ_t in ksi
Tensile Stress σ_t in MPa
Strain ε in %
1.7
1.2
0.6
0.0
12
8
4
0
0
0.2
0.4
0.6
0.8

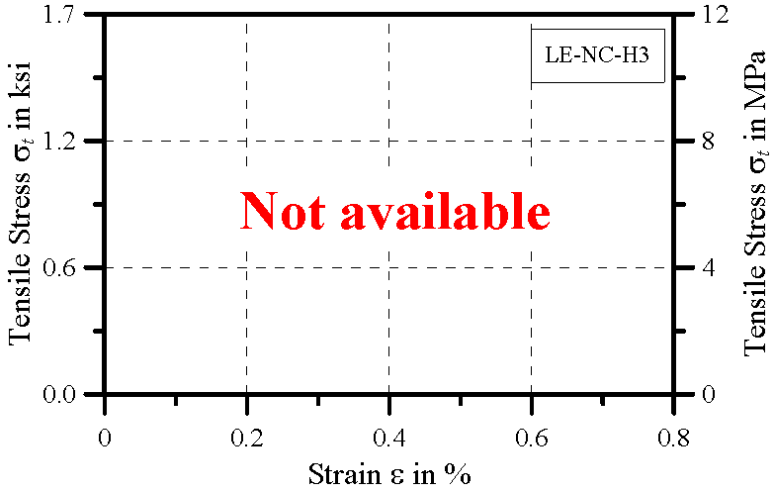
LE-NC-H3
Not available
Tensile Stress σ_t in ksi
Tensile Stress σ_t in MPa
Strain ε in %
1.7
1.2
0.6
0.0
12
8
4
0
0
0.2
0.4
0.6
0.8

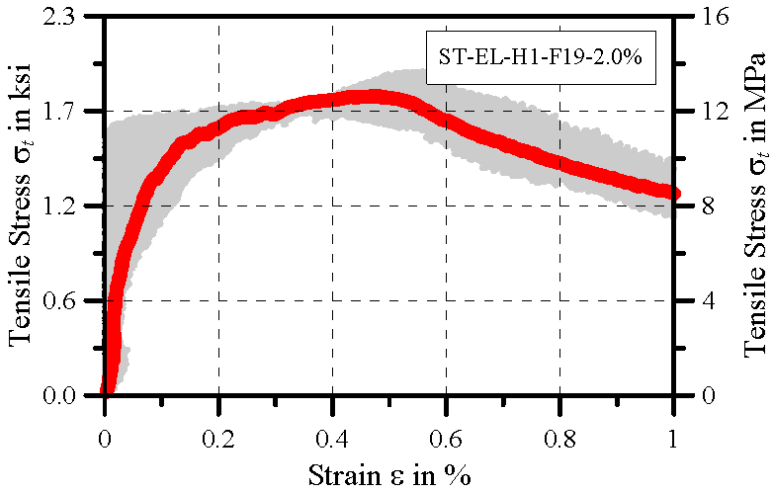
ST-EL-H1-F19-2.0%
Tensile Stress σ_t in ksi
Tensile Stress σ_t in MPa
Strain ε in %
2.3
1.7
1.2
0.6
0.0
16
12
8
4
0
0
0.2
0.4
0.6
0.8
1

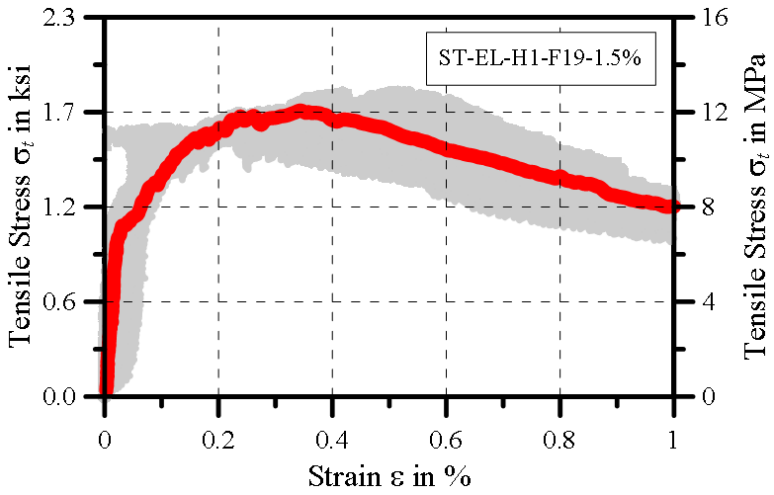
ST-EL-H1-F19-1.5%
Tensile Stress σ_t in ksi
Tensile Stress σ_t in MPa
Strain ε in %
2.3
1.7
1.2
0.6
0.0
16
12
8
4
0
0
0.2
0.4
0.6
0.8
1

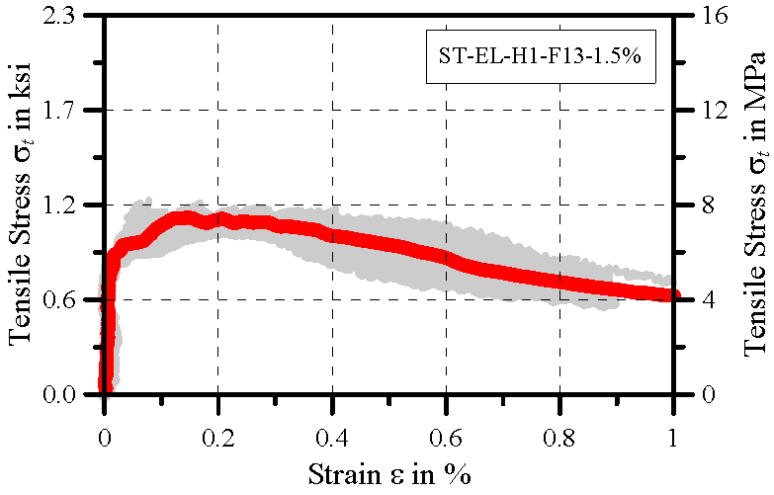
ST-EL-H1-F13-1.5%
Tensile Stress σ_t in ksi
Tensile Stress σ_t in MPa
Strain ε in %
2.3
1.7
1.2
0.6
0.0
16
12
8
4
0
0
0.2
0.4
0.6
0.8
1

10. APPENDIX B – RESULTS OF FREEZE-THAW TESTING – RILEM

This appendix lists the raw results from the freeze-thaw testing outlined in section 4.3.1. For each specimen, the internal damage as measured by the relative dynamic modulus; moisture uptake and salt scaling are listed.

F-T cycles	spec.no	surface scaling					moisture uptake			internal damage						
		U_f (g)	U_b (g)	U_s (g)	ΣU_s (g)	m_n (g/m^2)	W_n (g)	W_{nt} (g)	ΔW_n ((%)	t_{nx} (ms)	t_{ny} (ms)	τ_{nx}	τ_{ny}	$R_{u,nx}$	$R_{u,ny}$	$R_{u,nmin}$
0	EL(965)-H1-1.35					0.00	1667.63	1667.63	0.00	59.5	63.1	1	1	1	1	100
	EL(965)-H1-1.35					0.00	1697.28	1697.28	0.00	60.5	62.3	1	1	1	1	100
	EL(965)-H1-2.0					0.00	1766.02	1766.02	0.00	61.3	62.3	1	1	1	1	100
	EL(965)-H1-2.0					0.00	1888.93	1888.93	0.00	59.6	61.4	1	1	1	1	100
	EL(965)-H1-3.0					0.00	1797.22	1797.22	0.00	59.5	63	1	1	1	1	100
	EL(965)-H1-3.0					0.00	1888.69	1888.69	0.00	59.3	62	1	1	1	1	100
	NC-H1-3.0					0.00	1793.46	1793.46	0.00	60.3	63.3	1	1	1	1	100
	NC-H1-3.0					0.00	1771.29	1771.29	0.00	59.7	63.2	1	1	1	1	100
	EL(955)-H1-3.0					0.00	1868.1	1868.10	0.00	60.3	60.6	1	1	1	1	100
	EL(955)-H1-3.0					0.00	1802.52	1802.52	0.00	61.01	61.5	1	1	1	1	100
F-T cycles	spec.no	surface scaling					moisture uptake			internal damage						
		U_f (g)	U_b (g)	U_s (g)	ΣU_s (g)	m_n (g/m^2)	W_n (g)	W_{nt} (g)	ΔW_n ((%)	t_{nx} (ms)	t_{ny} (ms)	τ_{nx}	τ_{ny}	$R_{u,nx}$	$R_{u,ny}$	$R_{u,nmin}$
10	EL(965)-H1-1.35	3.64	4.04	0.4	0.4	39.68	1669.84	1670.24	0.02	59.9	63.7	0.99332	0.99058	0.98668	0.98124	98.66795
	EL(965)-H1-1.35	3.45	3.77	0.32	0.32	32.98	1699.2	1699.52	0.02	61.9	62.4	0.97737	0.99840	0.95525	0.99680	99.67953
	EL(965)-H1-2.0	3.62	4.05	0.43	0.43	43.88	1769.07	1769.50	0.02	61.1	61.9	1.00328	1.00647	1.00656	1.01297	101.29743
	EL(965)-H1-2.0	3.8	4.13	0.33	0.33	31.43	1892.08	1892.41	0.02	59.6	61.7	1.00000	0.99513	1.00000	0.99029	99.02934
	EL(965)-H1-3.0	3.63	4.14	0.51	0.51	52.12	1800.95	1801.46	0.03	59.9	63.1	0.99332	0.99841	0.98668	0.99683	98.66793
	EL(965)-H1-3.0	3.5	4.02	0.52	0.52	48.55	1892.29	1892.81	0.03	59.6	60.8	0.99496	1.01975	0.98995	1.03989	98.99517
	NC-H1-3.0	3.47	3.76	0.29	0.29	28.47	1796.16	1796.45	0.02	59.4	62.7	1.01516	1.00958	1.03055	1.01924	101.92417
	NC-H1-3.0	3.71	3.89	0.18	0.18	18.61	1774.56	1774.74	0.01	59.6	63.1	1.00168	1.00159	1.00336	1.00317	100.33611
	EL(955)-H1-3.0	3.65	4.06	0.41	0.41	37.91	1871.07	1871.48	0.02	60.2	60.4	1.00166	1.00331	1.00333	1.00664	100.33271
	EL(955)-H1-3.0	3.67	3.84	0.17	0.17	17.18	1805.78	1805.95	0.01	61	61.7	1.00016	0.99676	1.00033	0.99352	99.35234
F-T cycles	spec.no	surface scaling					moisture uptake			internal damage						
		U_f (g)	U_b (g)	U_s (g)	ΣU_s (g)	m_n (g/m^2)	W_n (g)	W_{nt} (g)	ΔW_n ((%)	t_{nx} (ms)	t_{ny} (ms)	τ_{nx}	τ_{ny}	$R_{u,nx}$	$R_{u,ny}$	$R_{u,nmin}$
26	EL(965)-H1-1.35	4.04	4.53	0.49	0.89	88.29	1669.94	1670.83	0.05	59.9	63.8	0.99332	0.98902	0.98668	0.97816	98.66795
	EL(965)-H1-1.35	3.77	3.84	0.07	0.39	40.20	1702.02	1702.41	0.02	61.5	62.4	0.98373	0.99840	0.96772	0.99680	99.67953
	EL(965)-H1-2.0	4.05	4.32	0.27	0.7	71.43	1770.78	1771.48	0.04	61.5	62.3	0.99675	1.00000	0.99350	1.00000	100.00000
	EL(965)-H1-2.0	4.13	4.01	-0.12	0.21	20.00	1893.02	1893.23	0.01	59.6	61.6	1.00000	0.99675	1.00000	0.99351	99.35132
	EL(965)-H1-3.0	4.14	4.42	0.28	0.79	80.74	1801.89	1802.68	0.04	59.9	62.8	0.99332	1.00319	0.98668	1.00638	98.66793
	EL(965)-H1-3.0	4.02	4.18	0.16	0.68	63.49	1894.28	1894.96	0.04	59.4	61.4	0.99832	1.00978	0.99663	1.01965	99.66336
	NC-H1-3.0	3.76	3.89	0.13	0.42	41.24	1797.34	1797.76	0.02	59.3	62.5	1.01688	1.01281	1.03404	1.02578	102.57792
	NC-H1-3.0	3.89	3.97	0.08	0.26	26.88	1776.43	1776.69	0.01	59.6	63.1	1.00168	1.00159	1.00336	1.00317	100.33611
	EL(955)-H1-3.0	4.06	4.33	0.27	0.68	62.87	1871.97	1872.65	0.04	60.1	60.5	1.00333	1.00165	1.00667	1.00331	100.33106
	EL(955)-H1-3.0	3.84	3.97	0.13	0.3	30.31	1806.25	1806.55	0.02	60.8	62	1.00346	0.99193	1.00692	0.98393	98.39258

F-T cycles	spec.no	surface scaling					moisture uptake			internal damage						
		U_f (g)	U_b (g)	U_s (g)	ΣU_s (g)	m_n (g/m^2)	W_n (g)	W_{nt} (g)	ΔW_n (%)	t_{nx} (ms)	t_{ny} (ms)	τ_{nx}	τ_{ny}	$R_{u,nx}$	$R_{u,ny}$	$R_{u,nmin}$
44	EL(965)-H1-1.35	4.53	4.95	0.42	1.31	129.96	1670.1	1671.41	0.08	60	63.8	0.99166	0.98902	0.98339	0.97816	98.33909
	EL(965)-H1-1.35	3.84	3.95	0.11	0.5	51.54	1700.01	1700.51	0.03	61.9	62.7	0.97737	0.99362	0.95525	0.98727	98.72732
	EL(965)-H1-2.0	4.32	4.59	0.27	0.97	98.98	1771.66	1772.63	0.05	61.6	62.3	0.99513	1.00000	0.99028	1.00000	100.00000
	EL(965)-H1-2.0	4.01	4.03	0.02	0.23	21.90	1893.59	1893.82	0.01	59.9	62.4	0.99499	0.98396	0.99000	0.96819	96.81869
	EL(965)-H1-3.0	4.42	4.67	0.25	1.04	106.29	1801.81	1802.85	0.06	60.1	6.32	0.99001	10.02297	0.98012	100.45994	98.01186
	EL(965)-H1-3.0	4.18	4.3	0.12	0.8	74.70	1894.39	1895.19	0.04	59.5	61.3	0.99664	1.01143	0.99328	1.02298	99.32842
	NC-H1-3.0	3.89	4.12	0.23	0.65	63.82	1797.39	1798.04	0.04	59.6	62.5	1.01175	1.01281	1.02364	1.02578	102.36447
	NC-H1-3.0	3.97	4.04	0.07	0.33	34.12	1776.8	1777.13	0.02	59.8	63.3	0.99833	0.99842	0.99666	0.99684	99.68411
	EL(955)-H1-3.0	4.33	4.6	0.27	0.95	87.83	1872.85	1873.80	0.05	60.2	60.6	1.00166	1.00000	1.00333	1.00000	100.00000
	EL(955)-H1-3.0	3.97	4.08	0.11	0.41	41.42	1807.18	1807.59	0.02	61.2	61.9	0.99689	0.99353	0.99380	0.98711	98.71095
F-T cycles	spec.no	surface scaling					moisture uptake			internal damage						
		U_f (g)	U_b (g)	U_s (g)	ΣU_s (g)	m_n (g/m^2)	W_n (g)	W_{nt} (g)	ΔW_n (%)	t_{nx} (ms)	t_{ny} (ms)	τ_{nx}	τ_{ny}	$R_{u,nx}$	$R_{u,ny}$	$R_{u,nmin}$
74	EL(965)-H1-1.35	4.95	5.39	0.44	1.75	173.61	1669.79	1671.54	0.10	60.4	64	0.98509	0.98593	0.97040	0.97206	97.20563
	EL(965)-H1-1.35	3.95	4.05	0.1	0.6	61.84	1699.84	1700.44	0.04	62.3	62.9	0.97109	0.99045	0.94301	0.98100	98.10008
	EL(965)-H1-2.0	4.59	4.95	0.36	1.33	135.71	1772.35	1773.68	0.08	61.6	62.5	0.99513	0.99680	0.99028	0.99361	99.36061
	EL(965)-H1-2.0	4.03	4.16	0.13	0.36	34.29	1893.11	1893.47	0.02	61.5	61.6	0.96909	0.99675	0.93913	0.99351	93.91266
	EL(965)-H1-3.0	4.67	5	0.33	1.37	140.01	1801.57	1802.94	0.08	60.3	63.3	0.98672	0.99526	0.97362	0.99054	97.36231
	EL(965)-H1-3.0	4.3	4.4	0.1	0.9	84.03	1893.56	1894.46	0.05	59.9	61.4	0.98998	1.00978	0.98005	1.01965	98.00540
	NC-H1-3.0	4.12	4.38	0.26	0.91	89.35	1796.97	1797.88	0.05	60.1	62.9	1.00333	1.00636	1.00667	1.01277	100.66713
	NC-H1-3.0	4.04	4.15	0.11	0.44	45.49	1776.11	1776.55	0.02	59.7	63.5	1.00000	0.99527	1.00000	0.99057	100.00000
	EL(955)-H1-3.0	4.6	4.93	0.33	1.28	118.34	1873.94	1875.22	0.07	60.3	60.06	1.00000	1.00900	1.00000	1.01807	100.00000
	EL(955)-H1-3.0	4.08	4.27	0.19	0.6	60.62	1807.12	1807.72	0.03	61.3	61.4	0.99527	1.00163	0.99055	1.00326	99.05543
F-T cycles	spec.no	surface scaling					moisture uptake			internal damage						
		U_f (g)	U_b (g)	U_s (g)	ΣU_s (g)	m_n (g/m^2)	W_n (g)	W_{nt} (g)	ΔW_n (%)	t_{nx} (ms)	t_{ny} (ms)	τ_{nx}	τ_{ny}	$R_{u,nx}$	$R_{u,ny}$	$R_{u,nmin}$
96	EL(965)-H1-1.35	5.39	5.79	0.4	2.15	213.29	1670.51	1672.66	0.13	61.7	63.7	0.96432	0.99058	0.92991	0.98124	98.12396
	EL(965)-H1-1.35	4.05	4.15	0.1	0.7	72.15	1700.41	1701.11	0.04	62.7	62.9	0.96489	0.99045	0.93101	0.98100	98.10008
	EL(965)-H1-2.0	4.95	5.27	0.32	1.65	168.37	1772.65	1774.30	0.09	61.8	62.4	0.99190	0.99840	0.98387	0.99680	99.67954
	EL(965)-H1-2.0	4.16	4.2	0.04	0.4	38.10	1894.43	1894.83	0.02	60.4	62.1	0.98675	0.98872	0.97367	0.97757	97.36679
	EL(965)-H1-3.0	5	5.37	0.37	1.74	177.82	1802.22	1803.96	0.10	60.3	63.4	0.98672	0.99369	0.97362	0.98741	97.36231
	EL(965)-H1-3.0	4.4	4.53	0.13	1.03	96.17	1894.51	1895.54	0.05	59.7	61.2	0.99330	1.01308	0.98664	1.02633	98.66359
	NC-H1-3.0	4.38	4.63	0.25	1.16	113.89	1798.26	1799.42	0.06	59.7	63.1	1.01006	1.00317	1.02022	1.00635	100.63529
	NC-H1-3.0	4.15	4.24	0.09	0.53	54.80	1772.12	1772.65	0.03	59.5	63.3	1.00336	0.99842	1.00674	0.99684	100.67391
	EL(955)-H1-3.0	4.93	5.26	0.33	1.61	148.85	1875.58	1877.19	0.09	59.9	60.7	1.00668	0.99835	1.01341	0.99671	99.67058
	EL(955)-H1-3.0	4.27	4.36	0.09	0.69	69.71	1808.57	1809.26	0.04	61.4	62	0.99364	0.99193	0.98733	0.98393	98.39258

11. APPENDIX C – RECOMMENDED SPECIAL PROVISION

Recommended special provisions were developed for the proposed UHPC blends. The provisions are necessary for MDOT to bid future UHPC projects and are designed to be adopted as is.

RECOMMENDED SPECIAL PROVISION
FOR
PRODUCTION OF MICHIGAN ULTRA HIGH PERFORMANCE CONCRETE (MI – UHPC)

OFS:SCK 1 of 4 APPR:XXX:YYY:00-00-19

a. Description. This special provision addresses the production of Michigan Ultra High Performance Concrete (Mi-UHPC). Mi-UHPC must be used at locations specified on the plans. All work must be in accordance with the standard specifications, except as modified herein.

b. Materials. The concrete mixture must contain the following materials per cubic yard. Four mixes are listed with different amounts of High Range Water Reducers (HRWR). Other amounts of HRWR and alternative material proportions may be used if the resulting mix is shown to achieve the performance outlined in section h of this special provision and approved by the Engineer.

Material	**Weight [lb/yd^3]**			
Cement Blend	Mix A[1]	Mix B[1]	Mix C[1]	Mix D[1]
Portland Type I	653			
Slag Cement	653			
Silica Sand				
Fine Sand[2]	398	396	395	394
Coarse Sand[3]	1590	1586	1982	1577
Silica Fume	327			
Water	276	272	268	264
High Range Water Reducer[4,5]	20	26	33	39
Steel Fibers[6]	265			

[1] Mixes A, B, C and D have HRWR dosages of 1.5%, 2%, 2.5% and 3%, respectively.
[2] Grain sizes 80-200 microns
[3] Grain sizes 400-800 microns
[4] Polycarboxylate ether-based high range water reducer
[5] High range water reducer dosage rates can be adjusted to meet the paste flowability requirements, Dosages range vary with the type of silica fume and range from 1.5% to 3.0% by weight of the cement.
[6] The steel fibers are 2% by volume.

Steel fibers – Straight cold-drawn wire conform to ASTM A820, Type I fibers. They must have a diameter of 0.008 in (0.2mm)-0.012 in (0.3 mm) and length of 0.5 in (13 mm)- 0.75 in (19 mm), and a minimum tensile strength of 285 ksi.

High Range Water Reducer – After confirmation, the brand and dosage may not be replaced without written approval of the engineer.

c. Equipment. Mixers capable of inducing sufficiently high shear to successfully mix the UHPC must be used. Pumping Mi-UHPC is not permitted.

d. Submittals. Submit the following to the Engineer, at least 21 days before placing for review and approval:

A. Material certifications and manufacturer's published product literature.

B. A quality control plan that must include, but is not limited to, the following:

(1) Mixing protocol.

(2) Casting procedure.

(3) Sampling and testing procedure.

(4) Curing procedure.

e. Pre-Pour Meeting. Prior to the initial placement of the Mi-UHPC, the Contractor must arrange for an onsite meeting with the Engineer and Construction Field Services. The objective of the meeting will be to clearly outline the procedures for mixing, transporting, finishing and curing of the Mi-UHPC, and to review the trial batch requirements.

f. Trial Batch. Conduct trial batches using the four mixes listed in this special provision subsection b. Select the mix with lowest amount of HRWR that meets the flowability requirements of subsection g.5 of this special provision. In order to ensure the same construction conditions, environmental conditions (e.g., time of day, weather, etc.) must be recorded and submitted to the engineer after conducting the trial batches.

Demonstrate that the selected mixture meets the requirements of this special provision a minimum of 21 days before concrete placement. The trial batch must be attended by the Engineer and Construction Field Services. The trial batch must be of sufficient size to complete the trial placement.

Trial Placement: Construct a full scale trial batch mix to use at least the minimum mix capacity of the equipment, including quantities for sampling and testing. The trial placement must use the equipment and the same forming, casting, and curing procedures that will be used during construction. The trial placement must be witnessed by the Engineer and Construction Field Services.

Provide the results of temperature, slump, density (unit weight), 3-day compressive strength, and 7-day compressive strength testing. Each compressive strength test must be conducted according to subsection g.6 of this special provision. Submit the results of all tests above to the Engineer for review and approval a minimum of 10 calendar days prior to the use of the Mi-UHPC in the field .

To be considered a successful trial batch, the slump flow must be within the range of 7 to 12 inches, and the compressive strength must meet 12 ksi at 3 days, and 15 ksi at 7 days.

To be considered a successful trial placement, there must be no segregation of the Mi-UHPC and no visible voids when the forms are removed.

If the trial batch or trial placement does not meet these requirements, discard the material and repeat the trial batch and trial placement at no additional cost to the Department.

g. Construction.

1. Storage. Assure the proper storage of constituent materials, fibers, and additives as required by the manufacturer's specifications in order to protect materials against exposure to moisture and loss of physical and mechanical properties.

2. Temperature Limitations. Do not place concrete at ambient air temperatures below 40 degrees F.

For cold weather casting, the top surface of the concrete must be covered with insulating blankets, having a minimum R Value as specified in Table 706-1 of the Standard Specifications for Construction, when the air temperature is below 60 degrees F. Insulating blankets must meet the requirements of subsection 903.07.C of the Standard Specifications for Construction. Leave insulating blankets in place for a minimum 7 calendar days.

For warm weather casting, replace a sufficient amount of the mix water with ice to keep the mixture below 85 degrees F.

3. Mixing Protocol. The following mixing protocol must be followed:

A. Mix cement, GGBS, silica fume, and 20% of the silica sands for 5 minutes.

B. Add water and superplasticizer till turnover and formation of thick slurry. Do not allow material to cake on the side of the mixer.

C. Incorporate remaining silica sand gradually and mix another 5 minutes.

D. Perform the slump flow test according to subsection g.5 of this special provision. If the slump flow is between 7 and 12 inches, add the steel fibers into the mix. Do not incorporate any Mi-UHPC into the project with slump flow outside the stated range.

E. Add fibers and continue to mix until fluidity is optimized (between 5 and 8 minutes).

4. Forms: The forms must be water tight and coated to prevent absorption of water. The formwork must be resistant to the hydraulic pressure of the mix.

5. Quality Control. Submit a copy of all quality control records to the Engineer within 24 hours after the date of concrete placement covered by the record.

Use a flow table to measure the slump flow for each batch of Mi-UHPC. Conduct the slump flow test in accordance with ASTM C1437 without compacting and without moving or impacting the base plate. Record the slump flow for each batch in the QC records. The slump flow must be within the range of 7 to 12 in. Do not incorporate Mi-UHPC into the project with slump flow outside the stated range.

6. Compression Testing Requirements. Make three sets of compressive strength test samples for each day of placement. Each set consists of three 2x2 inch cubes. All test samples must be cured using the same method of curing as outlined in the quality control plan. The compressive strength tests must be conducted on a minimum of three 2x2 inch cube

samples according to ASTM C109. Testing shall be performed by an approved testing laboratory.

7. Curing. Do not apply curing compound. The concrete surfaces must be continuously cured with wet burlap per subsection 706.03.N.1.b, except that the wet burlap must be applied immediately after casting.

h. Acceptance. The Engineer will sample the Mi-UHPC and test it for 4, 7, and 28 day compressive strength and table slump flow. If the Mi-UHPC achieves a minimum of 12 ksi at 3 days, 15 ksi at 7 days, the table slump flow is within 7 to 12 inches, and Mi-UHPC placement, segregation, and consolidation are acceptable, the Mi-UHPC for each representative placement will be accepted.

i. Measurement and Payment. The completed work, as described, will be measured and paid for at the contract unit price using the following pay item:

Pay Item	**Pay Unit**
Conc, Michigan Ultra High Performance	Cubic Yard

Conc, Michigan Ultra High Performance will be measured in cubic yards based on plan quantities. Payment for **Conc, Michigan Ultra High Performance** includes all labor, equipment, and materials required for the first trial batch, forming, furnishing, testing, placing, finishing, and curing the concrete according to this special provision. No additional compensation will be made for trial batches or trial placements that fail to meet the requirements of this special provision.